MATERIALS CHEMISTRY
FRONTIERS

CCS 中国化学会 CHINESE CHEMICAL SOCIETY
ICCAS
ROYAL SOCIETY OF CHEMISTRY

REVIEW

View Article Online
View Journal | View Issue

Cite this: *Mater. Chem. Front.*, 2023, **7**, 4304

A review of fused-ring carbazole derivatives as emitter and/or host materials in organic light emitting diode (OLED) applications

Saliha Oner and Martin R. Bryce *

Received 14th April 2023,
Accepted 14th June 2023

DOI: 10.1039/d3qm00399j

rsc.li/frontiers-materials

This review focuses on fused-ring carbazole derivatives, their molecular design, electronic and photophysical properties, and in particular their applications as the emitter and/or the host material in the emitting layer of organic light emitting diodes (OLEDs), with emphasis on recent developments. This review is timely because of the rapidly expanding research into fused-ring carbazoles, predominantly indolocarbazole, indenocarbazole, benzofurocarbazole, benzothienocarbazole and diindolocarbazole derivatives. To our knowledge this class of materials has not been reviewed previously. The appeal of fused-ring carbazoles is their extended π-electron systems with good thermal stability, tunable frontier orbital energies that enable a wide gamut (red, green, blue and white) emission colour, high photoluminescence quantum yields, and versatility for chemical functionalisation at different sites, leading to outstanding OLED efficiencies. This review is divided into sections according to the molecules' role in OLEDs: namely, as conventional luminescent emitters – especially in the deep-blue region; as state-of-the-art hosts for phosphorescent iridium-based emitters; as thermally activated delayed fluorescence (TADF) emitters with high external quantum efficiency; and as multiresonance (MR) emitters with unprecedented high colour purity. We conclude by highlighting the challenges and the great opportunities for fused-ring carbazole derivatives in OLEDs and other optoelectronic applications.

1. Introduction

Relevant general background information will be summarised before focusing on fused-ring carbazoles. Carbazole is a versatile building block for compounds that have been a wide variety of electronic applications such as organic light-emitting diodes (OLEDs),[1,2] solar cells,[3,4] sensors,[5,6] organic field effect transistors (OFETs),[7,8] molecular wires,[9] and electrochromic devices.[10,11] Carbazole is an electron-rich unit, providing good hole transporting properties,[12] high thermal and electrochemical stability,[13,14] high photoluminescence quantum yield (PLQY),[15] ease of functionalisation through different sites and tunable optical and electronic properties.[16] (Co)polymerisation of substituted carbazoles is also readily achieved yielding carbazole as a main-chain unit in luminescent and electroactive polymers.[17] However, it is important to note that commercial carbazole can contain trace amounts of isomeric impurities, identified as 1*H*-benzo[*f*]indole[18] and 5*H*-benzo[*b*]carbazole,[19] which have profound effects on the luminescent properties of the sample and derived products, notably giving enhanced PLQY and ultralong phosphorescence.

Through rational molecular design many carbazole derivatives have been developed as emitter and/or host materials for organic light emitting diode (OLED) applications.[1,2,20,21] OLED technology is growing rapidly in areas such as consumer electronics, flat panel displays, flexible screens, and solid-state lighting.[22] Further development of efficient and cheap OLED materials is still necessary to fully exploit the technology. As a prime example, there is a continued need for stable blue emitters and hosts.[23,24] First generation OLEDs were based on fluorescence which has a theoretical maximum of only 25% internal quantum efficiency (IQE) because spin statistics dictate that emissive singlets and non-emissive triplets are formed in a 1 : 3 ratio, thereby severely limiting the external quantum efficiency (EQE) of the OLEDs.[25] Second generation OLEDs utilised phosphorescent emitters which can theoretically achieve 100% IQE by harnessing both singlet and triplet excitons.[26] In phosphorescent OLEDs (PhOLEDs) organometallic complexes (predominantly Ir and Pt) can increase the spin–orbit coupling (SOC) due to the heavy atom effect and have favourable intersystem crossing (ISC) rates. By ISC, singlet excitons are transformed into the triplet state and are deactivated radiatively *via* phosphorescence. In PhOLEDs, the emitter (guest) is doped in a host material to prevent concentration quenching and triplet–triplet annihilation (TTA) processes that decrease the quantum efficiency.[27,28] Small-molecule and

Department of Chemistry, Durham University, Stockton Road, Durham DH1 3LE, UK. E-mail: m.r.bryce@durham.ac.uk

polymeric carbazole derivatives are ubiquitous host materials for PhOLEDs.[29–32] Regarding PhOLEDs, the low natural abundance of the heavy metals makes these complexes more expensive and less attractive for commercialisation compared to pure organic materials. Also, the complexes or their precursors may be toxic because of the presence of heavy metals, and their chemical modification is more limited, with some complexes being unstable especially for blue emission. Because of the above reasons, there is a great demand for organic compounds which are cheaper, more abundant, easy to modify and have high light emission efficiency. Emission mechanisms that are utilised to harvest both singlet and triplet excitons radiatively in pure organic materials include: triplet–triplet annihilation (TTA),[33,34] hybridised local and charge transfer (HLCT) excitation[35] and triplet–polaron annihilation (TPA).[36]

However, the mechanism that has had the most dramatic impact on the OLED field in the last decade is thermally activated delayed fluorescence (TADF) leading to third-generation organic electroluminescent materials. In this mechanism, T_1 excitons are converted into S_1 excitons (the subscript 1 denotes the lowest energy T and S states) by a reverse intersystem crossing (RISC) process, causing a delayed fluorescence, which allows theoretical 100% IQE. The basic TADF mechanism in organic materials was known since the 1960s (named "E-type delayed fluorescence").[37] However, its potential had lain dormant until the first report in 2009 from Adachi's group of a TADF organometallic complex in electroluminescence.[38] A pure organic compound (indolocarbazole based) was subsequently demonstrated as a TADF emitter in OLEDs, again by Adachi's group.[39] To obtain an efficient TADF emitter, a second-order vibronically coupled RISC mechanism is achieved by a molecular design which requires a small S_1–T_1 energy gap ($\Delta E_{ST} < \approx 200$ meV). TADF emitters generally have a highly twisted D–A structure (D = electron donor; A = electron acceptor), with optimised dihedral angle and distance between the D and A units, induced by steric hindrance and/or a molecular bridge. Thereby the highest occupied and lowest unoccupied molecular orbitals (HOMO and LUMO, respectively) are predominantly localised on the D and A units respectively, but at the expense of low values of oscillator strength.

For efficient TADF the emitter should have a small ΔE_{ST}, a large SOC, a fast $k_{RISC} \approx 10^6$ s^{-1} and a high photoluminescence quantum yield (PLQY). Additionally, for good colour purity the emission peak should have narrow full-width at half-maximum (FWHM). The latter is very challenging to achieve as the delayed fluorescence comes from a charge transfer (CT) excited state, which typically features significant structural relaxations leading to broadened emission (FWHM *ca.* 70–100 nm). According to El-Sayed's rules the direct conversion from T_1 to S_1 is not allowed because the large CT character of both excited states leads to vanishing SOC. However, an energetically close state (usually a locally excited D or A triplet state, ^{3}LE) comes to the rescue and an efficient spin–flip process can occur within the manifold of ^{1}CT, ^{3}CT and ^{3}LE states. This LE state is tuned by intramolecular vibrations which enhance the SOC, thereby enabling fast ISC and RISC to occur.[40]

An alternative to the standard D–A design of TADF molecules was first reported in 2016 by Hatakeyama *et al.*[41] The molecules are polycyclic aromatic compounds with electron-deficient boron and electron-rich nitrogen atoms embedded within the rigid carbon framework. Short-range charge transfer occurs through atomically separated frontier molecular orbitals (FMOs) leading to multi-resonance TADF (MR-TADF). Benefitting from the MR effect, the radiative decay constant of fluorescence (k_F) of some MR-TADF emitters is $\approx 10^7$ s^{-1} which is much higher than most TADF emitters. Narrow FWHM of the emission is achieved due to the presence of FMOs that suppress the vibrational relaxations that occur upon excitation. However, OLEDs based on such BN-based MR emitters tend to show serious efficiency roll-off at higher brightness, and poor device operation stability: a main reason is slow k_{RISC} rates which are generally within the range $\approx 10^3$–10^5 s^{-1}.

For thin film photophysical measurements and for OLED fabrication, the emitter molecules are typically dispersed in a host material to limit quenching mechanisms such as triplet–triplet annihilation (TTA) and aggregation caused quenching (ACQ).[42,43] A suitable host should possess: (i) higher triplet energies than those of the guest molecules to confine triplet excitons within the emitting layer (EML) by preventing exothermic reverse energy transfer; (ii) energy levels appropriately aligned with those of the neighbouring active layers for efficient charge carrier injection into the EML to achieve a low operating voltage; (iii) balanced charge carrier properties for holes and electrons; (iv) high glass transition temperature (T_g) to favour uniform and stable amorphous films and to minimise the possibility of phase separation upon heating, thus prolonging the operational lifetime of the device.

Four classes of hosts have been reported: (i) hole transporting, based on electron-donating units such as carbazole, arylamine and phenothiazine; (ii) electron transporting, based on electron-withdrawing units, such as triazine, oxadiazole, cyanoarene and phosphine oxide; (iii) bipolar, with both hole transporting and electron transporting units in the same molecule; (iv) mixed hosts that form intermolecular exciplexes. The latter two classes achieve a better balance of holes and electrons in the EML. A drawback of bipolar hosts can be a reduction of the HOMO–LUMO gap due to intramolecular charge transfer, which will lower the S and T energies, and consequently lead to unwanted back-transfer of energy from the guest to the host. Exciplex forming *co*-hosts have been used especially for PhOLEDs, but also for TADF-OLEDs and hyperfluorescent (TADF-sensitised fluorescence) OLEDs.[44,45] Compared to a single bipolar host molecule, an exciplex *co*-host has more spacially separated frontier molecular orbital distribution which results in reduced intramolecular charge transfer and a smaller ΔE_{ST}.[46] It is a challenge to fine tune the substituents and steric effects to design molecules with a high T energy which also possess a HOMO–LUMO gap appropriate for injection of both holes and electrons into the doped emitter layer from adjacent layers. It should be noted that E_T values can vary significantly between doped films and neat films (by as much as 0.24 eV higher in dilute doped film) ascribed to conformational demands of the molecule in the solid state. Therefore, caution should be used in comparing literature data obtained in different media.[47]

Classical hole-transporting host materials that are frequently used to benchmark the performance of new emitters or new hosts are 4,4′-bis(9-carbazolyl)biphenyl (CBP) and 1,3-bis(*N*-

carbazolyl)benzene (mCP). CBP has E_T 2.56 eV[48] and its T_g is 103 °C[49] determined by a melt-blending method, correcting earlier reported values of 62 and 112 °C from differential scanning calorimetry (DSC). mCP has significantly higher E_T 2.90 eV[50] but lower T_g 62 °C (with previous reports quoting 55, 60, 65 and 66 °C).[49] However, these hosts are prone to crystallisation, especially when the dopant concentration is low. The E_T and T_g values have been raised in conformationally restricted bi(carbazole) derivatives.[51,52] Established carbazole-based ambipolar hosts with sufficiently high triplet energies (>2.7 eV) for sky-blue and blue emitters include derivatives with electron accepting pyridine[29,53] or phosphine oxide[54] substituents. The large S_1–T_1 gap in conventional host materials causes a high triplet exciton density, which facilitates TTA, triplet–polaron annihilation (TPA) and electric field induced quenching processes, which contribute to detrimental efficiency roll-off in PhOLEDs.[55] Therefore, TADF host materials with small ΔE_{ST} and efficient RISC rate can overcome these drawbacks, by converting triplet excitons to the singlet state.

Fused-ring carbazole derivatives are having a major impact in the OLED field. Their structures lead to increased rigidity which has the benefit of restricting molecular deformations in the excited state and suppressing nonradiative energy dissipation. Section 2 considers their applications as conventional fluorescent emitters. Section 3 gives examples where fused carbazoles are hosts for phosphorescent iridium complexes. Section 4 is a major part of this review, showcasing how fused carbazoles are key components of some of the most efficient TADF emitters, imparting rigidity,[56] narrow band emission,[57] small ΔE_{ST}, high PLQY,[58,59] good thermal stability, and structural versatility. Most notably, indolocarbazole, indenocarbazole, benzofurocarbazole, benzothienocarbazole and diindolocarbazole derivatives are highlighted. Section 5 concerns the current hot topic of multi-resonance (MR) fused carbazoles. In Section 6 we conclude with perspectives on the future of this very active and expanding field. Throughout this article we have retained the nomenclature and abbreviations used for the compounds in the cited publications to facilitate cross-checking with the original data. Selected figures are included to illustrate key optoelectronic properties of the molecules. Synthetic routes will not be considered. In the chemical structures the carbazole frameworks in the fused rings are shown in blue.

2. Fused-ring carbazole derivatives as conventional fluorescent emitters

The emphasis of this section is on stable blue/deep-blue electroluminescence. An initial report that aryl substituted indolo[2,3-*a*]carbazole derivatives give blue/deep blue fluorescence in solution and in neat thin film set the stage. However, OLEDs were not reported in this work.[60] Subsequently, indeno[2,1-*b*]carbazole derivatives **IDC-PA** and **IDC-Py** were studied (Fig. 1a).[61] λ_{max}^{PL} was 450/439 nm in DCM solution, and 453/443 nm, respectively, in films. The negligible red-shifts indicated that there were almost no intermolecular interactions in the films and aggregation was suppressed by the twisted structures induced by the bulky anthracene and pyrene groups. The PLQYs were 0.84 and 0.78 (DCM solution). The T_gs were 186 and 157 °C for **IDC-PA** and **IDC-Py**, respectively. Non-doped OLEDs with a neat EML exhibited efficiencies of up to 4.80 and 4.13 cd A^{-1}, and EQE_{max} values of 4.41% and 6.08% with deep-blue Commission Internationale de l'Éclairage ($CIE_{x,y}$) coordinates (0.15, 0.10) and (0.15, 0.08) for **IDC-PA** and **IDC-Py** devices, with FWHM of 58 and 56 nm, respectively. There was negligible efficiency roll-off, even at increased voltage (Fig. 1b) and at a brightness of 5000 cd m^{-2} (EQEs 4.35% and 5.35%).

The bis(indolo[3,2-*b*]carbazole) derivative **BEDCE** (Fig. 2a) was studied.[62] Differential scanning calorimetry (DSC) exhibited a weak exothermic peak at 20 °C, corresponding to a glass transition temperature (T_g), which resulted in an elastomeric material at room temperature. The oligo-oxyethylene chains introduced large steric hindrance, modulating the strong π–π stacking tendency of the fused carbazole skeletons, and provided an amorphous structure. **BEDCE** showed λ_{max}^{PL} at 426 and 531 nm, with a PLQY of 88% (THF solution). Devices with a solution-processed, non-doped emitter layer had EQE_{max} 1.34% with CE_{max} of 4.56 cd A^{-1} and L_{max} of 10 320 cd m^{-2} with greenish-yellow EL, CIE(0.36, 0.59).

The indolo[2,3-*c*]carbazoles **1–4** (Fig. 2) have λ_{max}^{PL} (undoped films) of 437, 447, 451 and 539 nm, respectively.[63] The PL measurements at 77 K (in MeTHF) indicated a red-shifted and structured emission for **1–3** which was attributed to phosphorescence. This behaviour was not observed at room temperature. Monoexponential decays were observed for **1**

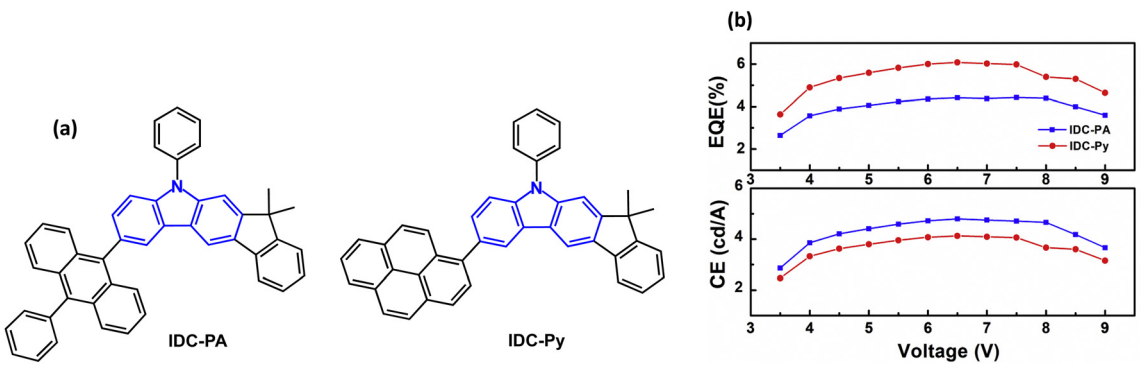

Fig. 1 (a) Molecular structures of **IDC-PA** and **IDC-Py**. (b) Current efficiency and EQE *versus* voltage.[61] Copyright 2018 Elsevier.

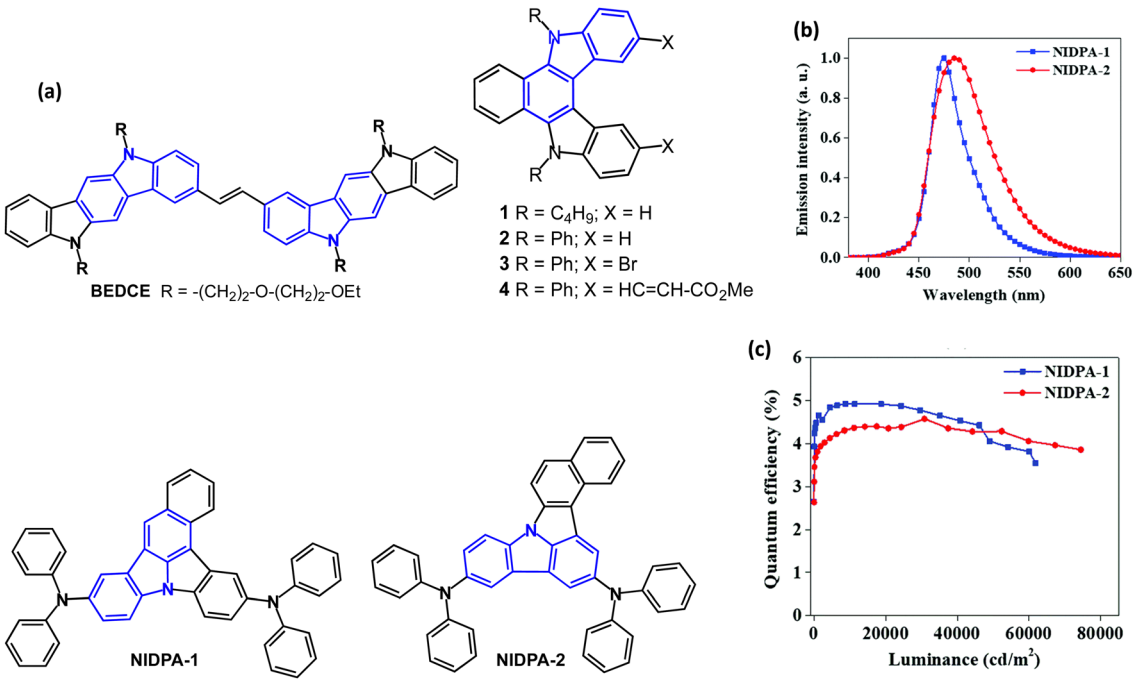

Fig. 2 (a) Molecular structures of **BEDCE**, **1**–**4**, **NIDPA-1** and **NIDPA-2**. (b) EL spectra. (c) EQE–luminance curves of doped OLEDs.[64] Copyright 2020 The Royal Society of Chemistry.

and **2**, indicating that only the S_1 state was emitting. Two components were obtained for compound **3**, due to fluorescence from the S_1 state and a limited degree of dimer formation. For compound **4**, all the decays were multiexponential and solvent-dependent. Two components were attributed to different torsional conformations of the ester group, and the third component with a longer lifetime was attributed to the small contribution of a CT state. EL spectra of single- and double-layer devices mostly resembled the PL spectra, but with additional contributions from electromers or electroplexes.

Isomeric benzo[*c*]carbazole chromophores **NIDPA-1** and **NIDPA-2** (Fig. 2) showed λ_{max}^{PL} at 473/484 nm with PLQYs of 51/54% (under N_2) and FWHMs of 46/71 nm (2 wt% doped in PANB host film) respectively.[64] The emission of both compounds in the neat film (489/502 nm) was red-shifted compared to the doped film due to strong intermolecular interactions. The excited-state lifetime of the **NIDPA-2** was longer than for **NIDPA-1** (26.6 *vs.* 12.6 ns). The compounds are conventional fluorescent emitters with ΔE_{ST} 0.67 and 0.89 eV (PL measurements in PANB host). OLEDs had a PANB:emitter (2 wt%) EML. The **NIDPA-1** device exhibited blue EL [λ_{max}^{EL} 475 nm, CIE(0.13, 0.22)], EQE_{max} 4.9% and narrow FWHM of 41 nm. The **NIDPA-2** device had broader EL [λ_{max}^{EL} 487 nm, CIE(0.16, 0.34)] and EQE_{max} 4.6%. High values of L_{max} 62 000/74 500 cd m^{-2} were obtained for **NIDPA-1** and **NIDPA-2** devices, respectively. Both devices showed excellent stability with a very low drop of EQE at high brightness (Fig. 2b and c).

The related indolocarbazole derivatives **IDCz-DPA** and **IDCz-2DPA** (Fig. 3) have λ_{max}^{PL} 451 and 457 nm, respectively, in toluene solution.[65] PLQYs were 48% and 56% with narrow FWHM of 41 and 37 nm doped in α-ADN films (under N_2). Using the same device architecture as for **NIDPA-1** and **NIDPA-2** (above) **IDCz-2DPA** showed higher OLED performance than **IDCz-DPA**, with EQE_{max} of 5.6% (*vs.* 5.3%), L_{max} 47 600 cd m^{-2} (*vs.* 23 700 cd m^{-2}), FWHM 35 nm (*vs.* 41 nm), CIE(0.13, 0.15) [*vs.* (0.14, 0.09)] with little EQE roll-off at high luminance. Lifetimes at 80% (LT_{80}) of the initial luminance (L_0) were 142 h and 50 h for **IDCz-2DPA** and **IDCz-DPA** devices, respectively. The longer lifetime for **IDCz-2DPA** was explained by the higher current efficiency and red-shifted colour coordinate (*i.e.*, lower emission energy) reducing stress on the device.

In 2021 indeno[2,1-*b*]carbazole derivative ***m*-FLDID** (Fig. 4a) was reported as a violet emitter.[66] The HOMO/LUMO energies were calculated by density functional theory (DFT) as 5.20/1.38 eV, resulting in a wide energy gap (E_g) of 3.82 eV. Electrochemical measurements gave E_g 3.32 eV. ***m*-FLDID** showed λ_{max}^{PL} 400 nm in THF solution and 404 nm as 1 wt% doped in mixed

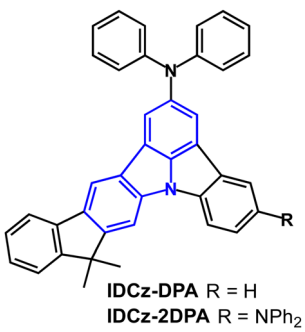

Fig. 3 Molecular structures of **IDCz-DPA** and **IDCz-2DPA**.

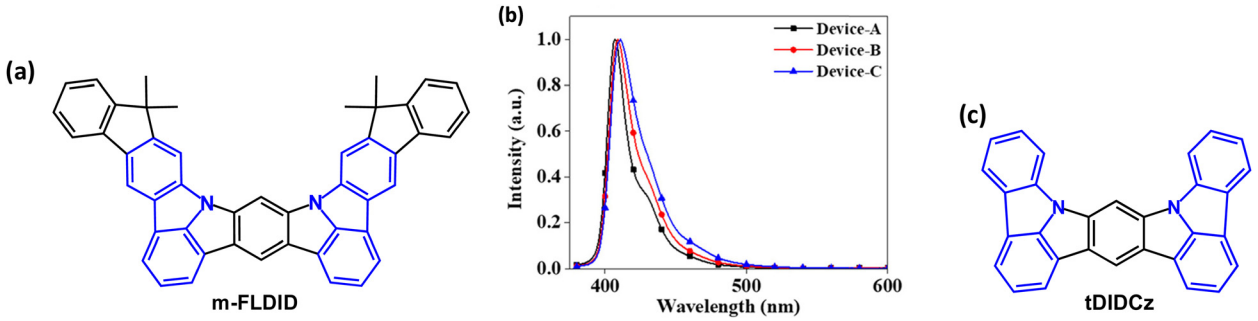

Fig. 4 (a) Molecular structure of ***m*-FLDID**. (b) EL spectra of ***m*-FLDID** Devices A (1 wt%) B (3 wt%) and C (5 wt%).[66] Copyright 2021 The American Chemical Society. (c) Molecular structure of **tDIDCz**.

mCP:TSPO1 host, with FWHM values of 23 and 22 nm, respectively. These values are comparable to the best multi-resonance (MR) type emitters (see Section 5).[67,68] The remarkably small FWHM, small Stokes shift (6 nm), and sharp emission of ***m*-FLDID** were attributed to an MR structure with alternating HOMO and LUMO distribution. $S_1/T_1/\Delta E_{ST}$ energies are 3.08/2.72/0.36 eV. ***m*-FLDID** had PLQY 71% in mixed mCP:TSPO1 host, which remained unchanged in air and nitrogen atmosphere, confirming that there was no contribution from triplet excitons (*i.e.* no TADF); τ_{PF} was 15.5 ns without a delayed component. OLEDs with mCP:TSPO1 host:***m*-FLDID** (25:50:*X* wt%) EML had EQE_{max} values of 4.4–5.2% with a narrow FWHM of 17–27 nm, depending on the doping concentration, and $CIE_y < 0.03$ (Fig. 4b). However, there was extensive efficiency roll-off to 2.7–3.2% at 100 cd m^{-2}.

A similar core structure **tDIDCz** (Fig. 4c) gave violet-emitting OLEDs with CIE(0.164, 0.018) and remarkably narrow FWHM of only 14 nm in mCBP:TSPO1 host. The EQE_{max} was 3.3% with extensive efficiency roll off to ≈1% at 100 cd m^{-2}.[69]

3 Fused-ring carbazole derivatives as host materials

Molecules that are both conventional fluorescent emitters and hosts are covered in this section. In many cases 1,3,5-triazine derivatives are prominent acceptors in these types of bipolar molecules. Two indolocarbazole donors were combined with a triazine acceptor to obtain **BICT**, **PBICT**, **POBICT** and **BBICT** (Fig. 5).[70] An additional electron-withdrawing or -donating group (substituent R) on the triazine tuned the energy levels, the transporting ability and the ΔE_{ST} values. Intramolecular π–π stacking was observed between the two indolocarbazole units (in single-crystal X-ray structures). DFT calculations indicated the dihedral angles between the D and A groups were in the range 41–44° for the four compounds. T_g values were in the range 164–202 °C. λ_{max}^{PL} red shifted sequentially from deep-blue to green for **POBICT**, **BICT**, **PBICT** and **BBICT** (412, 425, 469 and 516 nm in DCM solution). The T_1 energy decreased in the order of **BICT** ≈ **POBICT** (2.70 eV) > **PBICT** (2.66 eV) > **BBICT** (2.47 eV) (PL measurements). The ΔE_{ST} values varied between 0.34 eV for **POBICT** and 0.06 eV for **BBICT**. The compounds were host materials for PhOLEDs with the orange emitter iridium(III)bis(4-phenylthieno[3,2-*c*]pyridinato-*N*,*C*2′) acetylacetonate (PO-01) as the guest with 10 wt% doping in the EML. The highest EQE_{max} of 24.5% was obtained with **PBICT** host. All the devices showed small efficiency roll-off with 90% of the initial luminance at 10 000 cd m^{-2} which was attributed to the wide charge recombination zone in the EML due to the bipolar hosts.

BBPICT (Fig. 5) is a host for red PhOLEDs using the emitter $Ir(mphmq)_2(tmd)$.[71] **BBPICT** exhibited a broad peak at λ_{max}^{PL} 510 nm (toluene solution); $S_1/T_1/\Delta E_{ST}$ levels were 2.74/2.58/0.16 eV (PL measurements). The device structure used **BBPICT**:$Ir(mphmq)_2(tmd)$ (2 wt%) dopant as the EML. EQE_{max} 20.9% was obtained. The devices exhibited small efficiency roll-off of 1.7% at 1000 cd m^{-2}, and a long operational half-life LT_{50} of 1390 h at a brightness of 1000 cd m^{-2}. Comparable devices with CBP host had much higher efficiency roll-off of 17.3% at 1000 cd m^{-2} and shorter LT_{50} of 57 h, attributed to CBP's unbalanced carrier mobility and larger ΔE_{ST}, compared to **BBPICT**.

The isomeric indolo[3,2-*a*] and indolo[2,3-*b*]carbazole derivatives **m32aICT** and **m23bICT** (Fig. 5) are also efficient host materials.[72] They exhibit broad, featureless emission at λ_{max}^{PL} 493/482 nm (toluene solution), respectively. $S_1/T_1/\Delta E_{ST}$ levels were 2.90/2.89/0.01 eV and 2.92/2.72/0.20 eV, respectively (toluene solution). PL transient decay curves (pristine films) indicated the presence of delayed components for **m32aICT** related to its small ΔE_{ST}, whereas for **m23bICT** only a negligible delayed component was observed. The OLED structure used DACT-II (a carbazole–phenylene–triazine derivative) as a TADF sensitiser and Ph*t*BuPAD as a conventional anthracene-based fluorescent emitter, together with the new host in the EML. The **m32aICT** host device had green emission EQE_{max}/PE_{max} values of 23.2%/76.9 lm W^{-1}, remaining at 20.0% and 46.4 lm W^{-1} at 5000 cd m^{-2}, which was more efficient than the **m23bICT** device.

Dibenzothiophene-*S*,*S*-dioxide served as the acceptor in the bipolar indolocarbazole host **DBTO-IN/CAR** (Fig. 5) in PhOLEDs with the archetypal green emitter $Ir(ppy)_3$.[73] **DBTO-IN/CAR** has T_g 156 °C and E_T 2.71 eV (in toluene). PhOLEDs with a **DBTO-IN/CAR**:$Ir(ppy)_3$ (5 wt%) EML exhibited maximum $PE_{max}/CE_{max}/EQE_{max}$ of 45.36 lm W^{-1}, 51.98 cd A^{-1} and 19.03%, which were only slightly higher than the reference device with CBP host (42.01 lm W^{-1}, 50.81 cd A^{-1}, 17.72%). **DBTO-IN/CAR** was also used as a non-doped cyan fluorescence emitter in devices which exhibited 3.0 lm W^{-1}, 4.30 cd A^{-1} and EQE_{max} 2.47%, CIE(0.23, 0.41).

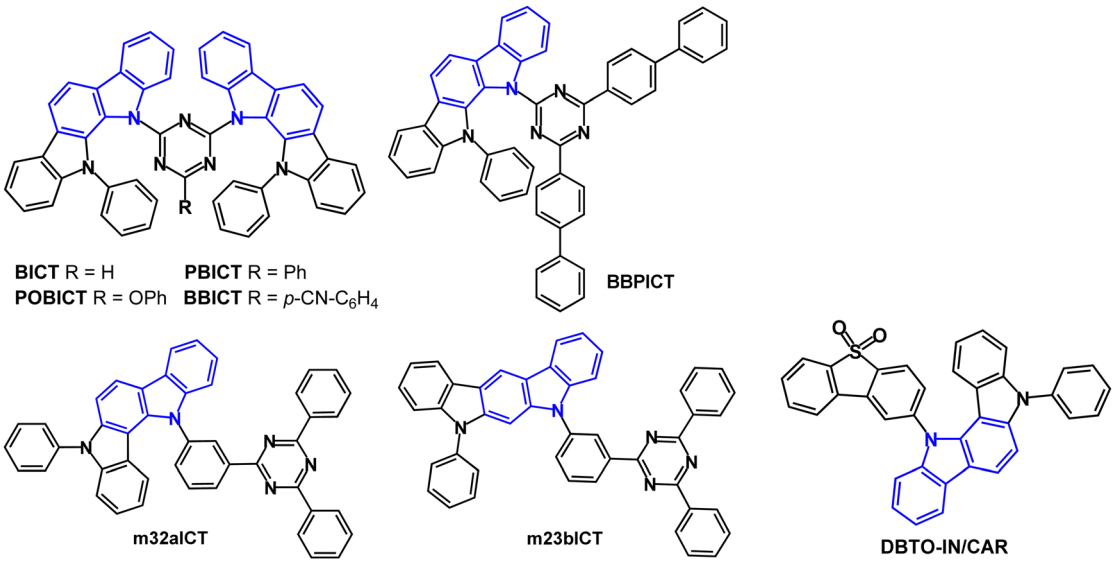

Fig. 5 Molecular structures of indolocarbazole derivatives **BICT**, **PBICT**, **POBICT**, **BBICT**, **BBPICT**, **m32aICT**, **m23bICT** and **DBTO-IN/CAR**.

Bipolar indenocarbazoles have also been studied. **DPDDC** (Fig. 6a) is a host for green PhOLEDs.[74] **DPDDC** has high thermal stability with a decomposition temperature (T_d) of 441 °C (corresponding to 5% weight loss), and T_g of 140 °C. The λ_{max}^{PL} was 475 nm (thin solid film) and $E_T/\Delta E_{ST}$ values were 2.79/0.18 eV, respectively (in 2Me-THF solution). Transient decay times of 10 wt% doped films of **DPDDC** in mCP were τ_{PF} 46.4 ns and τ_{DF} 12.3 μs. Green PhOLEDs with an EML comprising **DPDDC**:$(mdppy)_2Ir(acac)$ (5 wt%) exhibited EQE_{max} 23.6% with low efficiency roll-off of 5.5% at 5000 cd m^{-2}. The devices operated at room temperature and at a constant current density for an initial luminance of 5000 cd m^{-2} showed an improved lifetime LT_{90} of *ca.* 665 min compared to a device with CBP host (LT_{90} = 31 min). The long operating lifetime was attributed to the minimised interactions between the triplets on the Ir dopant and the polarons on the **DPDDC** host molecules.

A hole transporting indenocarbazole derivative **PCIC** (Fig. 6a) was developed.[75] The T_1 level is 2.75 eV (PL data in toluene) T_d

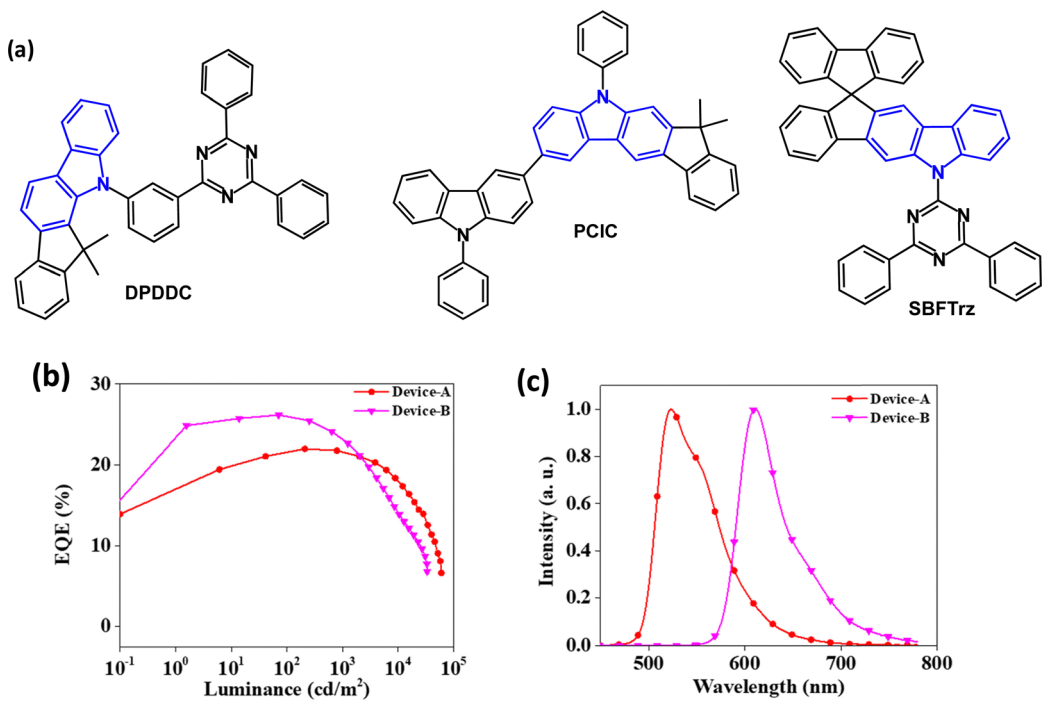

Fig. 6 (a) Molecular structures of indenocarbazoles **DPDDC**, **PCIC** and **SBFTrz**. (b) EQE–*L* data for **SBFTrz**-$Ir(ppy)_2acac$ (Device-A) and **SBFTrz**-$Ir(mphmq)_2tmd$ (Device-B).[76] (c) EL spectra of Device-A and Device-B.[76] Copyright 2021 Elsevier.

482 °C (TGA, 5% weight loss) and T_g (DSC) 98 °C. **PCIC** served as a host for the emitter Ir(mppy)$_3$ in green PhOLEDs with a solution processed EML. A lifetime of 1300 hours to LT_{50}, and CE 66.2 cd A^{-1} (at 1000 cd m^{-2}) was obtained for a device structure that included a bipolar exciton blocking layer with a high triplet level to suppress exciton migration from the green emissive layer. EQE data were not reported.

Theoretical studies of **SBFTrz** (Fig. 6a) indicated bipolar CT character with the spiro unit enforcing a highly twisted geometry.[76] The T_g of **SBFTrz** is 134 °C and $S_1/T_1/\Delta E_{ST}$ energies are 3.63/2.74/0.89 eV. Based on data from hole-only and electron-only devices, **SBFTrz** was treated as a predominantly electron transporting host and was combined with p-type BPBPCz (1 : 1 ratio) to develop an exciplex co-host system with improved charge balance in the EML. Green and red PhOLEDs had Ir(ppy)$_2$acac and Ir(mphmq)$_2$tmd emitters, respectively, at 5 wt% doping, with **SBFTrz**:BPBPCz:dopant as the EML. EQE_{max} values were 22.0 and 26.2%, λ_{max}^{EL} 523 nm, CIE(0.33, 0.63) and 610 nm, CIE(0.65, 0.35), and low efficiency roll-off up to 1000 cd m^{-2} (Fig. 6b and c). There was three- and five-fold enhancement in the operational lifetime of the exciplex-host green and red PhOLEDs, compared to the corresponding **SBFTrz** single-host devices.

Indolo[3,2,1-*jk*]carbazole derivatives **ICz-PPI** and **2ICz-PPI** (Fig. 7a) were studied as conventional fluorescent emitters and as hosts for PhOLEDs.[77] DFT studies indicated a small overlap between HOMO and LUMO with the ICz unit acting as the acceptor (Fig. 7b). **ICz-PPI** and **2ICz-PPI** are violet-blue emitters with λ_{max}^{PL} 398/414 nm in DCM and PLQYs of 72.5/63.9%, respectively. PL measurements in different polarity solvents suggested a weak ICT interaction. The emissions showed small red shifts (24 and 28 nm, respectively) in solid thin films, indicating that the π–π interactions in the solid state are suppressed by the twisted molecular structures. The T_1 energies were 2.48/2.80 eV (PL measurements). Introducing the additional ICz group (**2ICz-PPI**) significantly increased the T_1 energy and slightly decreased the PLQY. Non-doped blue-emitting OLEDs used **ICz-PPI** and **2ICz-PPI** as the EML. The **ICz-PPI** device had EQE_{max} 2.47%, CIE(0.153, 0.121), while the **2ICz-PPI** device had EQE_{max} 1.94%, CIE(0.161, 0.102). Based on data for hole-only and electron-only devices, **ICz-PPI** could be a better bipolar host material compared with **2ICz-PPI**.

ICz-PPI and **2ICz-PPI** were tested as hosts in green and red PhOLEDs, with host:Ir(ppy)$_3$ (8 wt%) or Ir(MDQ)$_2$acac (10 wt%) as the EMLs. The **ICz-PPI** devices were more efficient with CE_{max}/EQE_{max} 62.8 cd A^{-1} and 17.8% for Ir(ppy)$_3$, and 25.7 cd A^{-1} and 19.4% for Ir(MDQ)$_2$acac. The **ICz-PPI**:Ir(MDQ)$_2$acac device retained EQE of 14.9% at 10 000 cd m^{-2}. Furthermore, **ICz-PPI** served as both host and emitter in a warm-white OLED, CIE(0.427, 0.468) with EQE_{max} 14.4%, L_{max} 42 500 cd m^{-2}, through simultaneous emission from three layers in which Ir(MDQ)$_2$(acac), Ir(ppy)$_3$ and **ICz-PPI** were the red, green and blue components, respectively (Fig. 7c).

ICzPyr (Fig. 7a) is a host for the green TADF emitter 4CzIPN.[78] Theoretical calculations indicated that the HOMO was localised on the indolo[3,2,1-*jk*]carbazole unit while the LUMO was localised on the pyrimidine and peripheral phenyl units. The T_g of **ICzPyr** is 110 °C and $S_1/T_1/\Delta E_{ST}$ levels are 3.17/2.83/0.34 eV (PL data in solution). The PL spectrum of **ICzPyr** showed a very narrow FWHM of 22 nm. Green TADF-OLEDs with **ICzPyr**:4CzIPN (10 wt%) as the EML had EQE 10.0% at

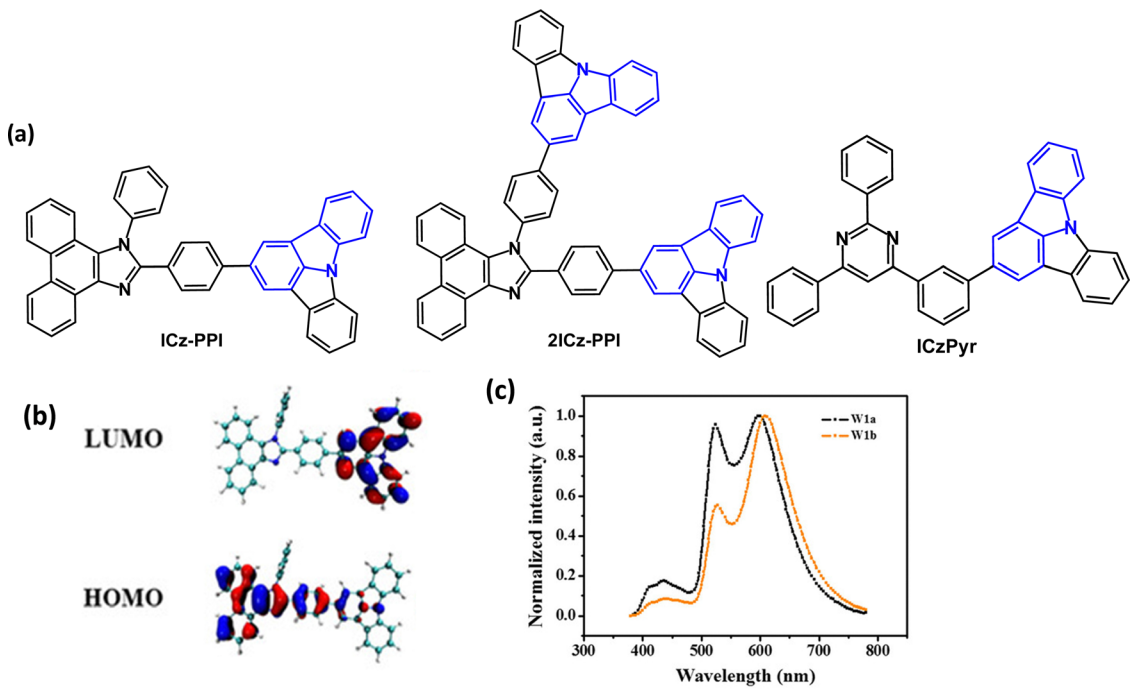

Fig. 7 (a) Molecular structures of **ICz-PPI**, **2ICz-PPI** and **ICzPyr**. (b) HOMO and LUMO plots for **ICz-PPI**.[77] (c) EL spectra of warm-white devices using Ir(MDQ)$_2$(acac), Ir(ppy)$_3$ and **ICz-PPI** in two different device configurations (W1a and W1b).[77] Copyright 2019 Wiley-VCH.

100 cd m^{-2} and 13.9% at 1000 cd m^{-2}. The device using **ICzPyr** showed a lower driving voltage, higher luminous efficiency, and a significantly longer lifetime of LT_{50} 5.5 h than using a conventional mCBP/4CzIPN emitter layer (LT_{50} 1.0 h) which was ascribed to the bipolar characteristics of **ICzPyr**.

Benzofuro- and benzothieno-carbazole derivatives **BFCz** and **BTCz** (Fig. 8) were designed as analogues of mCP.[50] The T_g of both compounds was significantly increased compared to mCP, to 147 °C (**BFCz**) and 157 °C (**BTCz**) due to the higher rigidity of the fused rings which had a positive effect on the film forming properties. The photophysical and device properties of **BFCz** and **BTCz** were very similar. The λ_{max}^{PL} was 365 and 362 nm, respectively (in solid polystyrene). The HOMO was distributed over the heteroaromatic core with the LUMO predominantly on the central phenylene ring, giving some bipolar character. The high T_1 energies of 2.94 and 2.93 eV enabled their use as hosts for sky-blue PhOLEDs with FIrpic guest emitter in the EML. The EQE_{max} values were 15.0 and 16.1%; the power efficiencies were 14.9 and 14.8 lm W^{-1}, respectively, with CIE(0.16, 0.37).

The isomeric benzothieno[3,2-*c*]carbazole (BTCz) derivatives **m1BTCBP** and **m4BTCBP** (Fig. 8a) were studied as host materials.[79] DFT calculations showed that the HOMO and LUMO were distributed on the phenylcarbazole units and biphenyl linkers, respectively. The π-expanded carbazole units provided deeper LUMO levels and shallower HOMO levels, compared to mCBP. Also, compared to mCBP, the BTCz group increased the bond dissociation energy (BDE) of the $C_{phenylene}$–N bond by 10% in the anionic state. The T_1 energies were calculated as 2.87 and 2.94 eV for **m1BTCBP**, and **m4BTCBP**, respectively. Thermal studies showed considerably higher T_g values (166–167 °C) compared to mCP. PhOLEDs using host:Ir(ppy)$_3$ emitter (12 wt%) as the EML, gave EQE_{max} > 20% and low turn-on voltages around 3.0 V at 1 cd m^{-2} and 4.0 V at 1000 cd m^{-2}. A comparable mCBP-based device had higher EQE_{max} (24%), but also higher efficiency roll-off (Fig. 8b). **m1BTCBP**:[Ir(ppy)$_3$] OLEDs exhibited LT_{50} 300 h at an initial luminance of *ca.* 12 000 cd m^{-2} (Fig. 8c). The LT_{50} at 1000 cd m^{-2} was estimated to be ≈ 23 000 h which was higher than that of mCBP-based OLEDs (LT_{50} ≈ 8500 h).

The lifetime improvement of green PhOLEDs with Ir(ppy)$_3$ emitter was demonstrated by using an exciplex host based on a mixture of a fused-ring pyrrolocarbazole hole transport component with a triazine type electron transport component.[80] The lifetime of the exciplex-host device to LT_{80} was ≈30 h which was >15 times longer than that of single-host devices.

4 Fused carbazole derivatives as TADF emitters

4.1 Indolocarbazole, indenocarbazole, benzofurocarbazole, benzothienocarbazole and pyrrolocarbazole derivatives

The rather weak electron donating ability of carbazole limits it use in TADF emitters. Alternative six-membered nitrogen heterocyclic donors such as phenothiazine, phenoxazine and 9,9-dimethyl-9,10-dihydroacridine have been successful, but their TADF efficiency can be complicated by different conformers in which the nitrogen lone pairs are oriented differently with respect to the acceptor.[81–83] Processes that decrease the efficiency of TADF emitters are concentration quenching and exciton annihilations, such as triplet–triplet annihilation (TTA), singlet–triplet annihilation (STA), and triplet–polaron annihilation (TPA).[84,85] Designs that combine two or more (non-fused) carbazole units,[86] or fused-ring carbazole units, have been widely exploited to impart increased donor strength and

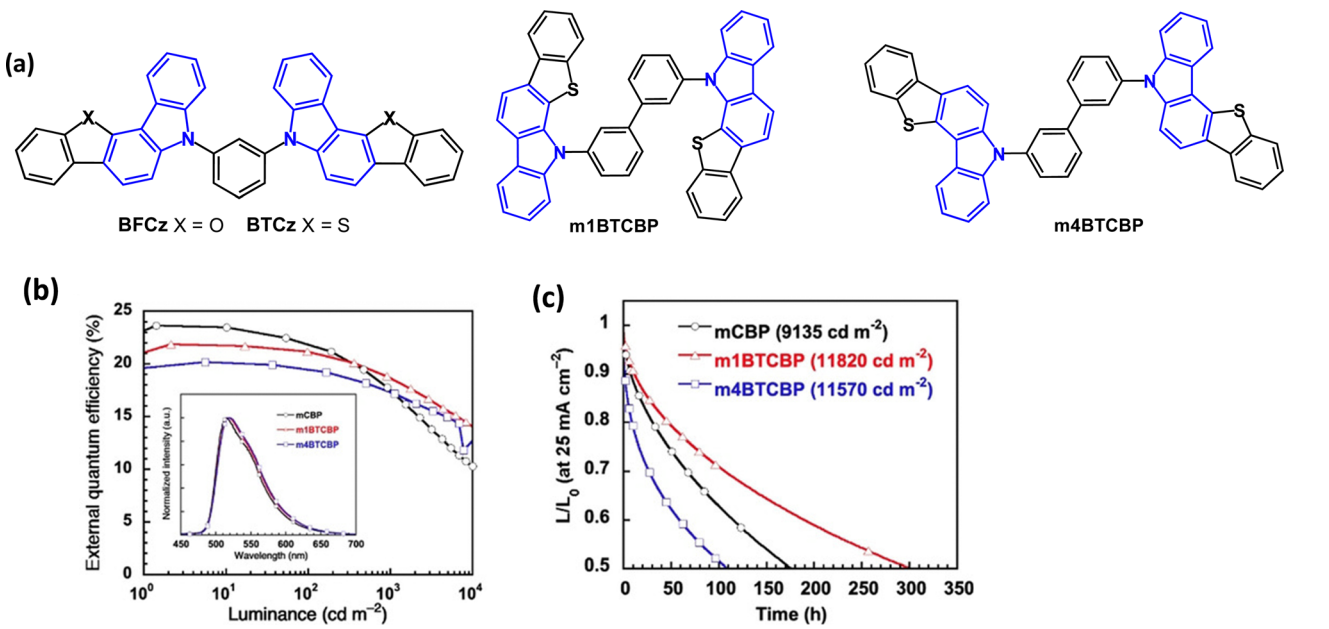

Fig. 8 (a) Molecular structures of **BFCz**, **BTCz**, **m1BTCBP** and **m4BTCBP**. (b) EQE–*L* characteristics.[79] (c) Operational lifetime at LT_{50} with Ir(ppy)$_3$ emitter.[79] Copyright 2021 Wiley-VCH.

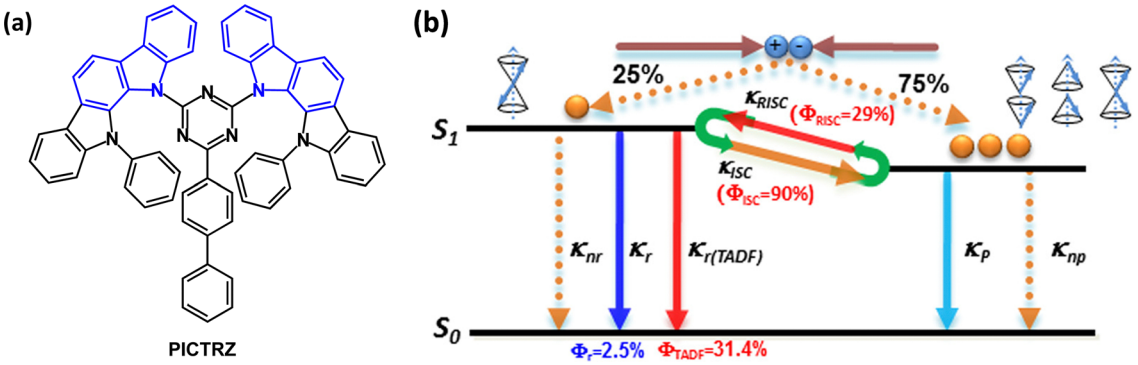

Fig. 9 (a) Molecular structure of **PICTRZ**. (b) A first approximation of the electroluminescence process involving TADF with efficient intersystem crossing from $T_1 \rightarrow S_1$.[39] Copyright 2011 The American Institute of Physics.

molecular rigidity, especially in very efficient green and blue TADF emitters. Fused-ring systems will now be considered.

Indolocarbazole derivatives are popular because of their ease of synthesis and systematic structural variation. Indeed, indolocarbazole has a special distinction as a component of the first all-organic TADF emitter **PICTRZ** used for OLEDs by Adachi's group in 2011 (Fig. 9a).[39] The two indolocarbazole units increase the steric hindrance between the D and A units of **PICTRZ** (compared to carbazole) leading to a well-separated HOMO and LUMO. The PL spectrum showed green emission with a large Stokes shift, indicating an efficient intramolecular charge transfer. $S_1/T_1/\Delta E_{ST}$ values were 2.66/2.55/0.11 eV for mCP:**PICTRZ** (6 wt%) film. The small ΔE_{ST} together with a high fluorescence radiative decay rate ($k_r \approx 10^7$) allowed the up-conversion from $T_1 \rightarrow S_1$ and efficient TADF (Fig. 9b). Transient decay times were $\tau_{PF} \approx 10$ ns and $\tau_{DF} \approx 230$ μs. The PLQYs for **PICTRZ** in non-degassed/degassed toluene solution were 10 ± 3%/35 ± 3%. The OLED with mCP host:**PICTRZ** (6 wt%) as the EML had EQE_{max} 5.3%. This landmark paper initiated a surge of interest in all-organic TADF-OLEDs.

The isomeric indolocarbazole–triazine D–A molecules **IndCzpTr-1** and **IndCzpTr-2** (Fig. 10) were reported in 2018.[58]

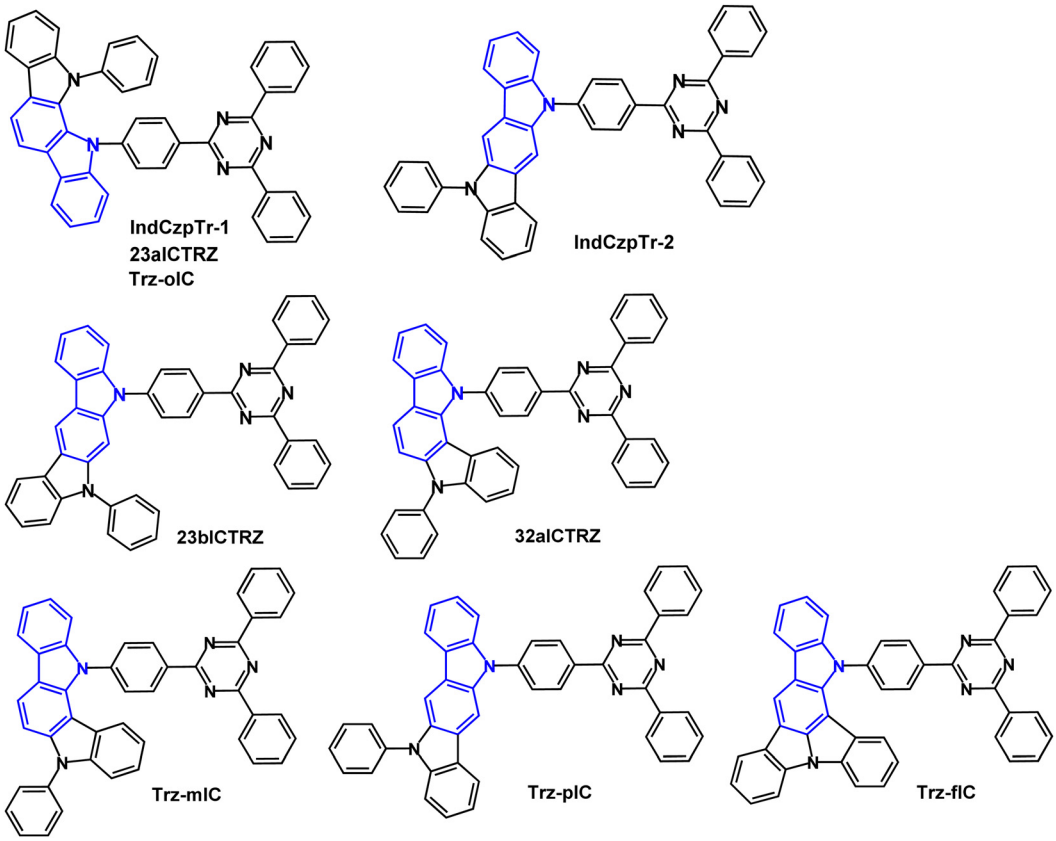

Fig. 10 Molecular structures of **IndCzpTr-1/23alCTRZ/Trz-olC**, **IndCzpTr-2**, **23blCTRZ**, **32alCTRZ**, **Trz-mlC**, **Trz-plC** and **Trz-flC**.

The calculated HOMO/LUMO values were −5.16/−1.91 and −4.92/−1.90 eV for **IndCzpTr-1** and **IndCzpTr-2**. The shallower HOMO of **IndCzpTr-2** indicates the stronger electron donating ability of indolo[3,2-*b*]carbazole compared to the [2,3-*a*] unit in **IndCzpTr-1**. λ_{max}^{PL} values were 480 and 490 nm (toluene solution); S_1/T_1/ΔE_{ST} values were 2.94/2.81/0.13 eV for **IndCzpTr-1** and 2.77/2.66/0.11 eV for **IndCzpTr-2** (PL measurements). PLQYs were >70% for **IndCzpTr-1** and **IndCzpTr-2** (mCBP doped films in air). OLEDs had an mCBP:emitter (10–20 wt%) EML. The **IndCzpTr-1** OLEDs exhibited EQE_{max} 14.5% with CE_{max} 28.1 cd A^{-1} (sky-blue emission) whereas **IndCzpTr-2** OLEDs had EQE_{max} 30.0% with CE_{max} of 82.6 cd A^{-1} (green emission) without any optical outcoupling technology. The high efficiency of the latter was explained by the more linear structure of **IndCzpTr-2** imparting a preferential horizontal dipole orientation which could enhance carrier mobility.

Another 2018 report on **IndCzpTr-1** (re-named as **23aICTRZ**), **23bICTRZ** and **32aICRTZ** (Fig. 10) focused on the importance of the phenylene group between the D and A units.[87] This work illustrates that well-separated HOMO/LUMO distributions are required to obtain a small ΔE_{ST}, although completely separated HOMO and LUMO leads to a relatively low radiative decay rate (k_r, usually 10^6 s^{-1}) according to Fermi's golden rule.[87,88] The enlarged separation between D and A increases the dipole moment change in the charge-transfer (CT) transition[89] and also controls the dihedral angle between D and A to modulate the FMO distributions. As a result, the compounds with a phenylene bridge have the potential to achieve high k_r and small ΔE_{ST} simultaneously. The analogue PIC-TRZ2, without a phenylene spacer, showed completely separated HOMO/LUMO distributions[88] whereas the FMOs of **23aICTRZ**, **23bICTRZ** and **32aICTRZ** showed some overlap resulting in higher oscillator strengths (*f*) of 0.123, 0.161, and 0.025, respectively, compared to PIC-TRZ2 (f 0.0012). T_g values were in the range 155–159 °C; T_1 energies were 2.69, 2.70 and 2.80 eV (PL in toluene) for **23aICTRZ**, **23bICTRZ**, and **32aICTRZ**, respectively, giving ΔE_{ST} values of 0.25, 0.27, and 0.15 eV. The lower T_1 value of the first two compounds indicates a stronger interaction between D and A, compared to **32aICTRZ**. Significant DF emission was observed for **32aICTRZ** (consistent with the smaller ΔE_{ST}) while DF was negligible for the other derivatives. The k_r values were very high, around 10^8 s^{-1}, compared to *ca.* 10^5 s^{-1} for PIC-TRZ2[88] which was attributed to the favoured FMO distributions of **23aICTRZ**, **23bICTRZ** and **32aICTRZ**. TADF-OLEDs with DPEPO host: **32aICTRZ** (10 wt%) EML exhibited EQE_{max} 25.1% and 21.5% at 5000 cd m^{-2} with λ_{max}^{EL} 512 nm. The devices based on **23aICTRZ** and **23bICTRZ** had much lower EQE_{max} 13.6% and 9.8%, respectively, with significant efficiency roll-off. Additionally, by utilising **32aICTRZ** as the host for green TADF-OLEDs with DACT-II as the emitter (15 wt%) impressively high EQE/PE of 26.2%/69.7 lm W^{-1} at a brightness of 5000 cd m^{-2} was obtained.

The TADF properties of the isomeric indolocarbazole derivatives **IndCzpTr-1** (re-named as **Trz-oIC**), **Trz-mIC** and **Trz-pIC**, and the fused ring analogue **Trz-fIC**, (Fig. 10) were subsequently reported.[90] The absorption spectrum of **Trz-pIC** was red-shifted compared to other isomers, because of a stronger ICT interaction. The non-fused carbazole analogue (PhCzTrz) had decreased donor strength and reduced ICT.[91] ΔE_{ST} increased in the sequence **Trz-mIC** (0.13 eV) < **Trz-oIC** (0.16 eV) < **Trz-pIC** (0.29 eV) < **Trz-fIC** (0.45 eV). The PLQY (DBFPO doped films) was highest for **Trz-mIC** (90%), which also showed the highest DF : PF component ratio (62 : 28) in the series. K_{RISC} rates in the series were in the range 4.03–11.90 × 10^{-5} s^{-1}. OLEDs with a DBFPO host:emitter (20 wt%) EML had EQE_{max} that increased in the order **Trz-fIC** (10.6%) < **Trz-oIC** (23.2%) < **Trz-pIC**

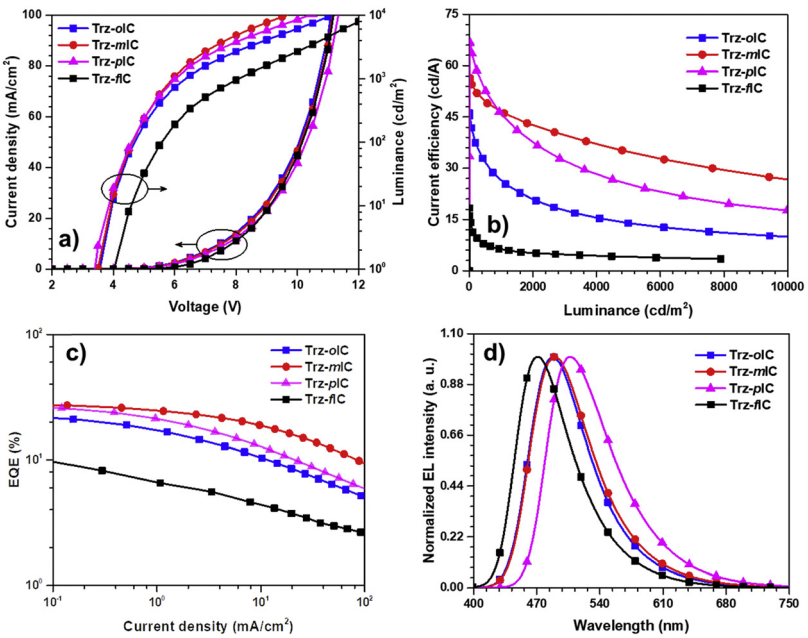

Fig. 11 Electroluminescence properties: (a) *J*–*V*–*L* plot; (b) current efficiency; (c) EQE and (d) EL spectra of **Trz-oIC**, **Trz-mIC**, **Trz-pIC** and **Trz-fIC**.[90] Copyright 2019 Elsevier.

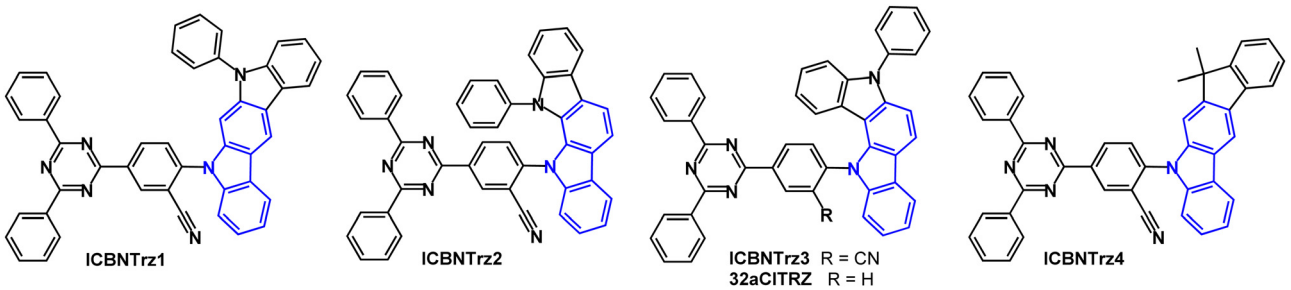

Fig. 12 Molecular structures of **ICBNTrz1**, **ICBNTrz2**, **ICBNTrz3**, **32aCITRZ** and **ICBNTrz4**.

(26.8%) < **Trz-mIC** (28.0%) with maximum current efficiencies of 18.4, 46.1, 66.8 and 56.5 cd A^{-1}, respectively. The devices showed sky-blue to green emission with λ_{max}^{EL} 470–507 nm and FWHM 75–85 nm (Fig. 11).

A series of green indolo- and indeno-carbazole TADF emitters reported in 2022 have diphenyltriazine as the main acceptor group and benzonitrile as a secondary acceptor which served to increase the bond dissociation energy (BDE) and the k_{RISC} for TADF emission (Fig. 12).[92] Compared to the non-CN analogue (**32aCITRZ**), **ICBNTrz3** has a much smaller ΔE_{ST} because the CN group stabilises the CT singlet state. **ICBNTrz3** was the most successful emitter of the series with PLQY 85% (5 wt% doped film in CzTrz), k_{RISC} 3.15 × 10^5 s^{-1}, ΔE_{ST} 0.04 eV (1 wt% doped film in polystyrene). Devices had CzTrz host:emitter (20 wt%) as the EML. The EQE_{max} of **ICBNTrz3** devices was 18.5%. The device lifetime was extended by more than 20 times compared to the **32aCITRZ** devices. The **ICBNTrz3** device had LT_{90} = 532 h at 1000 cd m^{-2} which is among the longest lifetimes achieved to date in green TADF OLEDs. The long lifetime correlates with the high k_{RISC} which reduces triplet exciton density.

The indolo[2,3-*a*]carbazole D–A emitters **ICz-DPS** and **ICz-BP** with sulfonyl and carbonyl units in the acceptor unit (Fig. 13) show both TADF and aggregation induced emission (AIE) properties.[93] AIE can be beneficial in OLEDs as some non-doped devices can show high efficiencies.[94–96] Large dihedral angles (>70°) between the D–A groups prevent intermolecular π–π stacking and the phenylene spacer between the D–A units interrupts the HOMO–LUMO spatial overlap. ΔE_{ST} was reduced from 0.21 eV (**ICz-DPS**) to 0.10 eV (**ICz-BP**): the deeper LUMO level of **ICz-BP** reflects the stronger electron-accepting ability of BP. **ICz-DPS** and **ICz-BP** have λ_{max}^{PL} 438 nm and 481 nm; PLQY 53% and 62%; k_{RISC} 30.5 and 39.7 × 10^5 s^{-1} (neat film). The excited state lifetimes were: **ICz-DPS** τ_{PF} = 22.7 ns, τ_{DF} = 616 ns; **ICz-BP** τ_{PF} = 21.1 ns, τ_{DF} = 448 ns (10 wt% films in DPEPO). OLEDs with a DPEPO host:emitter (10 w%) EML had λ_{max}^{EL} 435 nm (0.15, 0.08) and 475 nm (0.17, 0.28) with EQE_{max}/CE_{max} of 11.6%/30.1 cd A^{-1} and 17.7%/44.8 cd A^{-1} for the **ICz-DPS** and **ICz-BP** devices, respectively. Non-doped OLEDs based on **ICz-DPS** had efficiencies of 11.7% and 30.1 cd A^{-1}. The deep blue emission of **ICz-DPS** is notable.

The TADF emitter **PrCzPTrz** (Fig. 14) contains an unusual pyrrolocarbazole donor.[97] Fusion of the pyrrole unit increased the donor character compared to the parent carbazole, as indicated by the shallower calculated HOMO energy of PrCz. The PLQYs for **PrCzPTrz** were 0.13/0.80 under oxygen/nitrogen with ΔE_{ST} 0.03 eV (toluene solution) and τ_{DF} 15.8 μs. OLEDs with mCP host:**PrCzPTrz** (10–50 wt%) EML had EQE_{max} 17.7% with green emission, CIE(0.26, 0.47). The EQE was much higher than for a comparable device with a non-fused carbazole donor (EQE_{max} 4%) although lower than the dimethylacridine analogue DMAC-TRZ using an alternative device structure (EQE_{max} 26.5%).[98] The LT_{50} of the **PrCzPTrz** device (≈0.7 h) was improved compared to the DMAC analogue (<0.1 h).

A series of indolocarbazole derivatives with additional heterocyclic functionality in the bridge or in the acceptor has been reported. **IDCzTrzDBF** (Fig. 15) has dibenzofuran as a linker chosen for its rigidity, steric effect and high stability.[99] The HOMO and LUMO were largely separated with a small overlap on dibenzofuran. Theoretical calculations revealed a dihedral angle of 77° between the D and A units. $S_1/T_1/\Delta E_{ST}$ levels were 2.92/2.87/0.05 eV (PL, toluene solution). The PLQY under air/nitrogen was 77.3/85.4% (5 wt% doped in mCBPTrz). The transient PL decay showed τ_{DF} 2.8 μs. Green TADF-OLEDs with mCBPTrz host:**IDCzTrzDBF** (5 wt%) EML had EQE_{max} 12.2%,

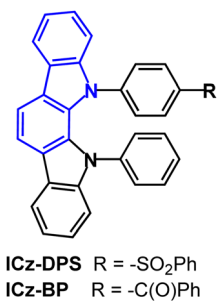

Fig. 13 Molecular structures of **ICz-DPS** and **ICz-BP**.

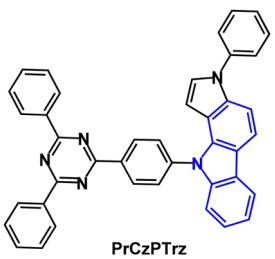

Fig. 14 Molecular structure of **PrCzPTrz**.

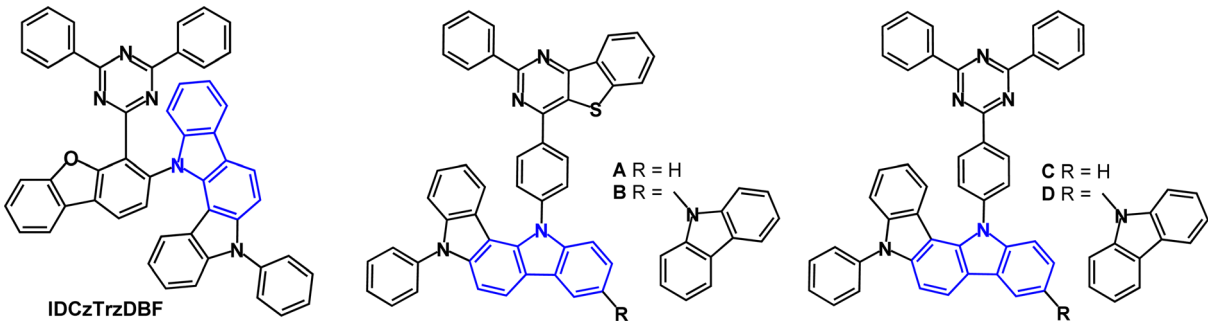

Fig. 15 Molecular structures of **IDCzTrzDBF** and **A–D**.

which was lower than analogues with di or tri(carbazole) instead of IDCz (EQE > 20%). The relatively low EQE_{max} of **IDCzTrzDBF**, despite its high PLQY, was attributed to the poor carrier balance in the EML as shown in the hole- and electron-only device measurements. The LT_{85} of the **IDCzTrzDBF** devices at an initial luminance (L_0) of 3000 cd m^{-2} was 56.9 h; the distorted structure of the molecule reduces the device lifetime compared to carbazole analogues.

Blue/sky-blue emitters **A–D** (Fig. 15) include two with the unusual thienopyrimidine acceptor (**A**, **B**) instead of triazine (**C**, **D**).[100] The calculated triplet energies were between 2.55 and 2.67 eV. PLQY measurements (toluene solution) indicated that **C** and **D** had slightly higher values (≈0.8) than **A** and **B** (≈0.7). The τ_{DF} values were 71.9, 108.6, 6.2 and 6.1 μs for **A** to **D**, respectively. Predictably, hole-only devices of **B** and **D** exhibited higher current densities than those of **A** and **C** due to the improved hole-transporting ability from the extra carbazole unit of **B** and **D**. Electron-only devices indicated that TRZ (in **C** and **D**) is a more efficient electron transport unit than thienopyrimidine (in **A** and **B**). OLEDs had a DPEPO host:emitter (15 wt%) EML. The EQE_{max} values for the **C** and **D** devices were slightly higher (21.4% and 22.3%) than the **A** and **B** devices (EQE_{max} 17.8% and 19.0%). Devices **A** and **B** showed high efficiency roll-off at 500 cd m^{-2}. λ_{max}^{EL} values were 492, 475, 484 and 475 nm for **A–D**, respectively. The higher EQE_{max} and lower efficiency roll-off of the **C** and **D** devices were attributed to the higher PLQY, smaller ΔE_{ST} and shorter exciton lifetimes of **C** and **D** compared with **A** and **B**. In summary, thienopyrimidine was less efficient than triazine in this series.

Indolo[2,3-*b*]carbazole TADF emitters **BBCz-*o*-TRZ** and **BBCz-*o*-2TRZ** feature an *o*-phenylene bridge between D and A units (Fig. 16).[101] PLQY values were 0.46/0.41 in toluene and 0.83/0.86 for 10 wt%-doped PYD2 films. $S_1/T_1/\Delta E_{ST}$ energies

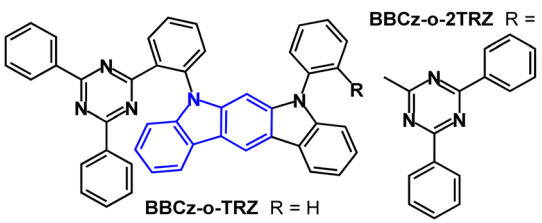

Fig. 16 Molecular structures of **BBCz-*o*-TRZ** and **BBCz-*o*-2TRZ**.

were 2.89/2.7/0.17 eV and 2.85/2.73/0.12 eV, respectively (PL in toluene). TADF components were observed with τ_{DF} 7.2/4.8 μs in the doped films. OLEDs with PYD2 host:emitter (30 wt%) as the EML gave bluish-green EL with EQE_{max} 15.3% and 16.6% for **BBCz-*o*-TRZ** and **BBCz-*o*-2TRZ** devices, which was comparable to analogous carbazole derivatives. The EQE roll-off was higher for the indolocarbazole devices than for the carbazole analogues. The half-life (LT_{50}) for **BBCz-*o*-TRZ** and **BBCz-*o*-2TRZ** devices was 345 h and 262 h, respectively, at an initial luminance (L_0) of 1000 cd m^{-2}. These data show that in this case increasing the number of acceptors in the emitter reduces the stability of the device, although it improves the balance between hole and electron transfer in the EML.

The A–D–A TADF emitter **ICzTRZ** (Fig. 17) had λ_{max}^{PL} 462 nm (toluene solution), 479 nm (5 wt% doped in mCBP) and 470 nm (10 wt% doped in PMMA).[102] $S_1/T_1/\Delta E_{ST}$ levels were 2.85/2.62/0.23 eV (5 wt% in mCBP); PLQY under air/N_2 was 59/70%. Devices with mCBP host:**ICzTRZ** (5 wt%) EML gave sky-blue emission with λ_{max}^{EL} 483 nm, CIE(0.17, 0.32), EQE_{max} 22.1% at 16 cd m^{-2}, EQE_{100} 17.3% and L_{max} 7805 cd m^{-2}. Simulations demonstrated that for a PLQY of 70% if the molecules were randomly orientated in the film the device EQE would be ≈15%. Therefore, it was inferred that there is strong horizontal orientation of the emitter molecules in the device, in line with polarization- and angle-dependent PL thin film experiments in DPEPO, mCP and mCBP hosts, leading to enhanced light outcoupling and higher EQE in the OLEDs.

The bis(indolocarbazole) twin $(A–D–A)_2$ TADF emitter **DICzTRZ** (Fig. 17) was subsequently reported.[103] The PLQY of **DICzTRZ** was 60% in degassed toluene and 44% after exposure to oxygen. $S_1/T_1/\Delta E_{ST}$ values were 2.80/2.59/0.21 eV (PL data). λ_{max}^{PL} in (9-(4-*t*-butylphenyl)-3,6-bis(triphenylsilyl)-9*H*-carbazole) (CzSi) host (30 wt% doping) was 488 nm, and only slightly red-shifted compared to that in toluene, and PLQY was 57%. The τ_{DF} values were 156.1 and 69.49 μs with ΔE_{ST} 0.03 and 0.19 eV for the doped films in PMMA and CzSi, respectively. OLEDs with a solution-deposited EML of CzSi host:**DICzTRZ** (20 wt%) had EQE_{max} 8.4%, λ_{max}^{EL} 494 nm; CIE(0.22, 0.47). The device efficiency of **DICzTRZ** was lower compared to the non-twin derivative **ICzTRZ** (EQE_{max} = 11.6%; λ_{max}^{EL} 485 nm; CIE(0.19, 0.37), solution deposited EML)[103] which was attributed to the lower PLQY and unfavourable vertical orientation of the transition dipole moment of **DICzTRZ** in the EML.

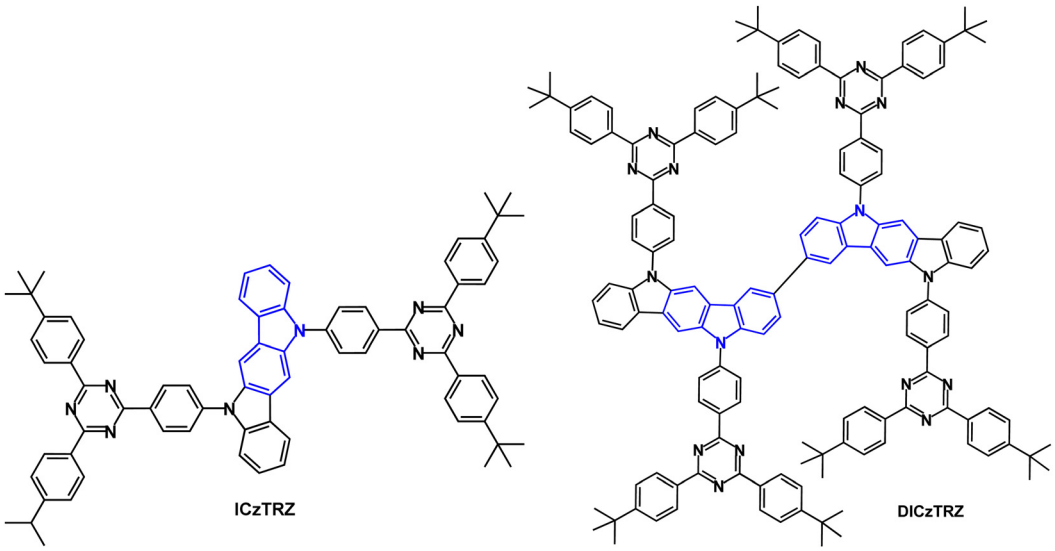

Fig. 17 Molecular structures of **ICzTRZ** and **DICzTRZ**.

Triarylboron derivatives have been widely used as acceptor groups in TADF emitters.[104–112] The vacant p orbital on boron imparts the electron accepting properties. For example, **TDBA-TPDICz** (Fig. 18a) has λ_{max}^{PL} 447 nm and ΔE_{ST} 0.41 eV (in toluene solution); ΔE_{ST} 0.29 eV in DBFPO host.[56] OLEDs with DBFPO:**TDBA-TPDICz** (20 wt%) as the EML gave EQE_{max} 16.9%, λ_{max}^{EL} 462 nm, CIE(0.14, 0.14). The results showed that the weaker cyclic boron acceptor significantly blue shifted the emission compared to a triazine analogue [λ_{max}^{EL} 509 nm, CIE(0.25, 0.53)].

Indolo[3,2-*a*]carbazole derivatives **BO-tCzPhICz** and **BOtCz-DICz** (Fig. 18a) with the same multi-resonance boron-based acceptor are deep-blue TADF emitters.[111] **BO-tCzPhICz** has a larger dihedral angle (68.3 *vs.* 59.8°) and smaller ΔE_{ST} (76.6 *vs.* 153 meV, film state) compared to **BO-tCzDICz**. Both compounds showed TADF with $\lambda_{max}^{PL} \approx 450$ nm (thin film), FWHM ≈ 50 nm and τ_{DF} 0.22–0.23 μs. OLEDs had a solution processed mCP host:emitter EML. The smaller ΔE_{ST}, faster RISC rate (34.4×10^5 *vs.* 20.9×10^5 s^{-1}) and higher PLQY (92.7 *vs.* 77.3%, film) of **BO-tCzPhICz** resulted in a higher EQE_{max} of 17.8% *vs.* 14.8% for **BOtCzDICz**. The devices have among the best EL performance for solution-processed deep-blue TADF-OLEDs with $CIE_y < 0.1$ and close to the National Television System Committee (NTSC)

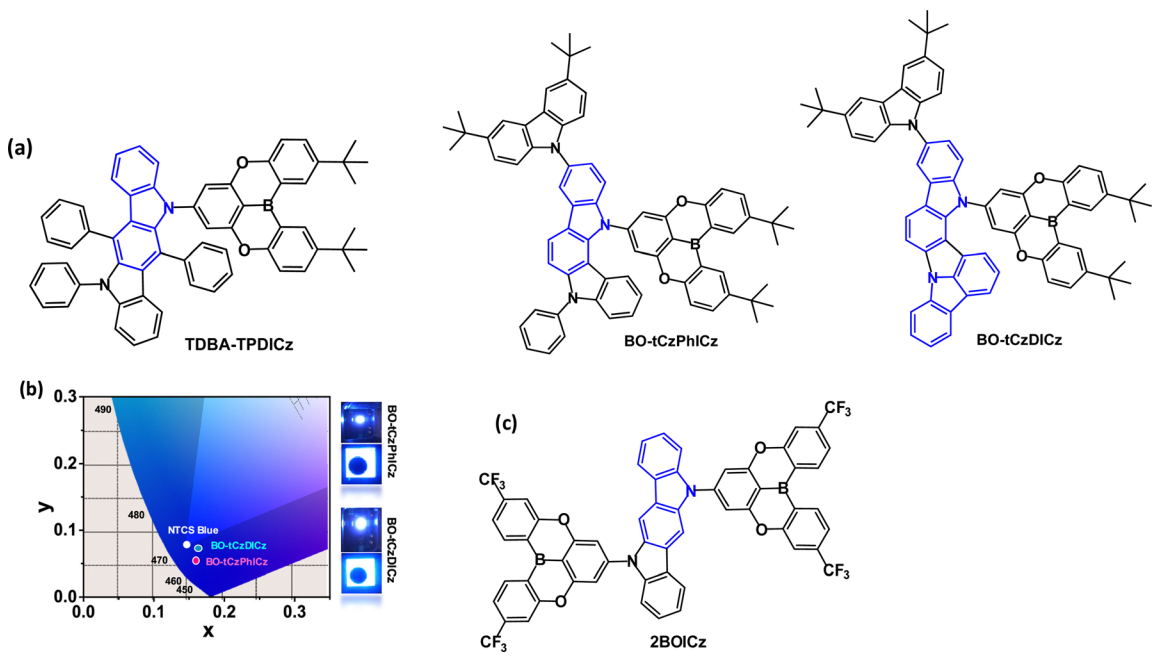

Fig. 18 (a) Molecular structures of **TPDA-TPDICz**, **BO-tCzPhICz** and **BOtCzDICz**. (b) CIE diagram and images of EL of devices of **BO-tCzPhICz** and **BOtCzDICz**.[111] Copyright 2021 The American Chemical Society. (c) Molecular structure of **2BOICz**.

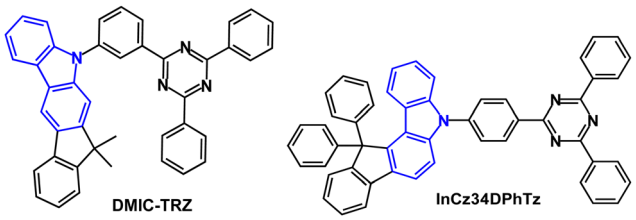

Fig. 19 Molecular structures of **DMIC-TRZ** and **InCz34DPhTz**.

standard blue (0.14, 0.08) (Fig. 18b). A narrow FWHM of 56 nm was retained in the **BO-tCzPhICz** device.

Two equivalent acceptors functionalised with CF_3 substituents have been attached to a sterically-uncrowded indolo[3,2-*b*]carbazole core to afford the A–D–A molecule **2BOICz** (Fig. 18c) as a fluorescent emitter with hybrid long- and short-range CT excitations.[113] The well-balanced rate constants of $k_r \gg k_{ISC} \approx k_{RISC} > 10^6\ s^{-1}$ lead to a short τ_{DF} of $\approx$ 0.88 μs. The quasi-planar structure of **2BOICz** gives a favoured dipole orientation for a large outcoupling efficiency. The OLEDs with mBPBC host:**2BOICz** (20 wt%) had green emission with EQE_{max} 40.4%. The LT_{50} of the device was $\approx$ 300 h at L_0 5000 cd m^{-2}.

Studies have addressed indenocarbazole donors as components of TADF emitters. For example, in 2017 it was reported that **DMIC-TRZ** (Fig. 19) had λ_{max}^{PL} was 466 nm (toluene solution) with ΔE_{ST} 0.14 eV (PL measurements).[114] The PL decay curve showed prompt and delayed components, and k_{RISC} was calculated to be $1.8 \times 10^5\ s^{-1}$. An OLED based on pure **DMIC-TRZ** film as the EML showed a low EQE_{max} of 1.93%. **DMIC-TRZ** was more successful as a host with sky-blue (5TCzBN), green (DMAC-BP) and orange (4TCzTPN) guest TADF emitters. The PLQYs of the doped films (6 wt% emitter) were $\approx$70% with τ_{DF} of 1.84, 2.67, and 4.07 μs for 5TCzBN, DMAC-BP, and 4TCzTPN, respectively. The sky-blue and green TADF devices had EQE_{max} values of 19.2% and 21.0%, respectively. Both devices showed small efficiency roll-offs: EQEs were 18.0% at 2000 cd m^{-2} and 14.2% at 5000 cd m^{-2} for 5TCzBN, and comparably 19.5% and 14.2% for DMAC-BP. Furthermore, the orange 4TCzTPN host: **DMIC-TRZ** OLEDs achieved EQE_{max} of 23.2%, (18.9% at 5000 cd m^{-2}) which was higher that a reference device with CBP host (EQE_{max} 15.4%). These data demonstrated the benefits of more balanced charge injection into **DMIC-TRZ** with similar hole and electron carrier mobilities within the EML, leading to a wide recombination zone and suppressed exciton annihilation rates in the **DMIC-TRZ**-guest EMLs.

A series of indenocarbazole-triazine blue TADF emitters were reported in 2019 of which **InCz34DPhTz** (Fig. 19) is the most noteworthy.[115] $S_1/T_1/\Delta E_{ST}$ levels were 2.90/2.79/0.11 eV. PL data indicated only a small TADF contribution due to a slow k_{RISC} ($1.6 \times 10^4\ s^{-1}$). TADF was confirmed by a linear dependence of DF with excitation power and slope $\approx$1, signifying a unimolecular process. The PLQY was 97.9% (doped in DPEPO film). TADF OLEDs with a DPEPO host:**InCz34DPhTz** (10 wt%) EML had EQE_{max} 25.9% although with extensive roll-off to 14.2% at 100 cd m^{-2}; λ_{max}^{EL} 472 nm; CIE(0.15, 0.24).

Benzofurocarbazole and benzothienocarbazole donors have been incorporated into TADF emitters, notably by J.-Y. Lee's group. Two established ways to increase k_{RISC} are: (i) to reduce ΔE_{ST}[116,117] and (ii) to enhance the SOC between S and T states of a TADF molecule. Introducing heteroatoms such as S, N or O into a TADF molecule can benefit the SOC and k_{RISC}.[118–123] For example, the blue TADF emitters **BFCz-2CN** and **BTCz-2CN** (Fig. 20)[124] both have E_T 2.46 eV (frozen THF), leading to ΔE_{ST} values 0.17 and 0.13 eV, respectively. PLQY values were $\approx$94% (mCP doped films), which is higher than the non-fused carbazole analogue 2CzPN.[125] Transient PL decay curves for

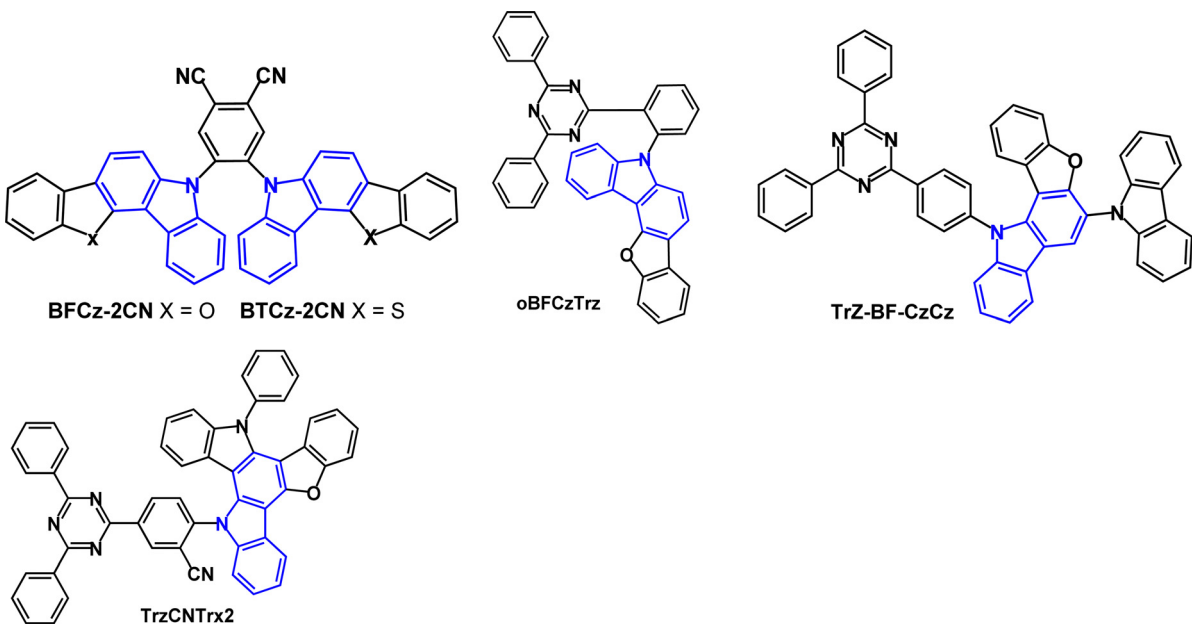

Fig. 20 Molecular structures of **BFCz-2CN**, **BTCz-2CN**, **oBFCzTrz**, **Trz-BF-CzCz** and **TrzCNTrx2**.

BFCz-2CN and **BTCz-2CN** indicated prompt and delayed emissions with τ_{DF} 2.60 and τ_{DF} 1.98 μs, which are shorter than 2CzPN (τ_{DF} 166 μs) because of the restricted molecular motion of the fused carbazole derivatives. OLEDs with an EML of mCP host:**BFCz-2CN** or **BTCz-2CN** (1 wt%) had λ_{max}^{EL} 486, FWHM 73 nm, $EQE_{max} \approx 12\%$ for both emitters, compared with 5% for 2CzPN.

Benzofuro[3,2-*c*]carbazole donor and triazine acceptor have been linked *via* an *o*-phenylene bridge in the emitter **oBFCzTrz** (Fig. 20).[126] **oBFCzTrz** has a very small experimental ΔE_{ST} value of 0.002 eV (compared to 0.191 and 0.302 eV for the *meta*- and *para*-phenylene isomers), τ_{DF} 5.4 μs and PLQY of 97.9% (under nitrogen). OLEDs with a DPEPO:**oBFCzTrz** (20 wt%) EML had EQE of 20.0% and 17.7% at 100 and 1000 cd m^{-2}, respectively with sky-blue emission and CIE(0.18, 0.31). Device lifetime studies gave LT_{95} of ≈3 h at a fixed current density of 5 mA cm^{-2}. Subsequently, different workers reported that OLEDs with a DPEPO host:**oBFCzTrz** (50 wt%) EML had EQE_{max} 25.5%, and a neat **oBFCzTrz** EML had EQE_{max} 14.0%.[127] Inspired by these results, a theoretical study suggested that *o*-linked D–A molecules may be an efficient design strategy for TADF emitters free of concentration quenching effects.[128]

The related benzofuro[3,2-*a*]carbazole derivative **Trz-BF-CzCz** (Fig. 20) had k_{RISC} 6.37 × 10^4 s^{-1} (doped film in DPEPO host) and gave OLEDs with EQE_{max} 23.3% and CIE(0.18, 0.32) using 20 wt% doping in DPEPO as the EML.[129]

TrzCNTrx2 (Fig. 20) was designed with enhanced donor rigidity to favour a faster RISC process.[130] The HOMO was mainly located on the Trx donor unit whereas the LUMO was on the diphenyltriazine acceptor and benzonitrile linker, with slight HOMO–LUMO overlap inside the donor unit. $S_1/T_1/\Delta E_{ST}$ levels were 2.83/2.75/0.08 eV (PL spectra in THF); PLQY 91% (doped film in CzTrz host) and k_{RISC} was raised to 5.13 × 10^5 s^{-1}. Green emitting OLEDs with an EML of CzTrz:**TrzCNTrx2** (5 wt%) had EQE_{max} 20.6% and CIE(0.30, 0.55) with very low roll-off to EQE 20.2% at 3000 cd m^{-2}. The devices had a lifetime up to 90% of initial luminance (LT_{90}) at 3000 cd m^{-2} of 141 h.

pBFCz-26DPPM and **pBTCz-26DPPM** (Fig. 21) are deep-blue TADF emitters based on benzofuro- and benzothieno-carbazole.[131] The HOMOs are localised on the BFCz and BTCz donors, while the LUMOs are predominantly on the 4,6-diphenylpyrimidine acceptor with some overlap on the phenylene bridge. The $S_1/T_1/\Delta E_{ST}$ values were 2.97/2.70/0.27 eV for **pBFCz-26DPPM** and 3.06/2.72/0.34 eV for **pBTCz-26DPPM**. The PLQYs were 71/75% for 10% doped films in DPEPO and 38/42% for the neat films for **pBFCz-26DPPM** and **pBTCz-26DPPM**, respectively. Transient PL data including temperature dependence indicated TADF emission for both compounds (10 wt% doped in DPEPO). OLEDs with DPEPO host:emitter (10 wt%) EML had low EQE_{max} 6.20, CIE(0.154, 0.054) and 5.36%, CIE(0.154, 0.052) for **pBFCz-26DPPM** and **pBTCz-26DPPM**, respectively.

The D–A–D bis(benzofurocarbazole) and bis(benzothienocarbazole) derivatives with a 2,5-pyrazine linkage were subsequently studied as blue TADF emitters (Fig. 21).[132] λ_{max}^{PL} values were 415 (**BFCZPZ1**), 444 (**BFCZPZ2**, **BFCZPZ3** and **BTCZPZ2**) and 456 nm (**BTCZPZ1**) (toluene solution) demonstrating a 41 nm red shift upon changing benzofuran to benzothiophene (**BFCZPZ1** to **BTCZPZ1**). The FWHMs were in the range 51–73 nm, which is narrower than a non-fused carbazole analogue (76 nm). **BTCZPZ1** had the highest SOCME 0.980 cm^{-1}, lowest ΔE_{ST} (0.24 eV, doped film in PPT host) and highest k_{RISC} (8.5 × 10^4 s^{-1}) of the five compounds. Devices with a PPT host:emitter (7 wt%) EML had EQE_{max} 21.1%, CIE(0.16, 0.17) for **BTCZPZ1** and EQE_{max} 21.3%, CIE(0.15, 0.10) for **BFCZPZ2** as the highest efficiencies in the series. The LT_{50} of the **BTCZPZ1** device (5.0 h) was the highest in the series.

Efficient hyperfluorescent OLEDs constitute a high E_T host co-doped with a TADF material and the final emitter. A fast

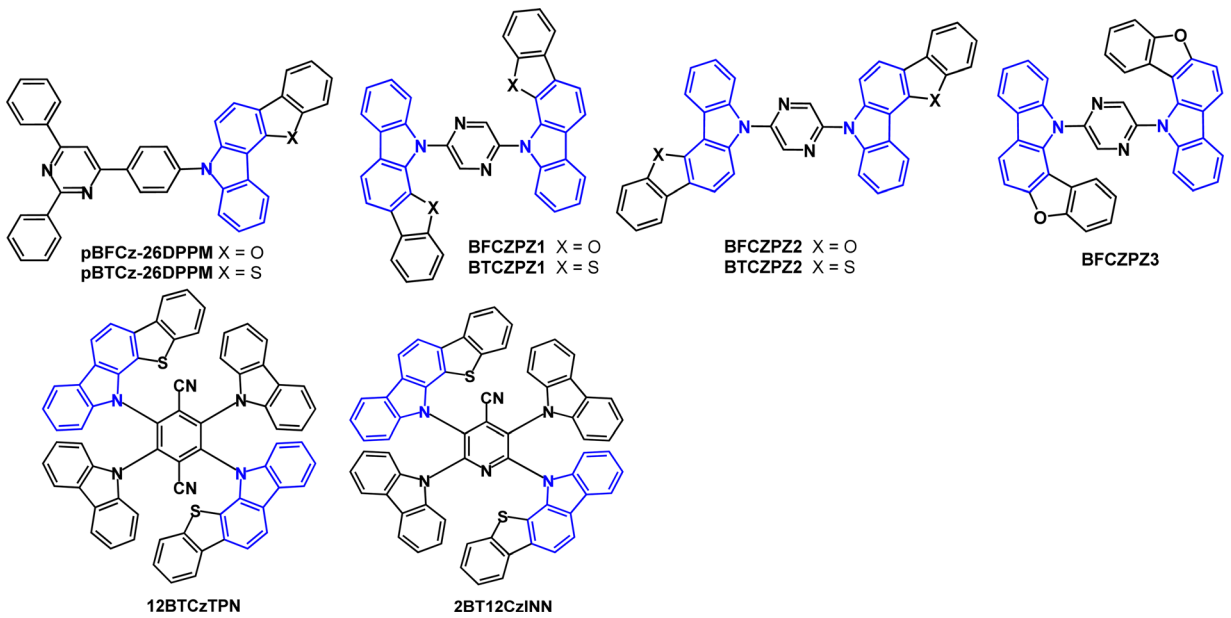

Fig. 21 Molecular structures of **pBFCz-26DPPM**, **pBTCz-26DPPM**, **BFCZPZ1**, **BTCZPZ1**, **BFCZPZ2**, **BTCZPZ2**, **BFCZPZ3**, **12BTCzTPN** and **2BT12CzINN**.

Förster resonance energy transfer (FRET) from the S_1 excited state of the TADF material to S_1 of the fluorescent emitter is needed to activate the hyperfluorescence. **12BTCzTPN** (Fig. 21)[133] has increased k_{RISC} of 3.67×10^6 s^{-1} due to the heavy atom effect of the two sulfur atoms compared to 4CzTPN (k_{RISC} 0.80×10^6 s^{-1}). **12BTCzTPN** served as the assistant dopant in a red hyperfluorescent device with 4*t*BuMB as the fluorescent emitter giving EQE_{max} 19.9% and CIE(0.64, 0.36). The pyridyl analogue **2BT12CzINN** (Fig. 21) has k_{RISC} of 10.9×10^5 s^{-1}. With the polycyclic aromatic hydrocarbon DBP as the fluorescent emitter hyperfluorescent **2BT12CzINN**:DBP devices in a PBICT:DBTTP1 host had EQE_{max} 14.7% and CIE(0.60, 0.39).[134] The EQE and the lifetime LT_{90} of 41.8 h at L_0 3000 cd m^{-2} were improved compared to a reference 4CzTPN:DBP device (EQE_{max} 11.3%; LT_{90} 27.8 h).

Benzofuro[3,2-*c*]carbazole and indeno[2,1-*b*]carbazole have been combined with an oxygen-bridged triarylboron acceptor to give D_2–π–A emitters **BBFCz** and **BICz** (Fig. 22; compare with Fig. 18a).[112] The structures are highly twisted with the HOMO and LUMO mainly distributed on the *ortho*-, *para*-substituted donors and the boron acceptor, respectively, and slightly extended to the adjacent phenylene core. PL data showed that **BBFCz** and **BICz** have very high T_1 values of 2.97 and 3.07 eV (toluene solution), ΔE_{ST} values of 0.26 and 0.15 eV leading to TADF, confirmed by temperature dependent studies. In contrast, the non-fused carbazole derivative (**BCz**) had ΔE_{ST} 0.40 eV and showed only conventional fluorescence. The electron donating ability increased in the order of **BCz** < **BBFCz** < **BICz**. The PLQYs were much higher in films than in solution, which was ascribed to AIE effects. Devices with a solution-processed neat EML gave deep-blue emission with λ_{max}^{EL} 412, 416 and 424 nm and CIE(0.18, 0.10), (0.17, 0.07) and (0.16, 0.08) and FWHM of 33, 42 and 61 nm, for **BCz**, **BBFCz** and **BICz** respectively. **BICz**, having the stronger donor and smaller ΔE_{ST}, gave the highest EQE_{max} of 10.1% in the series.

Blue/deep-blue emitters using indolo[3,2,1-*jk*]carbazole as the acceptor unit with carbazole and acridine donors have been reported (Fig. 23).[135] The λ_{max}^{PL} values for **ICzCz**, **ICzAc** and **ICzDAc** were 400, 439 and 449 nm, respectively (in toluene solution) and ΔE_{ST} values were 0.38, 0.20 and 0.17 eV (in polystyrene film). Transient PL experiments showed only prompt fluorescence for **ICzCz**, whereas **ICzAc** and **ICzDAc** had both prompt and delayed components, with τ_{DF} 9.86 μs and τ_{DF} 8.46 μs, respectively. The PLQYs of **ICzCz**, **ICzAc** and **ICzDAc**, as doped films in DPEPO under oxygen/nitrogen, were 0.40/0.53, 0.32/0.95 and 0.49/0.96. OLEDs with a DPEPO host:emitter (10 wt%) EML gave EQE_{max} values for **ICzCz**, **ICzAc**, and **ICzDAc** of 2.3%, 13.7% and 19.5%, with FWHM 49, 56, and 58 nm, and CIE(0.17, 0.04), (0.15, 0.09) and (0.15, 0.16) respectively.

The TADF emitter **CNICtCz** has enhanced acceptor character due to the cyano-functionalised indolocarbazole unit (Fig. 22).[136] DF was observed with τ_{DF} 6.25 μs (10 wt% in DPEPO film) and PLQYs were 0.33/0.50 under oxygen/nitrogen. The ΔE_{ST} of **CNICtCz** was 0.19 eV. Blue-emitting OLEDs with a DPEPO host:**CNICtCz**

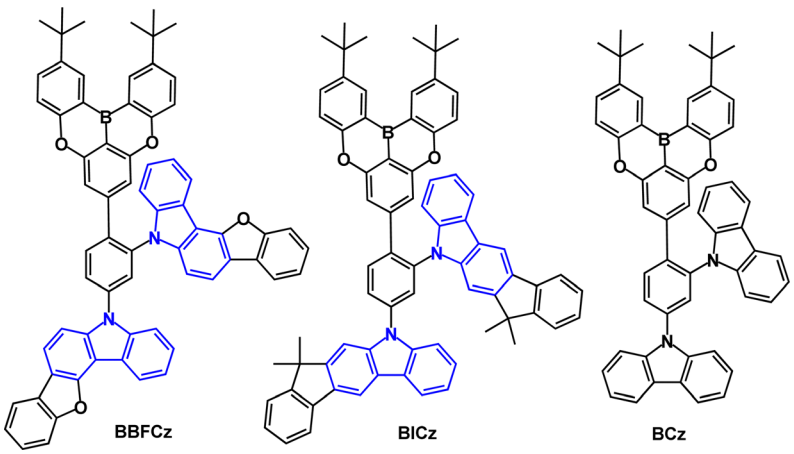

Fig. 22 Molecular structures of **BBFCz** and **BICz** and **BCz**.

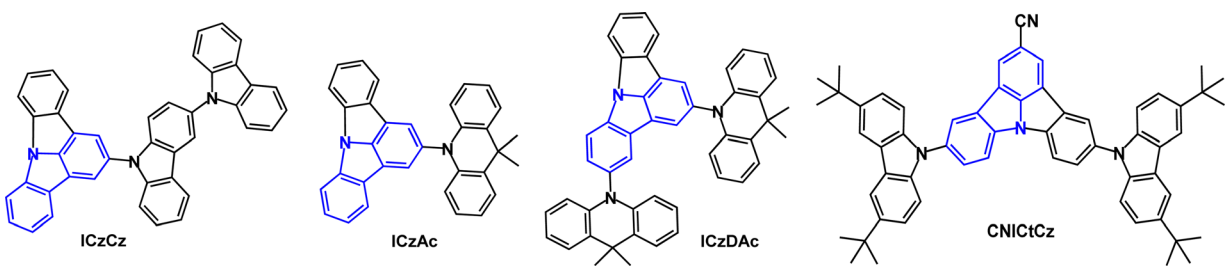

Fig. 23 Molecular structures of **ICzCz**, **ICzAc**, **ICzDAc** and **CNICtCz**.

(10 wt%) EML had EQE_{max} 16.0% (EQE 10.7% at 100 cd m^{-2}), λ_{max}^{EL} 456 nm, CIE(0.14, 0.13), FWHM 60 nm. The *t*-Bu substituents on **CNICtCz** significantly improved the device efficiency and slightly red-shifted the emission.

4.2 Diindolocarbazole (triazatruxene) derivatives

In the last few years, the C_3 symmetric, diindolocarbazole framework, also named triazatruxene, has become a popular near-planar, π-extended unit for TADF derivatives with a spacially large HOMO. Different D–A ratios can be obtained by attachment of an acceptor unit at one, two or three of the nitrogen atoms. Prominent examples will now be considered.

The D–A_3 structure **TAT-3DBTO$_2$** (Fig. 24a) was reported in 2018.[137] In the ground state geometry all the A units are tilted by 57° with respect to the TAT core.[138] After excitation the A units can rotate around the C-N bonds to minimise the orbital overlap. Calculations showed ten possible conformers of **TAT-3DBTO$_2$** all within 0.03 eV of each other, and ΔE_{ST} 0.01 eV was obtained from PL studies, with k_{RISC} as fast as 1×10^7 s^{-1} and PLQY ≈ 1, doped in BCPO film. Devices with a BCPO host:**TAT-3DBTO$_2$** (17 wt%) EML gave green emission, CIE(0.26, 0.46), EQE_{max} 30.9% and roll-off to 16.5% at 1000 cd m^{-2}; CE_{max} 50.8 cd A^{-1}.

The isomeric D–A_3 structure with the sulfone groups *meta* to the nitrogen atoms has a much larger ΔE_{ST} 0.28 eV compared to **TAT-3DBTO$_2$**.[139] As expected, this larger ΔE_{ST} strongly reduced the RISC rates. Calculations showed that the *meta* isomer is less conformationally restricted and rotation of its acceptor units lead to a lower T_1 energy, further away from the region of high density of states where larger vibronic coupling is found, favouring RISC.

The D–A molecule **TRZ-DI** (Fig. 24a) with a triazine acceptor has ΔE_{ST} 0.023 eV from PL studies, with k_{RISC} 1.63×10^6 s^{-1} and PLQY 0.87, doped in mixed TCTA:$Bepp_2$ film.[140] Devices with TCTA:$Bepp_2$ host:**TRZ-DI** (25 wt%) as the EML gave green emission, CIE(0.32, 0.58), EQE_{max} 31.4%. The analogous D–A_2 structure (**DTRZ-DI**) gave less efficient devices EQE_{max} 26.2% (Fig. 24b). It was noted that the high T_g values of **TRZ-DI** (203 °C) and **DTRZ-DI** (239 °C) should favour good morphological stability and electroluminescent lifetime.

An intricate triazatruxene-triazine cage molecule (Cage DA-1) is a TADF macrocyclic exciplex emitter. The cofacial D–A architecture induces efficient intramolecular through-space charge transfer with PLQY 35% in degassed toluene and a ΔE_{ST} of 0.049 eV. OLEDs were not reported.[141]

D–A–D molecules **TATC-BP** and **TATP-BP** (Fig. 25) exhibit multifunctional luminescence properties, namely, TADF, AIE and mechanoluminescence in the crystalline and powdered states.[142] PLQYs were very low in solution (0.8–1.9%) and were enhanced to 22–24% in neat films. From PL data ΔE_{ST} values were 0.125 and 0.129 eV, with τ_{DF} values 0.94 and 0.91 μs for **TATC-BP** and **TATP-BP**, respectively. Non-doped OLEDs with a solution-processed EML gave EQE_{max} ≈ 6%. Doped devices in H2 host (a dendritic polycarbazole derivative) with H2:**TATC-BP** (30 wt%) gave EQE_{max} 15.9% with low roll-off to 15.3% at 1000 cd m^{-2} and green emission, CIE(0.37, 0.53). For comparison the D–A_2 analogue **TAT-2BP** (Fig. 25) gave non-doped OLEDs with EQE_{max} 9.8% and very low roll-off to EQE 9.6% at 2000 cd m^{-2}.[143]

The D–A–D molecule **TAT-DBPZ** and the analogue **TAT-FDBPZ** with the more electron accepting fluorine-substituted dibenzophenazine unit have been reported (Fig. 26a).[144] Unusual features

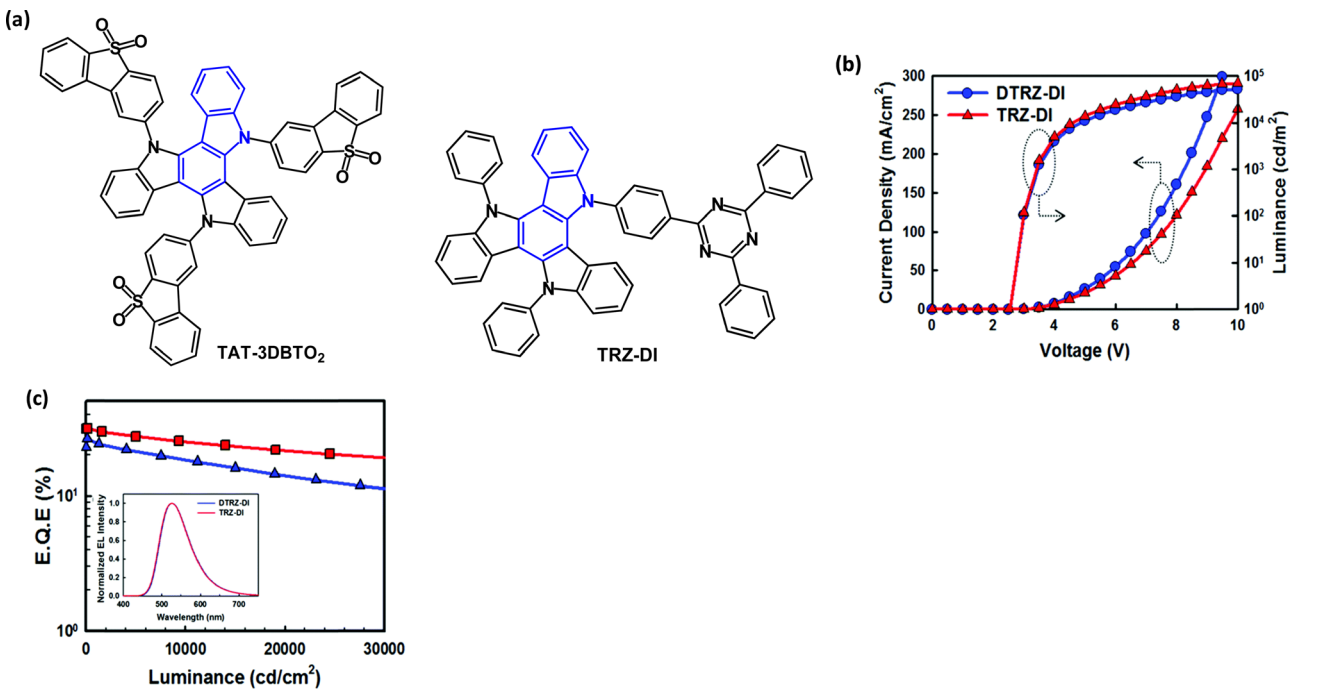

Fig. 24 (a) Molecular structures of **TAT-3DBTO$_2$** and **TRZ-DI**. (b) Current density–voltage–luminance (*J*–*V*–*L*) data. (c) EQE–*L* data; inset EL spectra for **TRZ-DI** and **DTRZ-DI** devices.[140] Copyright 2018 The Royal Society of Chemistry.

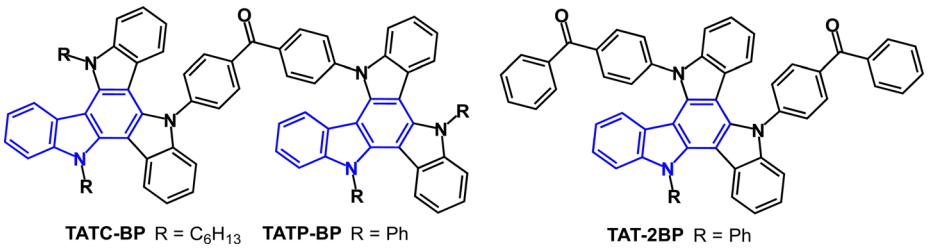

Fig. 25 Molecular structures of **TATC-BP**, **TATP-BP** and **TAT-2BP**.

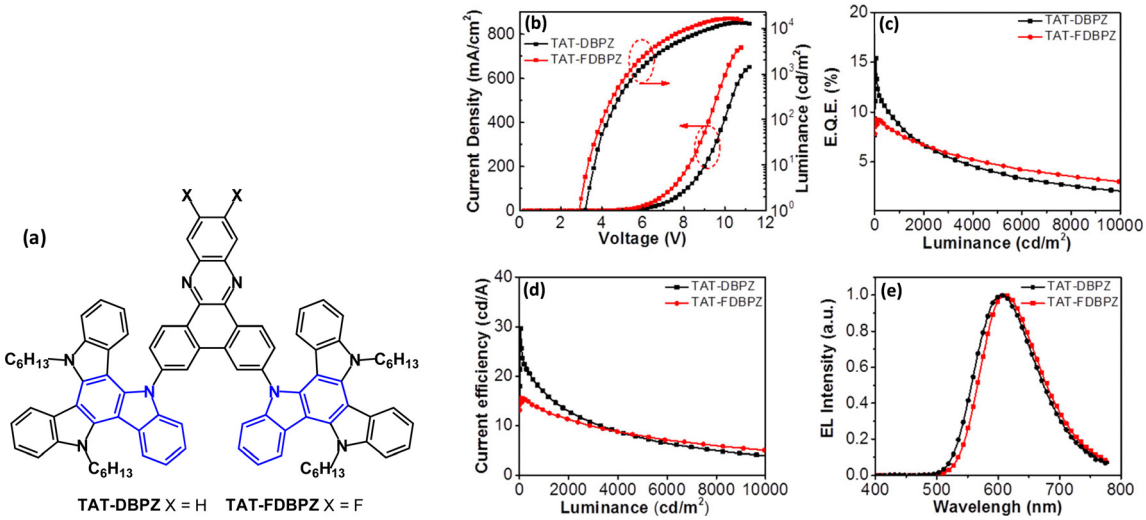

Fig. 26 (a) Molecular structures of **TAT-DBPZ** and **TAT-FDBPZ**. (b) Current density–voltage–luminance characteristics. (c) EQE–*L* curves. (d) CE–*L* curves. (e) EL spectra at 1000 cd m^{-2}.[144] Copyright 2020 The American Chemical Society.

of this work are that both compounds show AIE behaviour in neat films and red emission, with PLQYs 76% and 62% doped in CBP films. The large steric hindrance between the TAT and DBPZ moieties gave small ΔE_{ST} 0.16 and 0.10 eV for **TAT-DBPZ** and **TAT-FDBPZ**, respectively, leading to τ_{DF} values 2.30 and 1.51 μs and k_{RISC} 1.00 and 1.71 × 10^6 s^{-1}. The fluorine substituents in the FDBPZ unit imparted red-shifted emission and shorter DF lifetime and slightly decreased PLQY compared to **TAT-DBPZ**. The **TAT-DBPZ** device (20 wt% in CBP host as a solution processed EML) exhibited higher efficiency because of its higher PLQY and faster k_r giving EQE_{max} 15.4%; λ_{max}^{EL} 626 nm; CIE(0.61, 0.38) (Fig. 26b–d).

The D_3–A structure **TATC-TRZ** (Fig. 27) has flexible alkyl chains to enhance solubility, film forming ability and morphological stability that are beneficial for solution processed non-doped EMLs.[145] $S_1/T_1/\Delta E_{ST}$ values were 2.53/2.57/−0.04 eV (PL in neat films) and ΔE_{ST} 0.1 eV in doped films. The authors suggested that the very unusual negative ΔE_{ST} value in neat films might be due to a different geometrical arrangement in the fully relaxed S and T states. (Negative ΔE_{ST} values are a topic of current experimental and theoretical debate).[146] The PLQY of **TATC-TRZ** was only 2% in dilute toluene solution; this was raised to 22% in neat films, consistent with AIE. TADF characteristics were observed with τ_{PF} 17.5 ns, τ_{DF} 0.6 μs and k_{RISC} 2.9 × 10^6 s^{-1} in neat films. Green OLEDs fabricated with a neat **TATC-TRZ** EML had EQE_{max} 7.5%; λ_{max}^{EL} 560 nm. An EML of mCP host:**TATC-TRZ** (5 wt%) gave EQE_{max} 8.6%, lower roll-off (EQE 6.7% at 1000 cd m^{-2}) and λ_{max}^{EL} 530 nm.

Superior TADF behaviour has been demonstrated for the diindolocarbazole **BTPDIDCz** compared with the indolocarbazole analogues **BTPIDCz** and **BTP2IDCz**, all incorporating a thienopyrimidine acceptor (Fig. 28).[147] Cyclic voltammetric data gave a

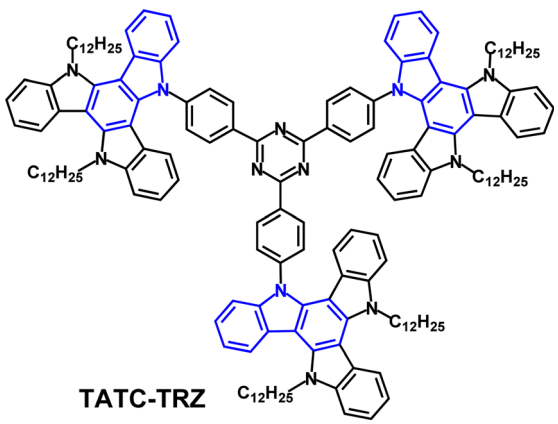

Fig. 27 Molecular structure of **TATC-TRZ**.

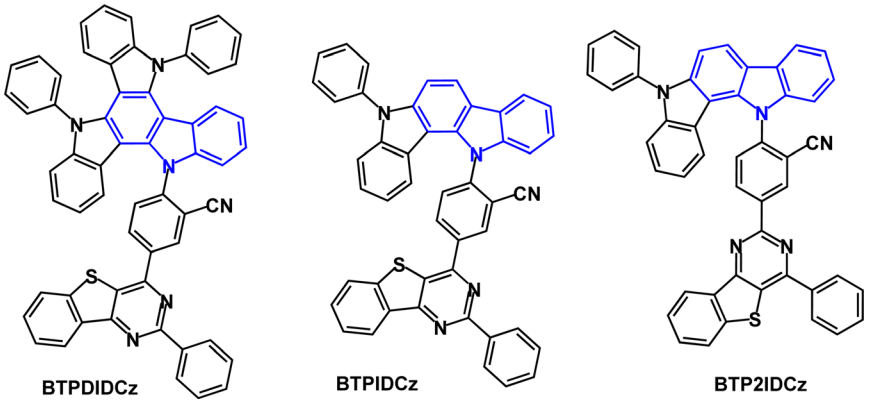

Fig. 28 Molecular structures of **BTPDIDCz**, **BTPIDCz** and **BTP2IDCz**.

shallower HOMO level for **BTPDIDCz** indicating the stronger electron donating ability of the diindolocarbazole group, compared to indolocarbazole. The $S_1/T_1/\Delta E_{ST}$ levels were 2.76/2.75/0/01 eV, 2.91/2.82/0.09 eV and 3.16/2.78/0.38 eV (PL measurements, THF solution) for **BTPDIDCz**, **BTPIDCz** and **BTP2IDCz**, respectively. Diindolocarbazole **BTPDIDCz** showed the smallest ΔE_{ST} and shortest τ_{DF} (4.1 μs) indicating its superior TADF behaviour. Conversely, the data for **BTP2IDCz** indicated only weak DF. PLQY values for the series were between 0.83–0.86. TADF-OLEDs had CzTrz host:emitter (5 or 20 wt%) EML. The best performance was achieved for **BTPDIDCz** with EQE_{max} 24.5%, λ_{max}^{EL} 530 nm; CIE(0.34, 0.57) and low efficiency roll-off to EQE 20.3% at 10 000 cd m^{-2}. The lifetimes of the devices were assessed by operating them at 5 mA cm^{-2}. In the series the **BTPDIDCz** device had the longest LT_{85} value of 93.4 h. This long lifetime can be correlated with the emitter's fast k_{RISC} of $\approx 1.0 \times 10^6$ s^{-1} which limits triplet exciton-triggered degradation mechanisms such as TTA and TPA which induce device failure.

To achieve colour tuning, alternative acceptors have been attached to diindolocarbazole. For examples, the D–A structures **TDBA-DI** and **β-DI-DBP** (Fig. 29) have sky-blue and orange/red emission, respectively. **TDBA-DI** has λ_{max}^{PL} 456 nm with FWHM of 55 nm (toluene solution).[104] The large dihedral angle between the D and A groups enables a small overlap between the HOMO and LUMO; $S_1/T_1/\Delta E_{ST}$ values are 3.06/2.95/0.11 eV (PL measurements). The PLQY of **TDBA-DI** as 20 wt% doped film in DBFPO host was 0.99. OLEDs with DBFPO host:**TDBA-DI** (20 wt%) as the EML had remarkably high EQE_{max} 38% (FWHM 65 nm; CIE 0.15, 0.28) while the analogous emitter with non-fused dimethylacridine as the D unit had EQE_{max} 26%, CIE(0.14, 0.15). The outstanding efficiency of **TDBA-DI** was attributed to its highly conjugated and rigid structure, which provided a high PLQY. Evidence was obtained that the horizontal molecular dipole orientation of **TDBA-DI** also contributed to the increased light out-coupling efficiency and high EQE. The operating lifetime of the DBFPO:**TDBA-DI** device was <2 h at 500 cd m^{-2}.

Theoretical studies of **β-DI-DBP** indicated a dihedral angle between D and A of 64.3°.[148] **β-DI-DBP** showed a broad emission with λ_{max}^{PL} 578 nm (toluene solution). The PLQY was 96.1% for a 5 wt% doped DIC-TRZ film with τ_{DF} 14.0 μs; $S_1/T_1/\Delta E_{ST}$ levels were 2.48/2.36/0.12 eV. **β-DI-DBP** showed a slightly faster k_{RISC} compared to the 9,9-dimethylacridine analogue β-DMAC-DBP, (1.79×10^5 s^{-1}, *versus* 1.53×10^5 s^{-1}) which may be due to the higher rigidity of the diindolocarbazole donor. OLEDs with DIC-TRZ host:**β-DI-DBP** (5 wt%) as the EML had EQE_{max} 23.8% with orange/red emission λ_{max}^{EL} 587 nm, CIE(0.53, 0.47) and broad FWHM of 102 nm. EQE_{max} was slightly higher and the efficiency roll-off at 1000 cd m^{-2} was considerably improved compared to β-DMAC-DBP devices (EQE_{max} 21.8%).

4.3 Carbazole fused with 6-membered rings

An interesting structural variant is the fused carbazole–acridine unit in the isomeric D–A emitters **12AcCz-PM** and **23AcCz-PM** (Fig. 30a) which have remarkably different photophysical behaviour.[149] **12AcCz-PM** has large steric hindrance between the D and A units leading to a quasi-axial acridine conformation (Fig. 30b) with no TADF character. In contrast, the reduced steric hindrance in **23AcCz-PM** allows a more favourable orthogonal

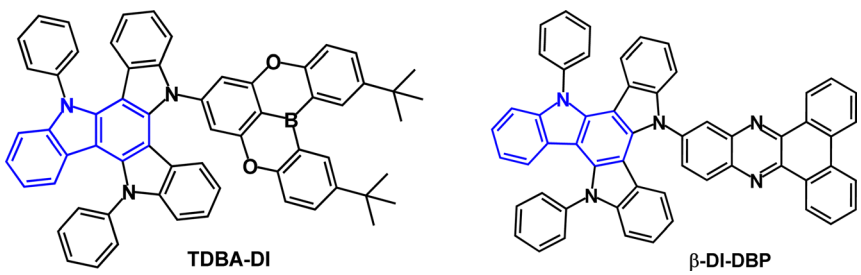

Fig. 29 Molecular structures of **TDBA-DI** and **β-DI-DBP**.

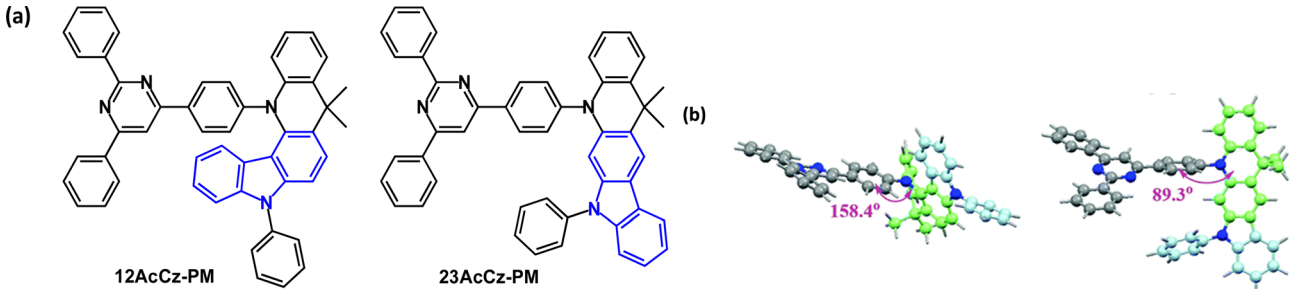

Fig. 30 (a) Molecular structures of **12AcCz-PM**, **23AcCz-PM** and (b) DFT computed optimal structures of **12AcCz-PM**, **23AcCz-PM**.[149] Copyright 2019 The Royal Society of Chemistry.

D–A structure with a quasi-equatorial acridine conformation (Fig. 30b) and efficient TADF. DFT indicated a large HOMO–LUMO overlap in **12AcCz-PM**, whereas the HOMO and LUMO were well separated in **23AcCz-PM**. $S_1/T_1/\Delta E_{ST}$ values were 3.06/2.67/0.39 eV and 2.73/2.67/0.06 eV for **12AcCz-PM** and **23AcCz-PM**, respectively (doped films in DPEPO). λ_{max}^{PL} values were 440 and 516 nm, with PLQYs of 78 and 95% for **12AcCz-PM** and **23AcCz-PM**. OLEDs had a DPEPO host:emitter (*X* wt%) EML. The **12AcCz-PM** doped device (20 wt%) had deep blue emission with CIE(0.15, 0.05) and EQE_{max} 6.4%. The 30 wt% **23AcCz-PM** device had blue-green emission with CIE(0.26, 0.55), EQE_{max}^{EL} 26.1%, 24.8% at 1000 cd m^{-2} and 20.7% at 5000 cd m^{-2}, indicating low efficiency roll-off and high operational stability.

A comparison of pyrimidine and triazine acceptors in **34AcCz-PM** and **34AcCz-Trz** (Fig. 31) showed superior devices for the pyrimidine analogue.[150] $S_1/T_1/\Delta E_{ST}$ levels were 2.72/2.57/0.15 eV and 2.62/2.50/0.12 eV (PL, doped films in CBP) for **34AcCz-PM** and **34AcCz-Trz**, respectively. λ_{max}^{PL} was 520/538 nm and PLQYs were 88/69% (doped films in CBP) and 67/42% (neat films) for **34AcCz-PM** and **34AcCz-Trz**, respectively. Both compounds showed DF with τ_{DF} of 0.73 and 0.88 μs (doped films in CBP). PL spectra in THF/water mixtures indicated that both compounds are AIE active. Doped and non-doped devices were reported. The EML of the doped devices for **34AcCz-PM** was 10 wt% in CBP; for **34AcCz-Trz** 5 wt% in CBP. The device with **34AcCz-PM** exhibited EQE_{max} 22.6% and CE_{max} 73.3 cd A^{-1} with 20.1% and 65.5 cd A^{-1} at 5000 cd m^{-2}, CIE(0.33, 0.58). The higher efficiency of the **34AcCz-PM** devices was attributed to its higher PLQY and higher k_{RISC} resulting from more prominent AIE compared to **34AcCz-Trz**. A non-doped OLED of **34AcCz-PM** exhibited EQE_{max} 14.1% and CE_{max} 45.2 cd A^{-1}.

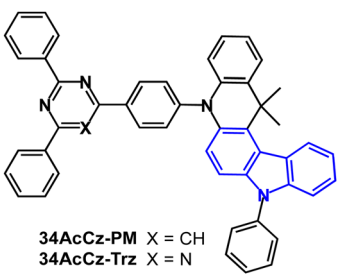

Fig. 31 Molecular structures of **34AcCz-PM** and **34AcCz-Trz**.

A series of unusual fused di-*t*-Bu-carbazole derivatives with peripheral carbazole (**2,3-**, **2,5-** and **2,6-CZ**), phenoxazine (**2,3-POA**) and diphenylamine (**2,3-DPA**) (Fig. 32) has been studied.[21] DFT calculations indicated that the HOMOs were mainly located on the peripheral donor units, whereas the LUMOs resided mainly on the central carbazole/carbonyl skeleton. **2,3-POA** had the shallowest HOMO, indicating its strong donor character. λ_{max}^{PL} ranged from blue (449 nm; **2,3-CZ**) to yellow-green (547 nm; **2,3-POA**) (toluene solution). All the compounds showed TADF with FWHM values increasing in the order **2,3-CZ** 36 nm < **2,5-CZ** 41 nm < **2,3-DPA** 57 nm < **2,6-CZ** 80 nm < **2,3-POA** 92 nm, with the narrow values ascribed to a potential multiresonance (MR) effect. ΔE_{ST} values were 0.26, 0.29, 0, 0.19 and 0.01 eV for **2,3-CZ**, **2,5-CZ**, **2,6-CZ**, **2,3-DPA** and **2,3-POA**, respectively. PLQYs ranged from 39.5% (**2,3-CZ**) to 82.5% (**2,3-POA**) (3.5 wt% doped in mCBP film). OLEDs used mCBP or 26DCzPPy as hosts in the EML. Notably, the pure-blue OLED with **2,5-CZ** had EQE_{max} 22.3% with CIE(0.13, 0.13) and FWHM 48 nm with significant efficiency roll-off. The yellow-green **2,3-POA** device had EQE_{max} 21.7%, CIE(0.30, 0.62) and FWHM 68 nm with low efficiency roll-off.

CBZANQ has a D–σ–A structure and orthogonal D and A units enforced by the spiro linkage (Fig. 33).[151] The molecule exhibited weak CT character and low PLQY of 18% (30 wt% doped in PMMA host) and ΔE_{ST} of 0.05 eV (in DPEPO host). OLEDs with DPEPO host:**CBZANQ** as the EML had low EQE_{max} 6.7% with λ_{max}^{EL} 492 nm. For comparison, devices with DPEPO:**PXZANQ** (Fig. 33) as the EML had EQE_{max} 22.1% and λ_{max}^{EL} 528 nm. The improved performance of this device was attributed to the increased donor strength of phenoxazine compared to carbazole.

Very recently TADF emitter **CCO-2** (Fig. 33) and close analogues[152] with different aryl substituents on the carbazole nitrogen atom have been reported. The molecular design combines a weak and rigid electron donor spiro[acridine-9,9′-xanthene] and a weak electron acceptor chromeno[3,2-*c*]carbazole that is also rigid. The molecules have high PLQY, high transition dipole ratios, fast k_r and fast k_{RISC} values. OLEDs fabricated with DPEPO host:**CCO-2** (15 wt%) gave blue emission with λ_{max}^{EL} 462 nm, CIE(0.14, 0.15) and EQE_{max} > 40% and roll-off to EQE 22.4% at 1000 cd m^{-2}. For 30–50 wt% devices there was a slight red shift to λ_{max}^{EL} 470 nm and reduced roll-off to EQE 31.3–33.7% at 1000 cd m^{-2}. Deep-blue and green hyperfluorescent OLEDs with **CCO-2** as sensitiser for multi-resonance

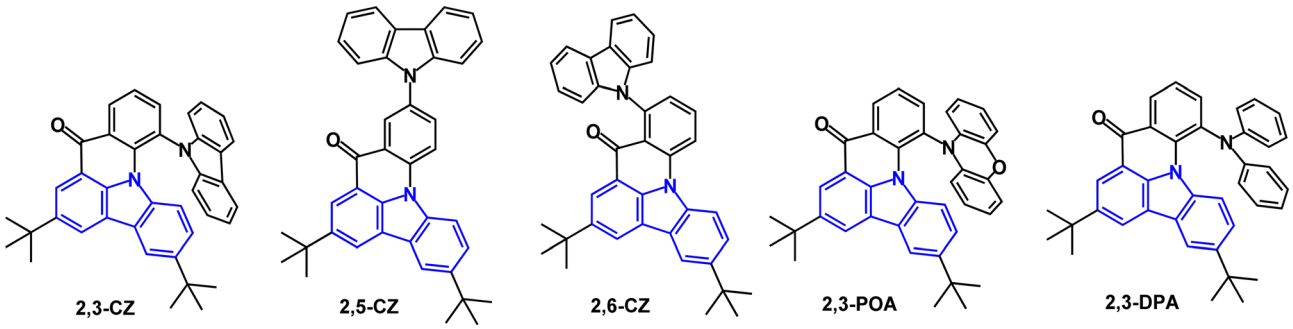

Fig. 32 Molecular structures of **2,3-CZ**, **2,5-CZ**, **2,6-CZ**, **2,3-POA** and **2,3-DPA**.

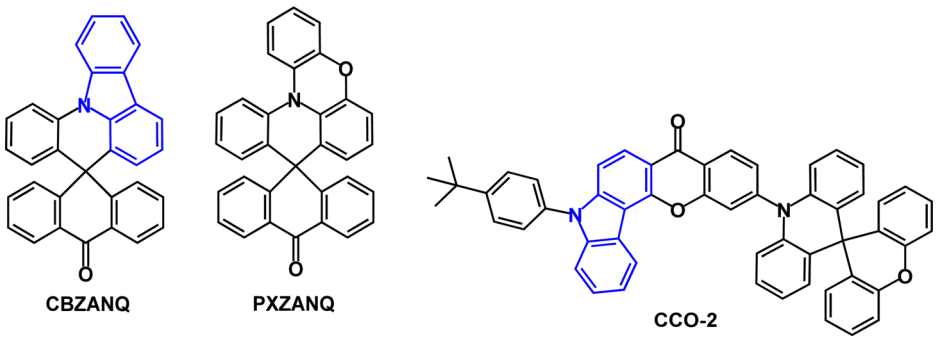

Fig. 33 Molecular structures of **CBZANQ**, **PXZANQ** and **CCO-2**.

delated fluorescent emitters had EQE_{max} 32.5%, CIE(0.14, 0.10) and EQE_{max} 37.6%, CIE(0.32, 0.64), respectively. The LT_{50} of the blue and green devices at L_0 100 cd m^{-2} was 1099 h and 34 669 h, respectively.

5. Multiresonance (MR) fused carbazole derivatives

5.1 Boron-containing molecules

As noted in the introduction section, multiresonance (MR) emitters are currently attracting great attention. Nitrogen and oxygen bridged triarylboron systems in D–A molecules show efficient TADF with narrow FWHM and small Stokes shifts because of their rigid structure and MR effects.[41,153] The MR-TADF mechanism is complex and is currently believed to involve crossing between T_1 and an upper T_2 (or higher) state *via* reverse internal conversion, followed by RISC from T_2 to S_1.[154] In 2018 it was reported that a carbazole-containing MR emitter with enhanced oscillator strength and faster k_{RISC} leads to pure-blue OLEDs with EQE_{max} of 32.1% and FWHM of only 27 nm.[67] The initially assigned molecular structure of this emitter has subsequently been corrected.[155] It was, therefore, logical to explore analogues with carbazole units embedded within a polycyclic B–C–N framework and this is now a fast-moving topic.

In 2019 **3F-BN** (Fig. 34) was reported to exhibit narrowband green emission (λ_{max}^{PL} 499 nm) and a very small Stokes shift (27 nm) suggesting a small change in the electronic configuration

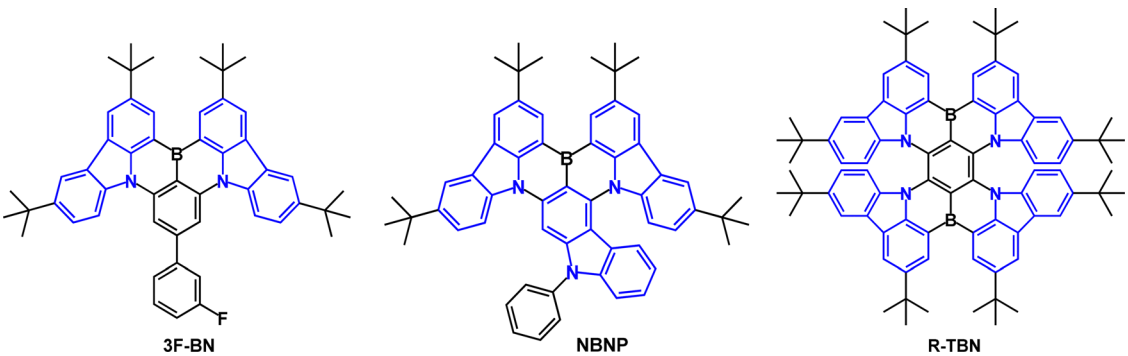

Fig. 34 Molecular structures of **3F-BN**, **NBNP** and **R-TBN**.

between ground and excited states, typical of the MR effect.[156] The PLQY was 83.4% (6 wt% doped in mCPBC films); $S_1/T_1/\Delta E_{ST}$ levels were 2.48/2.40/0.08 eV; k_F 4.66 × 10^7 s^{-1}; k_{RISC} 0.39 × 10^5 s^{-1}. PL decay curves of the films showed both PF and DF with τ_{DF} 16.7 μs. OLEDs with an EML of 5TCzBN host:**3F-BN** (6 wt%) gave EQE_{max} 22.7% with small efficiency roll-off (21.1% at 1000 cd m^{-2}), PE_{max} 72.2 lm W^{-1}, λ_{max}^{EL} 499 nm, FWHM 38.5 nm and CIE(0.20, 0.58).

The related tri-carbazole MR emitter **NBNP** (Fig. 34) was reported in 2022.[157] $S_1/T_1/\Delta E_{ST}$ levels for **NBNP** are 2.48/2.39/0.09 eV; k_{RISC} 3.0 × 10^5 s^{-1}. Large SOC matrix elements were also beneficial for activating TADF in **NBNP**. The PLQY was 93% with τ_{PF} 7.6 ns and τ_{DF} 3.8 μs (4 wt% doped in mCBP film). Green OLEDs used mCBP host:**NBNP** (4 wt%) as the EML giving EQE_{max} 28.0% with λ_{max}^{EL} 502 nm, FWHM 33 nm, CIE(0.12, 0.62), and maintaining EQE 18.8% at 5000 cd m^{-2}.

Tetra-carbazole derivative **R-TBN** (Fig. 34) is a deep-red emitter with λ_{max}^{PL} 692 nm (toluene solution) with ΔE_{ST} 0.16 eV; τ_{DF} 46.4 μs.[158] The PLQY is 100% both in solution and as 3 wt% doped in CBP film. OLEDs with CBP host:**R-TBN** EML gave EQE_{max} 24.7%. Because of the relatively long DF lifetime of **R-TBN** in doped film (0.71 ms) the EML also adopted a ternary system of CBP:Ir(mphmq)$_2$tmd (30 wt%):**R-TBN** (3 wt%) where Ir(mphmq)$_2$tmd is a phosphorescent sensitiser to assist exciton recycling. These devices gave EQE_{max} 27.6%, λ_{max}^{EL} 686 nm, FWHM 49 nm and CIE(0.721, 0.278). The devices with and without sensitiser gave identical EL spectra, confirming that EL is solely from **R-TBN**. The significant efficiency roll-off was partly attributed to the slow k_{RISC} 2.5 × 10^4 s^{-1} of **R-TBN**.

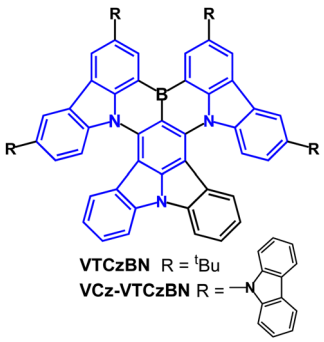

Fig. 35 Molecular structures of **VTCzBN** and **VCz-VTCzBN**.

The new multi-carbazole MR green emitters **VTCzBN** and **VCz-VTCzBN** (Fig. 35) were reported in 2022.[159] In particular, the pendant carbazole groups of **VCz-VTCzBN** extend the CT delocalisation leading to λ_{max}^{PL} 521 nm with FWHM of 29 nm in toluene solution and ΔE_{ST} < 0.01 eV. The PLQY of both **VTCzBN** and **VCz-VTCzBN** in doped films was 98%, with k_{RISC} 1.0 × 10^6 s^{-1} which is relatively high for MR B–N systems. Both compounds show prompt and delayed emissions with τ_{PF} 3.3 ns and τ_{DF} 9.9 μs for **VTCzBN**, and τ_{PF} 13.2 ns and τ_{DF} 8.7 μs for **VCz-VTCzBN**. OLEDs with an EML comprising 2,6-DCzppy host: emitter (4 wt%) gave high efficiencies of 91.0 cd A^{-1}, EQE_{max} 31.7% for **VTCzBN**, and 129.3 cd A^{-1}, EQE_{max} 32.2% for **VCz-VTCzBN** with FWHM 37–38 nm. There was considerable roll-off to EQE 24.8% and 18.0% at 100 cd m^{-2}. The peripheral carbazole units of **VCz-VTCzBN** red shifted the emission to λ_{max}^{EL} 524 nm, CIE(0.22, 0.71), compared to 499 nm, CIE(0.14, 0.56) for **VTCzBN**.

Molecules for full-colour narrow-band and high efficiency EL by modular design combining carbazole and tricoordinate boron fragments, were reported (Fig. 36).[160] PLQY values were in the range 85–98%; k_{RISC} values were in the range 1.2–18 × 10^4 s^{-1}; OLEDs with mCP as host achieved EQE_{max} values of 29.3%, 31.8% and 22.0% for blue, green and red, respectively.

Devices comprising **Cz2DABNA-NP-M/TB** and **CzB2-M/P** (Fig. 37) as emitters (1 wt% in DOBNA-Tol host) exhibited sky-blue and green emission at λ_{max}^{EL} 477 and 497 nm with FWHM 27 and 29 nm, respectively, and EQE_{max} of 21.8 and 26.7%. The LT_{80} value of the **Cz2DABNA-NP-M/TB** device was 91 h at L_0 100 cd m^{-2}, whereas the LT_{80} value of the **CzB2-M/P** device was 74 h at L_0 500 cd m^{-2}.[155]

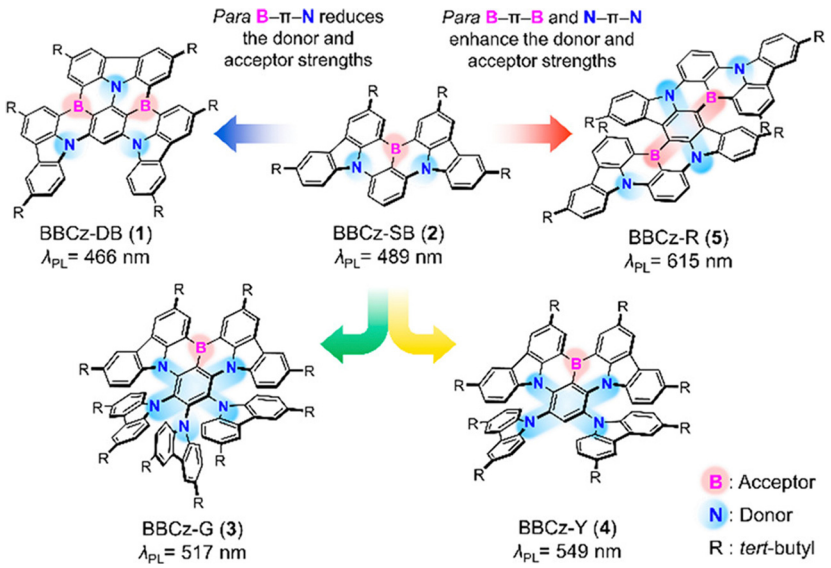

Fig. 36 Modular design for full-colour emitters **1–5**.[160] Copyright 2020 American Chemical Society.

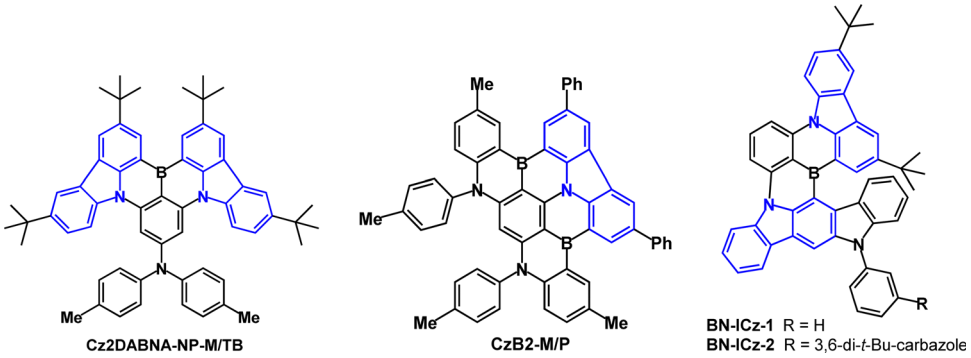

Fig. 37 Molecular structures of **Cz2DABNA-NP-M/TB**, **CzB2-M/P**, **BN-ICz-1** and **BN-ICz-2**.

The emitters **BN-ICz-1** and **BN-ICz-2** (Fig. 37) fuse an MR fragment onto an indolo[3,2-*b*]carbazole skeleton to achieve extended π-conjugation, increased molecular rigidity and reduced vibrational frequency.[161] The devices in mCBP host showed ultra-pure green emission with λ_{max} 523 nm and FWHM 23 nm; CIE(0.22, 0.74) and (0.21, 0.73) for **BN-ICz-1** and **BN-ICZ-2**, with EQE_{max} values ≈30%.

TCZ-F-DABNA (Fig. 38a) has a linearly extended π-system and emission shifted to the orange-red region.[162] The DABNA core of **TCZ-F-DABNA** imparts the MR properties and a small ΔE_{ST} of 0.12 eV (S_1/T_1 2.21/2.09 eV) for efficient TADF. The HOMO and LUMO distributions are similar to other DABNA derivatives and are less distributed on the fused carbazoles (Fig. 38b), although some extension of the HOMO introduces weak CT interaction with the DABNA core leading to a narrower band gap. **TCZ-F-DABNA** has a significantly twisted conformation (X-ray crystal structure and theoretical calculations) which can prevent molecular close packing and relieve concentration quenching of the emission. The PLQY was 99% with τ_{PF} 7.9 ns and τ_{DF} 20.2 μs (8 wt% doped in PhCzBCz film). This host was selected because of its high triplet level (2.96 eV) and balanced bipolar characteristics. OLEDs had PhCzBCz host:**TCZ-F-DABNA** (*X* wt%) as the EML. In the doping range 1–30%, EQE_{max} values were >30%, peaking at 39.2% for 8 wt%, with λ_{max}^{EL} 588 nm, CIE(0.54, 0.44) and FWHM 61 nm (Fig. 38c). A high horizontal molecular orientation ratio of 96% helped to boost the outcoupling efficiency and hence raise the EQE_{max}. Nonetheless, all the devices exhibited serious efficiency roll-off ascribed to the rather slow k_{RISC} of 7.80×10^4 s^{-1}.

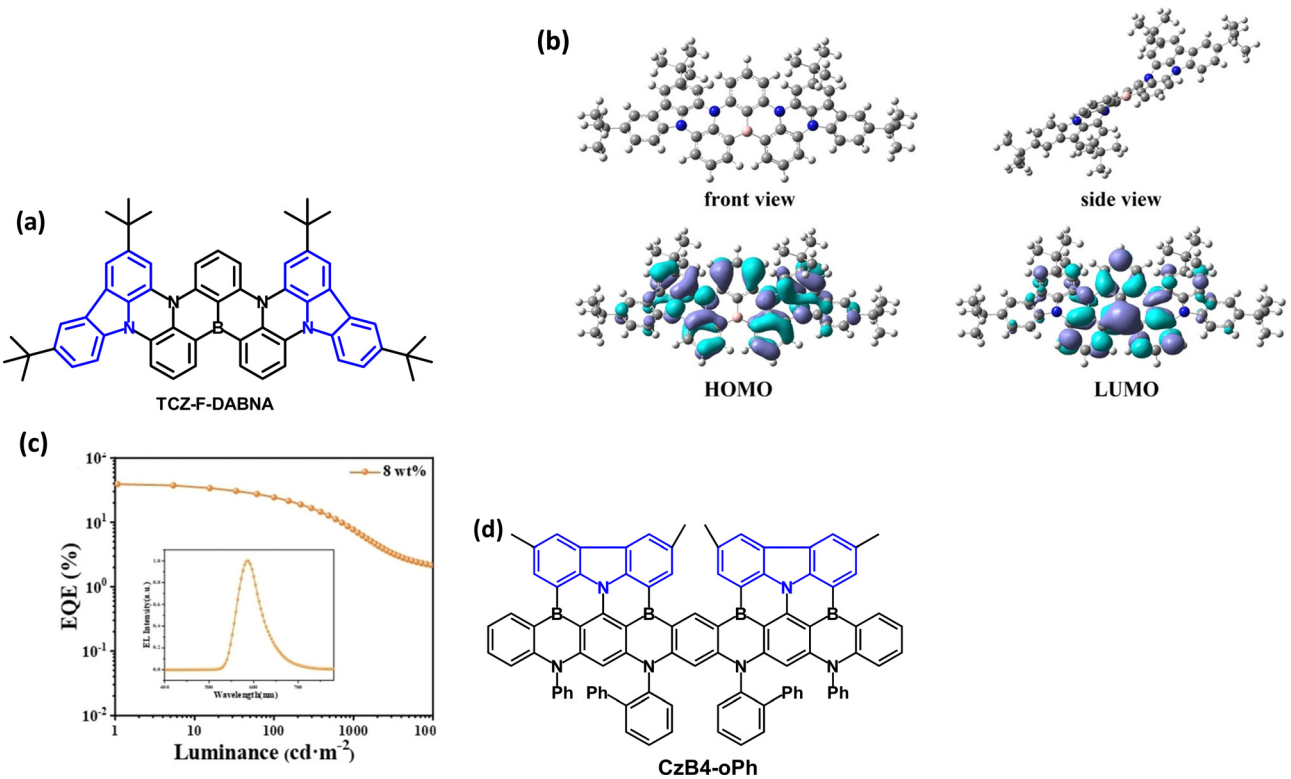

Fig. 38 (a) Molecular structure of **TCZ-F-DABNA**; (b) optimised molecular geometry and HOMO and LUMO distributions from DFT calculations; (c) EQE–*L* characteristics; inset shows the EL spectrum.[162] Copyright 2022 Wiley-VCH. (d) Molecular structure of **CzB4-oPh**.

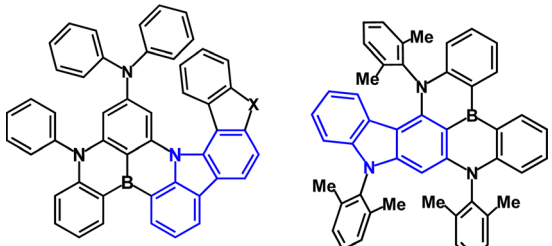

Fig. 39 Molecular structures of **mICz-DABNA**, **BFCz-DABNA** and **tri-*mx*-Cz-DABNA**.

Very recently multi-carbazole-fused BN-embedded nonacene, tridecacene and heptadecacene with more extended ladder frameworks were constructed.[163] The molecules exhibited ultra-narrowband green emission with FWHM 12–16 nm and k_{RISC} of $\approx 10^5$ s^{-1} doped in polystyrene films. The nonacene derivative **CzB4-oPh** (Fig. 38d) was used as an emitter in OLEDs with EQE_{max} 28.7% and EQE_{1000} 25.8%; λ_{max} 490 nm; FWHM 21 nm. The operational lifetime LT_{80} was 43 h at L_0 1000 cd m^{-2}.

In the search for new blue MR-TADF emitters, **mICz-DABNA** and **BFCz-DABNA** have been studied (Fig. 39).[164] PLQY values were ≈93%, ΔE_{ST} 0.20 eV and $\tau_{DF} \approx 18$ μs for 3 wt% emitters doped in mCBP-CN film. OLEDs had EQE_{max} 26.4 and 28.0% for **mICz-DABNA** and **BFCz-DABNA**, respectively, with λ_{max}^{EL} 466 and 463 nm; CIE(0.13, 0.11) and (0.13, 0.09) and very narrow FWHM of 26 nm. There was, however, severe efficiency roll-off to ≤8% at 400 cd m^{-2} due to the slow $k_{RISC} \approx 10^4$ s^{-1}. Very recently it has been reported that integrating *meta*-xylene rotors in **tri-*mx*-CzDABNA** (Fig. 39) leads to an enhanced k_{RISC} of 2.85×10^5 s^{-1} (in mCBP host). Devices gave pure blue emission with λ_{max}^{EL} 472 nm; CIE(0.13, 0.19), FWHM 34 nm and reduced efficiency roll-off with EQE_{max} 26.9%; EQE 24.8% at 100 cd m^{-2}.[165]

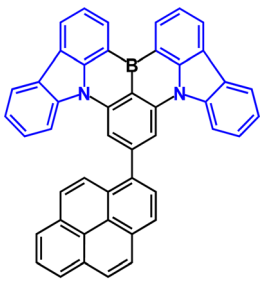

Fig. 40 Molecular structure of **CzBNPyr**.

It is well established that MR emitters as TADF molecules can achieve high efficiency OLEDs with narrow-band emission. However, device durability can be limited because of the instability of triplet states due to the rather slow k_{RISC} and long triplet lifetimes. Instead of striving to shorten the DF lifetime by molecular design, the quick scavenging of triplets has been achieved by a new strategy of attaching a pyrene unit with a low-lying T_1 level onto the MR emitter.[166] **CzBNPyr** (Fig. 40) is TADF-inactive with experimental ΔE_{ST} 0.62 eV (compared to unsubstituted and naphthalene-substituted CzBN analogues which are TADF-active with ΔE_{ST} 0.15 eV). Blue hyperfluorescent-OLEDs based on **CzBNPyr** gave EQE_{max} 19.4% and a substantial improvement in device stability to LT_{95} 29.1 h at L_0 1000 cd m^{-2}, compared to analogous devices with standard MR emitters. The authors note that this strategy should be applicable to enhancing device lifetimes of other HF-OLEDs with blue, green and red MR emitters without sacrificing efficiency and colour purity.

Chalcogen atoms have been incorporated into fused carbazole MR emitters in the series **CzBO**, **CzBS** and **CzBSe** (Fig. 41a).[167] The motivation for this work was to utilise a heavy atom effect in **CzBS** and **CzBSe** to enhance the SOC between the T and S states and thereby boost k_{RISC}. Indeed, k_{RISC} is claimed to be as high a 1.8×10^8 s^{-1} for **CzBSe**, accelerated by ≈800 and ≈20 000 times compared to **CzBS** and **CzBO**, respectively. In contrast to **CzBO** and **CzBS**, the PF component was negligible in **CzBSe** demonstrating that the typical $k_{RISC} \ll k_F$ situation that gives rise to both PF and DF components is not applicable for **CzBSe**. The ΔE_{ST} values for **CzBO**, **CzBS** and **CzBSe** were all in the range 0.14–0.16 eV (PL in 1 wt% doped in mCBP film) with PLQY values of 98–99%. Narrowband emission was observed in the doped films with λ_{max}^{PL} 448, 472 and 479 nm for **CzBO**, **CzBS** and **CzBSe**, respectively, with FWHM ≈ 30 nm (Fig. 41b). OLEDs with an EML of mCBP host:emitter (1 wt%) exhibited deep-blue to sky-blue emission with λ_{max}^{EL} 448, 473 and 481, CIE(0.15, 0.05), (0.11, 0.16), and (0.10, 0.24), FWHM 30–33 nm for **CzBO**, **CzBS**

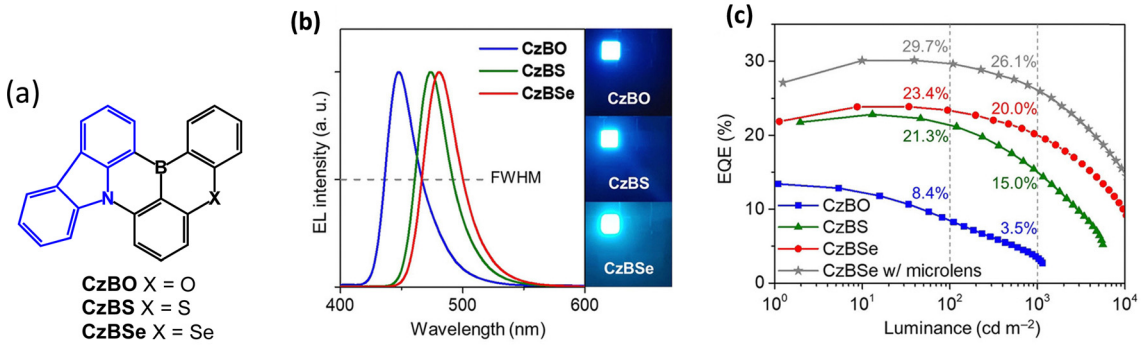

Fig. 41 (a) Molecular structures of **CzBO**, **CzBS** and **CzBSe**. (b) EL spectra and device images. (c) EQE–*L* data for the OLEDs.[167] Copyright 2022 Wiley-VCH.

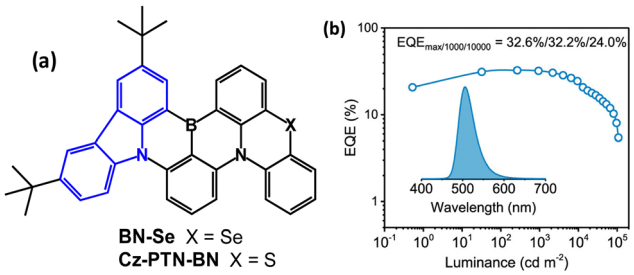

Fig. 42 (a) Molecular structures of **BN-Se** and **Cz-PTN-BN**. (b) EQE–*L* data for the **BN-Se** OLEDs.[168] Copyright 2022 The American Chemical Society.

and **CzBSe**, respectively. These devices gave EQE_{100} 8.4, 21.3 and 23.4%, which was increased with the use of a microlens array to enhance light outcoupling (Fig. 41c). The **CzBSe**-based device exhibited a longer operational lifetime of LT_{50} 7.48 h than the **CzBS**- and **CzBO**-devices (4.23 h and 0.16 h, respectively) at L_0 100 cd m^{-2}. The data clearly demonstrate interesting trends on implanting a chalcogen atom into MR-TADF emitters.

A more extended MR skeleton incorporating a selenium atom was designed (Fig. 42a).[168] **BN-Se** exhibited higher PLQY (99%), and faster k_{RISC} (1.6×10^6 s^{-1}) compared to the previously reported sulfur analogue **Cz-PTN-BN** (91%; 0.81×10^5 s^{-1}).[169] The ΔE_{ST} value for **BN-Se** was 0.08 eV. OLEDs with an EML of DMICTRZ host:**BN-Se** (1 wt%) exhibited λ_{max}^{EL} 506 nm, CIE(0.15, 0.62) with FWHM 45 nm. Without any outcoupling optimisation, EQE_{max} 32.6%, CE_{max} 95.9 cd A^{-1} and PE_{max} 103.9 lm W^{-1} were obtained with ultralow efficiency roll-off to EQE 32.2% at 1000 cd m^{-2} (Fig. 42b). For comparison OLEDs with emitter **Cz-PTN-BN** had enhanced roll-off. The operational lifetime of the **Cz-PTN-BN** device was LT_{50} 10.3 h at L_0 500 cd m^{-2}; the data were not reported for **BN-Se**. Furthermore, **BN-Se** was proposed as a photosensitiser for solar-powered applications such as photocatalysis.

In the context of OLEDs, the benefits of sulfur and selenium may be compound-specific and not universal. There is a very recent suggestion that the similar size of oxygen and carbon atoms may optimise narrowband MR emission compared to a sulfur analogue, as the larger sulfur atom can reduce both the π-conjugation and the molecular rigidity, thereby increasing geometrical relaxation energies which broaden the FWHM.[170] Also, there is evidence that device operational lifetimes can be adversely affected by the heavier chalcogen atoms,[171] perhaps due to the higher chemical reactivity of C-X bonds (X = S, Se), although this is not the case with the **CzBO**, **CzBS** and **CzBSe** series (Fig. 41a).

5.2 Boron-free MR fused-ring carbazole derivatives

This section will highlight recent reports of boron-free MR-TADF emitters with no standard acceptor groups present in the molecules. Indolocarbazole systems embedded within the π-framework have been prominent in this regard.

A rational molecular design strategy focused on the synergistic effect of *para*-positioned nitrogen atoms to enhance electronic coupling and to decrease the emitting energy gap.[57] Accordingly, **pICZ** and **pICZ-TPA** (Fig. 43a) are deep-blue emitters with λ_{max}^{PL} 441 and 447 nm, FWHM of 18 and 21 nm and PLQY ≈ 90% in toluene solution. HOMO–LUMO distributions throughout the core confirm the MR character of these molecules (Fig. 43b). PL decay curves showed a single exponential feature with τ_{PF} 8.37 ns

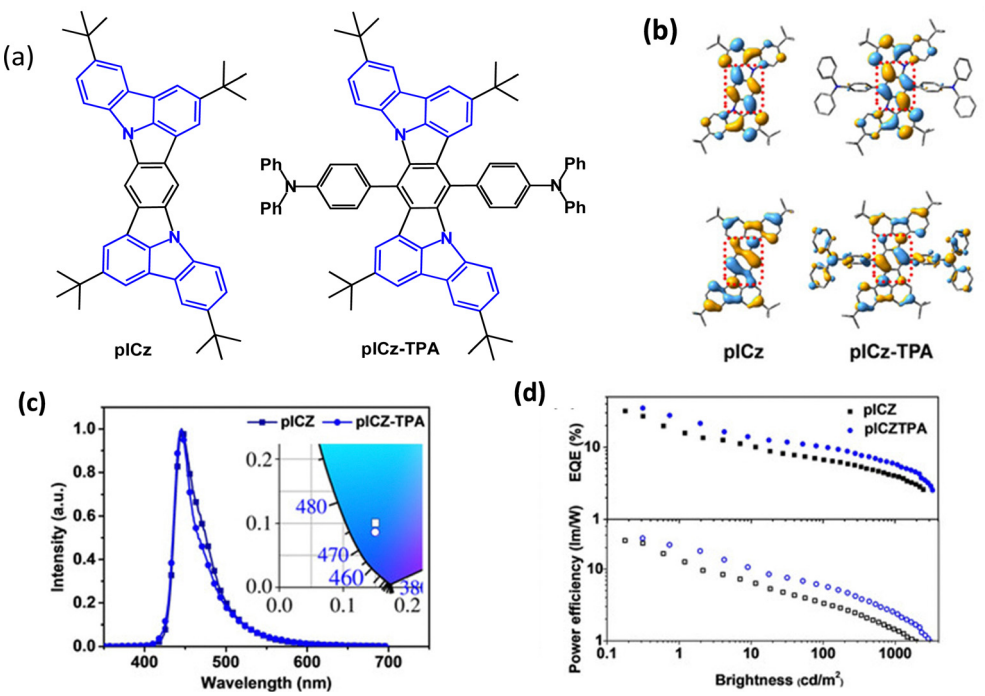

Fig. 43 (a) Molecular structures of **pICZ** and **pICZ-TPA**. (b) Calculated HOMO and LUMO distributions of **pICZ** and **pICZ-TPA**. (c) EL spectra of the OLEDs recorded at 1000 cd m^{-2}. (d) EQE–brightness and power efficiency–brightness curves.[57] Copyright 2021 Wiley-VCH.

and 6.70 ns for **pICZ** and **pICZ-TPA**, respectively, suggesting their non-TADF character, which is consistent with their ΔE_{ST} values of 0.29 and 0.32 eV. Nonetheless, impressive EL performance was obtained using an EML with a ternary composition, namely **pICZ** or **pICZ-TPA** (fluorophor):PPF (a wide energy gap host):DPAc-DtCzBN (a TADF sensitiser to assist exciton recycling). Recombination of charges on the TADF sensitizer, will be followed by $T_1 \rightarrow S_1$ upconversion, then energy transfer to the fluorophore for emission. EQE_{max} values as high as 32% and 34.7% were obtained with **pICZ** or **pICZ-TPA**, respectively, with $CIE_y \leq 0.10$ and FWHM 41 and 30 nm (Fig. 43b and c). Efficiency was enhanced by the high horizontal dipole ratio (0.84–0.85) of the emitters in the doped films. The large efficiency roll-off was ascribed mainly to the insufficient RISC rate ($k_{RISC} \approx 10^5\ s^{-1}$) of the sensitiser.

ICz-Mes$_3$ and **DiICz-Mes$_4$** are based on indolocarbazole units (Fig. 44a).[172] λ_{max}^{PL} was 387 and 441 nm, with very small FWHM values of 21 and 17 nm (toluene solution) for **ICz-Mes$_3$** and **DICz-Mes$_4$**, respectively. The PLQY values were 66/70% under N_2 and 43/47% in air saturated solutions, and the corresponding ΔE_{ST} values were 0.39/0.26 eV. **ICzMes$_3$** did not show TADF due to its large ΔE_{ST}, whereas **DiICzMes$_4$** showed weak, but unambiguous TADF. OLEDs had an EML of DPEPO host:**DiICzMes$_4$** (10 wt%). The very slow RISC rate of **DiICzMes$_4$** (k_{RISC} $1.8 \times 10^2\ s^{-1}$) was insufficient to enable triplet harvesting even at low current densities, and **DiICzMes$_4$** acted as a fluorescent dopant by harvesting only the singlet excitons, giving $EQE_{max} < 5\%$. Therefore, **DiICzMes$_4$** was utilised as a terminal emitter in a hyperfluorescent OLED with a D–A–D TADF co-host which was co-evaporated at 35 wt% in the EML, alongside 1% **DiICzMes$_4$** and bulk host DPEPO. The resulting OLEDs showed deep-blue emission from **DiICzMes$_4$** [CIE of (0.15, 0.11)] with an EQE_{max} 16.5% enabled by triplet harvesting of the D–A–D co-host.

The related tricarbazole molecules **t3IDCz** and **p3IDCz** (Fig. 44a) were reported very recently.[173] Blue photoluminescence was obtained with PLQYs 92–100% and λ_{max}^{PL} 470 nm (doped film). The calculated k_{RISC} values were in the range 0.68–$1.00 \times 10^4\ s^{-1}$, which are consistent with the experimental thin film data. ΔE_{ST} values were ≈0.20 eV (in frozen THF). Using an EML of mixed mCP:mCBP-1CN host:emitter (1 wt%) both **t3IDCz** and **p3IDCz** gave blue OLEDs (λ_{max}^{EL} 472 nm, FWHM 23–28 nm) with $EQE_{max} > 30\%$, but with extensive roll-off at 100 cd m^{-2} (Fig. 44b and c). The tricarbazole derivative ***t*Bu-TiTAT** (Fig. 44a) has ΔE_{ST} 0.36 eV in toluene, PLQY 76% (1% doped in mCP film) and gave blue OLEDs (λ_{max}^{EL} 454 nm, FWHM 55 nm) with EQE_{max} 12.6% and EQE 7.1% at 100 cd m^{-2}.[174]

The MR effect has been exploited to induce narrow emission in the indoloacridine derivatives **pSFlAc1** and **pSFlAc2** (Fig. 45a).[175] Both the emitters show deep-blue emission with λ_{max}^{PL} 443 and 450 nm and FWHM 18 nm in toluene solution, and ΔE_{ST} 0.29 and 0.31 eV. The PLQY values were >80% in DPEPO host films. OLEDs with an EML of α,β-ADH host:emitter (*X* wt%) gave EQE_{max} ≈ 9% and only limited roll-off to 7.3% and 8.2% at 5000 cd m^{-2} (Fig. 45c). The emission was deep-blue with CIE(0.147, 0.054) and (0.142, 0.066) for **pSFlAc1** and **pSFlAc2** devices, respectively, with FWHM 19 nm for both devices (Fig. 45b). All devices showed the same EL spectra within the dopant range 1–15% which was assigned to alleviated intermolecular interactions due to the orthogonal spirofluorene units. Furthermore, TADF-sensitised devices with an EML of mCBP:m4TCzPhBN (30 wt%):**pSFlAc1** or **pSFlAc2** (1–3 wt%) gave EQE_{max} 24.9% and 31.4%, respectively, retaining deep-blue emission, but with extensive efficiency roll-off at high brightness.

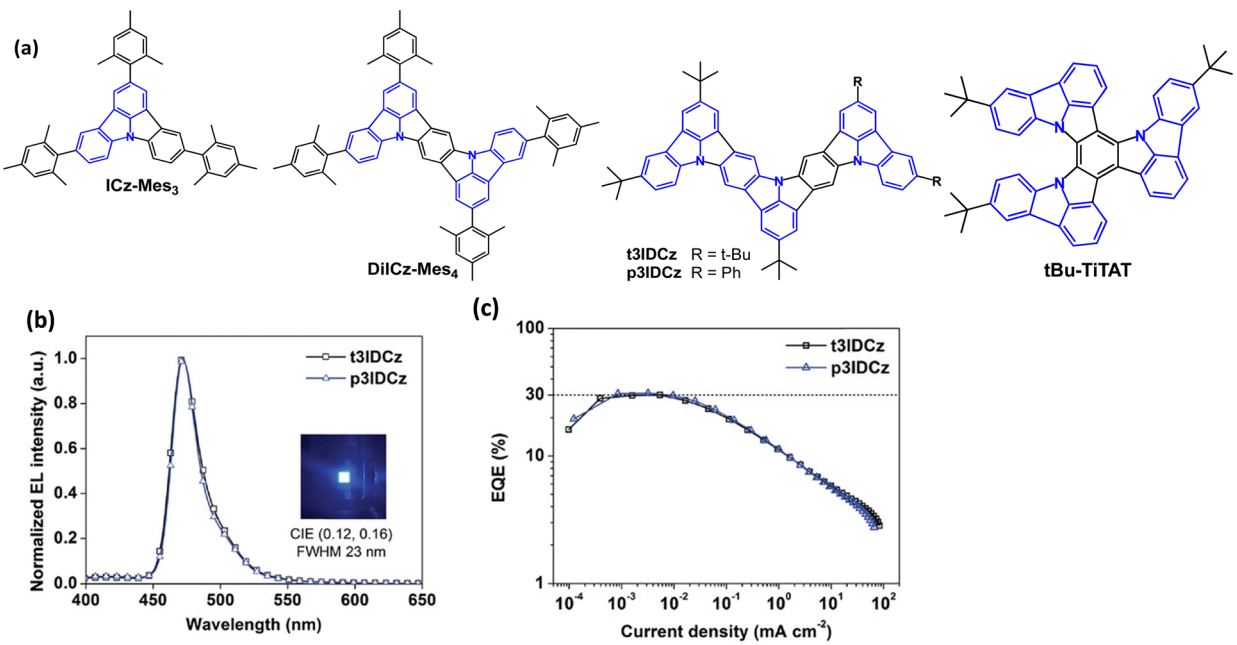

Fig. 44 (a) Molecular structures of **ICz-Mes$_3$** and **DiICz-Mes$_4$**, **t3IDCz**, **p3IDCz** and ***t*Bu-TiTAT**. (b) EL spectra of **t3IDCz** and **p3IDCz**. (c) EQE–current density curves.[173] Copyright 2022 Wiley-VCH.

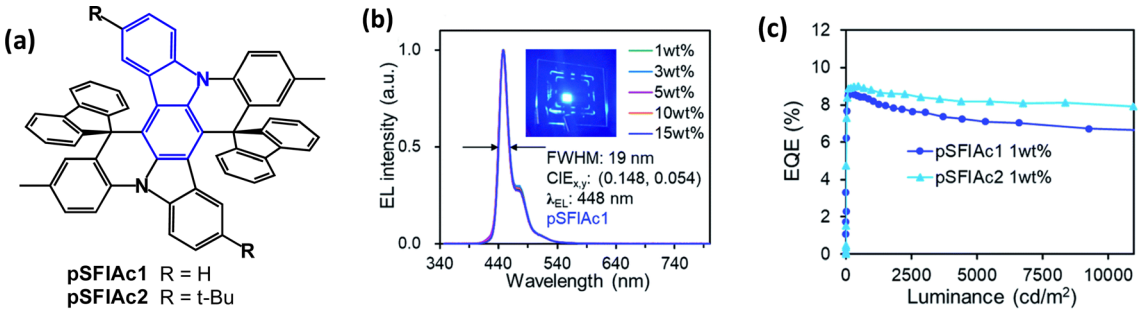

Fig. 45 (a) Molecular structures of **pSFIAc1** and **pSFIAc2**. (b) EL spectra and (c) EQE–luminance curves.[175] Copyright 2022 The Royal Society of Chemistry.

5 Conclusions and outlook

This review has demonstrated how in the last decade fused-ring carbazole derivatives have had a major impact in all the key aspects of OLED materials development – namely, traditional fluorophores, stable bipolar hosts for PhOLEDs, TADF emitters and MR emitters. These advances are set to continue at a rapid pace with a combination of precise molecular engineering, detailed photophysical analysis, high-level theory and device fabrication strategies. Fused carbazoles offer the benefits of inherent molecular rigidity, narrow band emission, small ΔE_{ST}, high PLQY, good thermal stability and structural versatility. MR-TADF emitters are currently stealing the show and further striking advances are no doubt already in the pipeline: improving k_{RISC} is a key issue for limiting the OLED efficiency roll-off. As noted recently,[172] a direct comparison between reported RISC rates from different research teams is challenging because of the different methods that can be used to obtain the data. Moreover, TD-DFT calculations which are routinely used to probe the S and T states of D–A TADF emitters, may not be reliable for MR-TADF emitters, thus hindering computationally guided molecular design.[176] The race to achieve ever higher EQE values is only part of the story. As highlighted in recent reviews, a critical goal is to achieve long-lifetime OLEDs at higher brightness and lower operating voltage for global commercialisation in phones, laptops, smart consumer devices and lighting, especially in the blue region where there are critical issues with short operational lifetimes.[177,178] To this end, further work is needed in understanding material degradation phenomena and device failure mechanisms under electrical stress. The continued development of narrowband pure-red emitters to meet the BT.2020 colour standard for ultra-high-definition displays is also imperative, with high colour purity especially important to offset the reduced sensitivity of humans' eyes in the red region.

We are not aware of any reports of fused carbazoles as units in emissive polymers, although TADF polymers, some of which incorporate (non-fused) carbazole, are prominent materials in OLEDs. Doped or non-doped polymer EMLs have been tailored for orange-red, green or blue emission.[179–182] Solution-processing and ink-jet printing of polymers has a high material utilisation rate and does not require harsh fabrication conditions for the EML. The technology, therefore, offers advantages over vacuum evaporation techniques, especially for large-area production on flexible substrates, as reviewed recently.[183] TADF-active polymer nanoparticles and films also have great potential in sensing and imaging applications.[184] Indeed, recent conferences have featured exciting new directions that are at the frontiers of electroluminescent materials including wearable and implantable light emitters for healthcare monitoring, biophotonics, and information and quantum optics.[185–187] TADF molecules have also been applied in X-ray scintillation and radiation detection.[188] Fused-ring carbazoles should be readily adaptable by smart synthetic chemistry to play enhanced roles in all these cutting-edge topics. Indolocarbazoles have very recently been demonstrated as efficient afterglow materials for proof-of-concept data protection, further realising their promise as versatile building blocks.[189]

In conclusion, we hope that readers are inspired by the menu of fused-ring carbazole derivatives that is now on the banquet table of optoelectronic materials, and that many colleagues will join the party and contribute to the exciting new interdisciplinary science that is on offer!

Author contributions

S. O. and M. R. B. contributed equally to writing this manuscript.

Conflicts of interest

There are no conflicts to declare.

Acknowledgements

S. O. thanks the Scientific and Technical Research Council of Turkey (TUBITAK) for the award of an International Postdoctoral Research Fellowship to visit Durham University.

References

1 B. Wex and B. R. Kaafarani, Perspective on carbazole-based organic compounds as emitters and hosts in TADF applications, *J. Mater. Chem. C*, 2017, **5**, 8622–8653.
2 P. Ledwon, Recent advances of donor-acceptor type carbazole-based molecules for light emitting applications, *Org. Electron.*, 2019, **75**, 105422.

3 G. Sathiyan, E. K. T. Sivakumar, R. Ganesamoorthy, R. Thangamuthu and P. Sakthivel, Review of carbazole based conjugated molecules for highly efficient organic solar cell application, *Tetrahedron Lett.*, 2016, **57**, 243–252.
4 L. Gao, T. H. Schloemer, F. Zhang, X. Chen, C. Xiao, K. Zhu and A. Sellinger, Carbazole-Based Hole-Transport Materials for High-Efficiency and Stable Perovskite Solar Cells, *ACS Appl. Energy Mater.*, 2020, **3**, 4492–4498.
5 L. Yang, J. Wang, L. Yang, C. Zhang, R. Zhang, Z. Zhang, B. Liu and C. Jiang, Fluorescent paper sensor fabricated by carbazole-based probes for dual visual detection of Cu^{2+} and gaseous H_2S, *RSC Adv.*, 2016, **6**, 56384–56391.
6 A. Pundi, C.-J. Chang, J. Chen, S.-R. Hsieh and M.-C. Lee, A chiral carbazole based sensor for sequential ''on-off-on'' fluorescence detection of Fe^{3+} and tryptophan/histidine, *Sens. Actuators, B*, 2021, **328**, 129084.
7 M. Más-Montoya, J. P. Cerón-Carrasco, S. Hamao, R. Eguchi, Y. Kubozono, A. Tárraga and D. Curiel, Synthesis and characterization of carbazolo[2,1-*a*]carbazole in thin film and single crystal field-effect transistors, *J. Mater. Chem. C*, 2017, **5**, 7020–7027.
8 C.-H. Chen, Y. Wang, T. Michinobu, S.-W. Chang, Y.-C. Chiu, C.-Y. Ke and G.-S. Liou, Donor–Acceptor Effect of Carbazole-Based Conjugated Polymer Electrets on Photoresponsive Flash Organic Field-Effect Transistor Memories, *ACS Appl. Mater. Interfaces*, 2020, **12**, 6144–6150.
9 L. J. O'Driscoll, X. Wang, M. Jay, A. S. Batsanov, H. Sadeghi, C. J. Lambert, B. J. Robinson and M. R. Bryce, Carbazole-Based Tetrapodal Anchor Groups for Gold Surfaces: Synthesis and Conductance Properties, *Angew. Chem., Int. Ed.*, 2020, **59**, 882–889.
10 E. G. Cansu-Ergun and A. M. Önal, Carbazole based electrochromic polymers bearing ethylenedioxy and propylenedioxy scaffolds, *J. Electroanal. Chem.*, 2018, **815**, 158–165.
11 Z. Xu, Y. Zhang, B. Wang, Z. Liu, J. Zhao and Y. Xie, Yellow-to-blue switching of indole[3,2-*b*]carbazole-based electrochromic polymers and the corresponding electrochromic devices with outstanding photopic contrast, fast switching speed, and satisfactory cycling stability, *Electrochim. Acta*, 2019, **302**, 373–384.
12 P. Gratia, A. Magomedov, T. Malinauskas, M. Daskeviciene, A. Abate, S. Ahmad, M. Grätzel, V. Getautis and M. K. Nazeeruddin, A Methoxydiphenylamine-Substituted Carbazole Twin Derivative: An Efficient Hole-Transporting Material for Perovskite Solar Cells, *Angew. Chem., Int. Ed.*, 2015, **54**, 11409–11413.
13 J. Ji, P. Li, Q. Tian, W. Feng and C. Wu, Three new carbazole derivatives with high thermal stability as host for efficient green phosphorescent organic-light emitting diodes, *Dyes Pigm.*, 2019, **171**, 107670.
14 F. Liu, J. Zou, Q. He, C. Tang, L. Xie, B. Peng, W. Wei, Y. Cao and W. Huang, Carbazole end-capped pyrene starburst with enhanced electrochemical stability and device performance, *J. Polym. Sci., Part A: Polym. Chem.*, 2010, **48**, 4943–4949.
15 X.-D. Zhu, Q.-S. Tian, Q. Zheng, X.-C. Tao, Y. Yuan, Y.-J. Yu, Y. Li, Z.-Q. Jiang and L.-S. Liao, A sky-blue thermally activated delayed fluorescence emitter based on multi-modified carbazole donor for efficient organic light-emitting diodes, *Org. Electron.*, 2019, **68**, 113–120.
16 I. A. Pocock, A. M. Alotaibi, K. Jagdev, C. Prior, G. R. Burgess, L. Male and R. S. Grainger, Direct formation of 4,5-disubstituted carbazoles via regioselective dilithiation, *Chem. Commun.*, 2021, **57**, 7252–7255.
17 J.-F. Morin, M. Leclerc, D. Adès and A. Siove, Polycarbazoles: 25 Years of Progress, *Macromol. Rapid Commun.*, 2005, **26**, 761–778.
18 C. Chen, K. C. Chong, Y. Pan, G. Qi, S. Xu and B. Liu, Revisiting Carbazole: Origin, Impurity, and Properties, *ACS Mater. Lett.*, 2021, **3**, 1081–1087.
19 H. Xiao, D.-S. Zheng, L.-Y. Zhang, L.-J. Xu and Z.-N. Chen, Ultra-Long Room Temperature Phosphorescence with the Efficiency Over 64% Induced by 1‰ Impurity Doping, *Adv. Funct. Mater.*, 2023, 2214241.
20 N. A. Kukhta, T. Matulaitis, D. Volyniuk, K. Ivaniuk, P. Turyk, P. Stakhira, J. V. Grazulevicius and A. P. Monkman, Deep-Blue High-Efficiency TTA OLED Using *Para*- and *Meta*-Conjugated Cyanotriphenylbenzene and Carbazole Derivatives as Emitter and Host, *J. Phys. Chem. Lett.*, 2017, **8**, 6199–6205.
21 X.-F. Luo, F.-L. Li, J.-W. Zou, Q. Zou, J. Su, M.-X. Mao and Y.-X. Zheng, A Series of Fused Carbazole/Carbonyl Based Blue to Yellow-Green Thermally Activated Delayed Fluorescence Materials for Efficient Organic Light-Emitting Diodes, *Adv. Opt. Mater.*, 2021, **9**, 2100784.
22 G. Hong, X. Gan, C. Leonhardt, Z. Zhang, J. Seibert, J. M. Busch and S. Bräse, A Brief History of OLEDs---Emitter Development and Industry Milestones, *Adv. Mater.*, 2021, **33**, 2005630.
23 M. Godumala, S. Choi, M. J. Cho and D. H. Choi, Thermally activated delayed fluorescence blue dopants and hosts: from the design strategy to organic light-emitting diode applications, *J. Mater. Chem. C*, 2016, **4**, 11355–11381.
24 A. Monkman, Why Do We Still Need a Stable Long Lifetime Deep Blue OLED Emitter?, *ACS Appl. Mater. Interfaces*, 2022, **14**, 20463–20467.
25 M. A. Baldo, D. F. O'Brien, M. E. Thompson and S. R. Forrest, Excitonic singlet-triplet ratio in a semiconducting organic thin film, *Phys. Rev. B: Condens. Matter Mater. Phys.*, 1999, **60**, 14422–14428.
26 C. Adachi, M. A. Baldo, M. E. Thompson and S. R. Forrest, Nearly 100% internal phosphorescence efficiency in an organic light-emitting device, *J. Appl. Phys.*, 2001, **90**, 5048–5051.
27 Y. Kawamura, J. Brooks, J. J. Brown, H. Sasabe and C. Adachi, Intermolecular Interaction and a Concentration-Quenching Mechanism of Phosphorescent Ir(III) Complexes in a Solid Film, *Phys. Rev. Lett.*, 2006, **96**, 17404.
28 J. H. Yun, J. Lim, W. J. Chung and J. Y. Lee, Exciton stabilizing high triplet energy n-type hosts for blue phosphorescent organic light-emitting diodes, *Dyes Pigm.*, 2021, **190**, 109297.

29 C.-J. Zheng, J. Ye, M.-F. Lo, M.-K. Fung, X.-M. Ou, X.-H. Zhang and C.-S. Lee, New Ambipolar Hosts Based on Carbazole and 4,5-Diazafluorene Units for Highly Efficient Blue Phosphorescent OLEDs with Low Efficiency Roll-Off, *Chem. Mater.*, 2012, **24**, 643–650.
30 M. Hong, M. K. Ravva, P. Winget and J.-L. Brédas, Effect of Substituents on the Electronic Structure and Degradation Process in Carbazole Derivatives for Blue OLED Host Materials, *Chem. Mater.*, 2016, **28**, 5791–5798.
31 W. Qu, Z. Gao, W. Li, X. Fan, Y. Shi, Y. Miao, Z. Wu, J. Huang, H. Wang and B. Wei, Carbazole/triazine based host materials for high-performance green PhOLEDs, *Dyes Pigm.*, 2022, **199**, 110086.
32 M.-J. Yang and T. Tsutsui, Use of Poly(9-vinylcarbazole) as Host Material for Iridium Complexes in High-Efficiency Organic Light-Emitting Devices, *Jpn. J. Appl. Phys.*, 2000, **39**, 828.
33 C.-J. Chiang, A. Kimyonok, M. K. Etherington, G. C. Griffiths, V. Jankus, F. Turksoy and A. P. Monkman, Ultrahigh Efficiency Fluorescent Single and Bi-Layer Organic Light Emitting Diodes: The Key Role of Triplet Fusion, *Adv. Funct. Mater.*, 2013, **23**, 739–746.
34 V. Jankus, C.-J. Chiang, F. Dias and A. P. Monkman, Deep Blue Exciplex Organic Light-Emitting Diodes with Enhanced Efficiency; P-type or E-type Triplet Conversion to Singlet Excitons?, *Adv. Mater.*, 2013, **25**, 1455–1459.
35 Y. Liu, H. Liu, Q. Bai, C. Du, A. Shang, D. Jiang, X. Tang and P. Lu, Pyrene[4,5-*d*]imidazole-Based Derivatives with Hybridized Local and Charge-Transfer State for Highly Efficient Blue and White Organic Light-Emitting Diodes with Low Efficiency Roll-Off, *ACS Appl. Mater. Interfaces*, 2020, **12**, 16715–16725.
36 A. Obolda, Q. Peng, C. He, T. Zhang, J. Ren, H. Ma, Z. Shuai and F. Li, Triplet–Polaron-Interaction-Induced Upconversion from Triplet to Singlet: a Possible Way to Obtain Highly Efficient OLEDs, *Adv. Mater.*, 2016, **28**, 4740–4746.
37 C. A. Parker and C. G. Hatchard, Triplet–singlet emission in fluid solutions. Phosphorescence of eosin, *Trans. Faraday Soc.*, 1961, **57**, 1894–1904.
38 A. Endo, M. Ogasawara, A. Takahashi, D. Yokoyama, Y. Kato and C. Adachi, Thermally Activated Delayed Fluorescence from Sn^{4+}–Porphyrin Complexes and Their Application to Organic Light Emitting Diodes—A Novel Mechanism for Electroluminescence, *Adv. Mater.*, 2009, **21**, 4802–4806.
39 A. Endo, K. Sato, K. Yoshimura, T. Kai, A. Kawada, H. Miyazaki and C. Adachi, Efficient up-conversion of triplet excitons into a singlet state and its application for organic light emitting diodes, *Appl. Phys. Lett.*, 2011, **98**, 083302.
40 M. K. Etherington, J. Gibson, H. F. Higginbotham, T. J. Penfold and A. P. Monkman, Revealing the spin–vibronic coupling mechanism of thermally activated delayed fluorescence, *Nat. Commun.*, 2016, **7**, 13680.
41 T. Hatakeyama, K. Shiren, K. Nakajima, S. Nomura, S. Nakatsuka, K. Kinoshita, J. Ni, Y. Ono and T. Ikuta, Ultrapure Blue Thermally Activated Delayed Fluorescence Molecules: Efficient HOMO–LUMO Separation by the Multiple Resonance Effect, *Adv. Mater.*, 2016, **28**, 2777–2781.
42 A. Chaskar, H.-F. Chen and K.-T. Wong, Bipolar Host Materials: A Chemical Approach for Highly Efficient Electrophosphorescent Devices, *Adv. Mater.*, 2011, **23**, 3876–3895.
43 Y. Tao, C. Yang and J. Qin, Organic host materials for phosphorescent organic light-emitting diodes, *Chem. Soc. Rev.*, 2011, **40**, 2943–2970.
44 Q. Wang, Q.-S. Tian, Y.-L. Zhang, X. Tang and L.-S. Liao, High-efficiency organic light-emitting diodes with exciplex hosts, *J. Mater. Chem. C*, 2019, **7**, 11329–11360.
45 T. B. Nguyen, H. Nakanotani, T. Hatakeyama and C. Adachi, The Role of Reverse Intersystem Crossing Using a TADF-Type Acceptor Molecule on the Device Stability of Exciplex-Based Organic Light-Emitting Diodes, *Adv. Mater.*, 2020, **32**, 1906614.
46 C.-C. Lee, N. R. Al Amin, J.-J. Xu, B.-C. Wang, D. Luo, K. Sutanto, S. Biring, S.-W. Liu and C.-H. Chen, Structural effect of phenylcarbazole-based molecules on the exciplex-forming co-host system to achieve highly efficient phosphorescent OLEDs with low efficiency roll-off, *J. Mater. Chem. C*, 2021, **9**, 9453–9464.
47 I. A. Wright, A. Danos, S. Montanaro, A. S. Batsanov, A. P. Monkman and M. R. Bryce, Conformational Dependence of Triplet Energies in Rotationally Hindered N- and S-Heterocyclic Dimers: New Design and Measurement Rules for High Triplet Energy OLED Host Materials, *Chem. – Eur. J.*, 2021, **27**, 6545–6556.
48 M.-H. Tsai, Y.-H. Hong, C.-H. Chang, H.-C. Su, C.-C. Wu, A. Matoliukstyte, J. Simokaitiene, S. Grigalevicius, J. V. Grazulevicius and C.-P. Hsu, 3-(9-Carbazolyl)carbazoles and 3,6-Di(9-carbazolyl)carbazoles as Effective Host Materials for Efficient Blue Organic Electrophosphorescence, *Adv. Mater.*, 2007, **19**, 862–866.
49 Y. Tsuchiya, N. Nakamura, S. Kakumachi, K. Kusuhara, C.-Y. Chan and C. Adachi, A convenient method to estimate the glass transition temperature of small organic semiconductor materials, *Chem. Commun.*, 2022, **58**, 11292–11295.
50 M.-S. Gong, J.-R. Cha and C. W. Lee, Synthesis and device properties of mCP analogues based on fused-ring carbazole moiety, *Org. Electron.*, 2017, **42**, 66–74.
51 M. Gantenbein, M. Hellstern, L. Le Pleux, M. Neuburger and M. Mayor, New 4,4′-Bis(9-carbazolyl)–Biphenyl Derivatives with Locked Carbazole–Biphenyl Junctions: High-Triplet State Energy Materials, *Chem. Mater.*, 2015, **27**, 1772–1779.
52 I. A. Wright, H. A. Al-Attar, A. S. Batsanov, A. P. Monkman and M. R. Bryce, Conformationally-restricted bicarbazoles with phenylene bridges displaying deep-blue emission and high triplet energies: systematic structure–property relationships, *Phys. Chem. Chem. Phys.*, 2018, **20**, 11867–11875.
53 S.-J. Su, H. Sasabe, T. Takeda and J. Kido, Pyridine-Containing Bipolar Host Materials for Highly Efficient Blue Phosphorescent OLEDs, *Chem. Mater.*, 2008, **20**, 1691–1693.
54 D. Kim, L. Zhu and J.-L. Brédas, Electronic Structure of Carbazole-Based Phosphine Oxides as Ambipolar Host Materials for Deep Blue Electrophosphorescence: A Density

Functional Theory Study, *Chem. Mater.*, 2012, **24**, 2604–2610.

55 S. Lee, K.-H. Kim, D. Limbach, Y.-S. Park and J.-J. Kim, Low Roll-Off and High Efficiency Orange Organic Light Emitting Diodes with Controlled Co-Doping of Green and Red Phosphorescent Dopants in an Exciplex Forming Co-Host, *Adv. Funct. Mater.*, 2013, **23**, 4105–4110.

56 J. H. Maeng, D. H. Ahn, H. Lee, Y. H. Jung, D. Karthik, J. Y. Lee and J. H. Kwon, Rigid indolocarbazole donor moiety for highly efficient thermally activated delayed fluorescent device, *Dyes Pigm.*, 2020, **180**, 108485.

57 J. Wei, C. Zhang, D. Zhang, Y. Zhang, Z. Liu, Z. Li, G. Yu and L. Duan, Indolo[3,2,1-*jk*]carbazole Embedded Multiple-Resonance Fluorophors for Narrowband Deep-blue Electroluminescence with EQE $\approx$ 34.7% and CIE_y $\approx$ 0.085, *Angew. Chem., Int. Ed.*, 2021, **60**, 12269–12273.

58 S. Xiang, X. Lv, S. Sun, Q. Zhang, Z. Huang, R. Guo, H. Gu, S. Liu and L. Wang, To improve the efficiency of thermally activated delayed fluorescence OLEDs by controlling the horizontal orientation through optimizing stereoscopic and linear structures of indolocarbazole isomers, *J. Mater. Chem. C*, 2018, **6**, 5812–5820.

59 R. Braveenth, H. Lee, J. D. Park, K. J. Yang, S. J. Hwang, K. R. Naveen, R. Lampande and J. H. Kwon, Achieving Narrow FWHM and High EQE Over 38% in Blue OLEDs Using Rigid Heteroatom-Based Deep Blue TADF Sensitized Host, *Adv. Funct. Mater.*, 2021, **31**, 2105805.

60 S. Yang, D. Guan, M. Yang, J. Tian, W. Chu and Z. Sun, Synthesis and characterization of novel butterfly-shaped aryl-substituted indolo[2,3-*a*]carbazole derivatives, *Tetrahedron Lett.*, 2015, **56**, 2223–2227.

61 Y.-X. Zhang, Y. Yuan, Q. Wang, Y. Hu, A. Khan, Z.-Q. Jiang and L.-S. Liao, Highly efficient non-doped deep-blue organic light-emitting diodes by employing a highly rigid skeleton, *Dyes Pigm.*, 2018, **158**, 396–401.

62 R. Mai, X. Wu, Y. Jiang, Y. Meng, B. Liu, X. Hu, J. Roncali, G. Zhou, J.-M. Liu, K. Kempa and J. Gao, An efficient multifunctional material based on polyether-substituted indolocarbazole for perovskite solar cells and solution-processed non-doped OLEDs, *J. Mater. Chem. A*, 2019, **7**, 1539–1547.

63 F. de Jong, M. Daniels, L. Vega-Castillo, K. Kennes, C. Martín, G. de Miguel, M. Cano, M. Pérez-Morales, J. Hofkens, W. Dehaen and M. Van der Auweraer, 5,10-Dihydrobenzo[*a*]indolo[2,3-*c*]carbazoles as Novel OLED Emitters, *J. Phys. Chem. B*, 2019, **123**, 1400–1411.

64 V. V. Patil, K. H. Lee and J. Y. Lee, Isomeric fused benzocarbazole as a chromophore for blue fluorescent organic light-emitting diodes, *J. Mater. Chem. C*, 2020, **8**, 8320–8327.

65 V. V. Patil, K. H. Lee and J. Y. Lee, A novel fluorene–indolocarbazole hybrid chromophore to assemble high efficiency deep-blue fluorescent emitters with extended device lifetime, *J. Mater. Chem. C*, 2020, **8**, 3051–3057.

66 V. V. Patil, J. Lim and J. Y. Lee, Strategic Synchronization of 7,7-Dimethyl-5,7-dihydroindeno[2,1-*b*]carbazole for Narrow-Band, Pure Violet Organic Light-Emitting Diodes with an Efficiency of $>5\%$ and a CIE_y Coordinate of <0.03, *ACS Appl. Mater. Interfaces*, 2021, **13**, 14440–14446.

67 X. Liang, Z.-P. Yan, H.-B. Han, Z.-G. Wu, Y.-X. Zheng, H. Meng, J.-L. Zuo and W. Huang, Peripheral Amplification of Multi-Resonance Induced Thermally Activated Delayed Fluorescence for Highly Efficient OLEDs, *Angew. Chem., Int. Ed.*, 2018, **57**, 11316–11320.

68 D. Sun, S. M. Suresh, D. Hall, M. Zhang, C. Si, D. B. Cordes, A. M. Z. Slawin, Y. Olivier, X. Zhang and E. Zysman-Colman, The design of an extended multiple resonance TADF emitter based on a polycyclic amine/carbonyl system, *Mater. Chem. Front.*, 2020, **4**, 2018–2022.

69 H. L. Lee, W. J. Chung and J. Y. Lee, Narrowband and Pure Violet Organic Emitter with a Full Width at Half Maximum of 14 nm and y Color Coordinate of Below 0.02, *Small*, 2020, **16**, 1907569.

70 D. Zhang, L. Duan, Y. Li, H. Li, Z. Bin, D. Zhang, J. Qiao, G. Dong, L. Wang and Y. Qiu, Towards High Efficiency and Low Roll-Off Orange Electrophosphorescent Devices by Fine Tuning Singlet and Triplet Energies of Bipolar Hosts Based on Indolocarbazole/1,3,5-Triazine Hybrids, *Adv. Funct. Mater.*, 2014, **24**, 3551–3561.

71 Y. Li, D. Zhang and L. Duan, High efficiency red phosphorescent organic light-emitting diodes with low dopant concentration, low roll-off and long lifetime based on a novel host material with thermally activated delayed fluorescent properties, *Org. Electron.*, 2018, **57**, 53–59.

72 X. Song, D. Zhang, Y. Lu, C. Yin and L. Duan, Understanding and Manipulating the Interplay of Wide-Energy-Gap Host and TADF Sensitizer in High-Performance Fluorescence OLEDs, *Adv. Mater.*, 2019, **31**, 1901923.

73 R. Braveenth, I.-J. Bae, K. Raagulan, S. Kim, S. Kim, M. Kim and K. Y. Chai, Dibenzothiophene-indolocarbazole-based bipolar material: Host for green phosphorescent OLEDs and non-doped fluorescent emitter, *Dyes Pigm.*, 2019, **162**, 466–474.

74 K. Guo, H. Wang, Z. Wang, C. Si, C. Peng, G. Chen, J. Zhang, G. Wang and B. Wei, Stable green phosphorescence organic light-emitting diodes with low efficiency roll-off using a novel bipolar thermally activated delayed fluorescence material as host, *Chem. Sci.*, 2017, **8**, 1259–1268.

75 E. Y. Park, D. H. Lee, T. N. Le, C.-M. Shin, J. Lee and M. C. Suh, An indenocarbazole-based host material for solution processable green phosphorescent organic light emitting diodes, *RSC Adv.*, 2021, **11**, 29115–29123.

76 V. V. Patil, J. Lim and J. Y. Lee, C2-, C3- spirobifluorene fused carbazole modified triazine as an electron transport type host of exciplex, *Dyes Pigm.*, 2021, **189**, 109247.

77 X.-H. Zheng, J.-W. Zhao, T.-T. Huang, X. Chen, C. Cao, G.-X. Yang, Z.-H. Lin, Q.-X. Tong, S.-L. Tao and D. Liu, Versatile Host Materials for Highly-Efficient Green, Red Phosphorescent and White Organic Light-Emitting Diodes, *ChemElectroChem*, 2019, **6**, 5810–5818.

78 Y. Hiraga, R. Kuwahara and T. Hatta, Novel indolo[3,2,1-*jk*]carbazole-based bipolar host material for highly efficient

thermally activated delayed-fluorescence organic light-emitting diodes, *Tetrahedron*, 2021, **94**, 132317.

79 A. Arai, H. Sasabe, K. Nakao, Y. Masuda and J. Kido, π-Extended Carbazole Derivatives as Host Materials for Highly Efficient and Long-Life Green Phosphorescent Organic Light-Emitting Diodes, *Chem. – Eur. J.*, 2021, **27**, 4971–4976.

80 J. M. Choi, J. H. Kim, Y. J. Kang and J. Y. Lee, Development of an exciplex type mixed host using a pyrrolocarbazole type material for extended lifetime in green phosphorescent organic light-emitting diodes, *Org. Electron.*, 2017, **49**, 393–399.

81 P. L. dos Santos, J. S. Ward, A. S. Batsanov, M. R. Bryce and A. P. Monkman, Optical and Polarity Control of Donor–Acceptor Conformation and Their Charge-Transfer States in Thermally Activated Delayed-Fluorescence Molecules, *J. Phys. Chem. C*, 2017, **121**, 16462–16469.

82 K. Wang, C.-J. Zheng, W. Liu, K. Liang, Y.-Z. Shi, S.-L. Tao, C.-S. Lee, X.-M. Ou and X.-H. Zhang, Avoiding Energy Loss on TADF Emitters: Controlling the Dual Conformations of D–A Structure Molecules Based on the Pseudoplanar Segments, *Adv. Mater.*, 2017, **29**, 1701476.

83 D.-G. Chen, T.-C. Lin, C.-L. Chen, Y.-T. Chen, Y.-A. Chen, G.-H. Lee, P.-T. Chou, C.-W. Liao, P.-C. Chiu, C.-H. Chang, Y.-J. Lien and Y. Chi, Optically Triggered Planarization of Boryl-Substituted Phenoxazine: Another Horizon of TADF Molecules and High-Performance OLEDs, *ACS Appl. Mater. Interfaces*, 2018, **10**, 12886–12896.

84 K. Masui, H. Nakanotani and C. Adachi, Analysis of exciton annihilation in high-efficiency sky-blue organic light-emitting diodes with thermally activated delayed fluorescence, *Org. Electron.*, 2013, **14**, 2721–2726.

85 C. S. Oh, H. L. Lee, S. H. Han and J. Y. Lee, Rational Molecular Design Overcoming the Long Delayed Fluorescence Lifetime and Serious Efficiency Roll-Off in Blue Thermally Activated Delayed Fluorescent Devices, *Chem. – Eur. J.*, 2019, **25**, 642–648.

86 R. K. Konidena, K. R. J. Thomas and J. W. Park, Recent Advances in the Design of Multi-Substituted Carbazoles for Optoelectronics: Synthesis and Structure–Property Outlook, *ChemPhotoChem*, 2022, **6**, e202200059.

87 D. Zhang, X. Song, M. Cai, H. Kaji and L. Duan, Versatile Indolocarbazole-Isomer Derivatives as Highly Emissive Emitters and Ideal Hosts for Thermally Activated Delayed Fluorescent OLEDs with Alleviated Efficiency Roll-Off, *Adv. Mater.*, 2018, **30**, 1705406.

88 K. Sato, K. Shizu, K. Yoshimura, A. Kawada, H. Miyazaki and C. Adachi, Organic Luminescent Molecule with Energetically Equivalent Singlet and Triplet Excited States for Organic Light-Emitting Diodes, *Phys. Rev. Lett.*, 2013, **110**, 247401.

89 Q. Zhang, H. Kuwabara, W. J. Potscavage, S. Huang, Y. Hatae, T. Shibata and C. Adachi, Anthraquinone-Based Intramolecular Charge-Transfer Compounds: Computational Molecular Design, Thermally Activated Delayed Fluorescence, and Highly Efficient Red Electroluminescence, *J. Am. Chem. Soc.*, 2014, **136**, 18070–18081.

90 D. Karthik, S. Y. Lee, D. H. Ahn, H. Lee, J. Y. Lee, J. H. Kwon and J. H. Park, Comparative analysis of various indolocarbazole-based emitters on thermally activated delayed fluorescence performances, *Org. Electron.*, 2019, **74**, 282–289.

91 M. Kim, S. K. Jeon, S.-H. Hwang, S.-S. Lee, E. Yu and J. Y. Lee, Correlation of Molecular Structure with Photophysical Properties and Device Performances of Thermally Activated Delayed Fluorescent Emitters, *J. Phys. Chem. C*, 2016, **120**, 2485–2493.

92 H. J. Lee, H. L. Lee, S. H. Han and J. Y. Lee, Novel secondary acceptor based molecular design for superb lifetime in thermally activated delayed fluorescent organic light-emitting diodes through high bond energy and fast up-conversion, *Chem. Eng. J.*, 2022, **427**, 130988.

93 J. Wang, J. Zhang, C. Jiang, C. Yao and X. Xi, Effective Design Strategy for Aggregation-Induced Emission and Thermally Activated Delayed Fluorescence Emitters Achieving 18% External Quantum Efficiency Pure-Blue OLEDs with Extremely Low Roll-Off, *ACS Appl. Mater. Interfaces*, 2021, **13**, 57713–57724.

94 M. R. Bryce, Aggregation-induced delayed fluorescence (AIDF) materials: a new break-through for nondoped OLEDs, *Sci. China: Chem.*, 2017, **60**, 1561–1562.

95 J. Guo, X.-L. Li, H. Nie, W. Luo, R. Hu, A. Qin, Z. Zhao, S.-J. Su and B. Z. Tang, Robust Luminescent Materials with Prominent Aggregation-Induced Emission and Thermally Activated Delayed Fluorescence for High-Performance Organic Light-Emitting Diodes, *Chem. Mater.*, 2017, **29**, 3623–3631.

96 D. Liu, J. Y. Wei, W. W. Tian, W. Jiang, Y. M. Sun, Z. Zhao and B. Z. Tang, Endowing TADF luminophors with AIE properties through adjusting flexible dendrons for highly efficient solution-processed nondoped OLEDs, *Chem. Sci.*, 2020, **11**, 7194–7203.

97 J. H. Kim, M. Eum, T. H. Kim and J. Y. Lee, A novel pyrrolocarbazole donor for stable and highly efficient thermally activated delayed fluorescent emitters, *Dyes Pigm.*, 2017, **136**, 529–534.

98 W.-L. Tsai, M.-H. Huang, W.-K. Lee, Y.-J. Hsu, K.-C. Pan, Y.-H. Huang, H.-C. Ting, M. Sarma, Y.-Y. Ho, H.-C. Hu, C.-C. Chen, M.-T. Lee, K.-T. Wong and C.-C. Wu, A versatile thermally activated delayed fluorescence emitter for both highly efficient doped and non-doped organic light emitting devices, *Chem. Commun.*, 2015, **51**, 13662–13665.

99 J. G. Yu, S. H. Han, H. L. Lee, W. P. Hong and J. Y. Lee, A novel molecular design employing a backbone freezing linker for improved efficiency, sharpened emission and long lifetime in thermally activated delayed fluorescence emitters, *J. Mater. Chem. C*, 2019, **7**, 2919–2926.

100 H. Kang, S. O. Jeon, Y. S. Chung, M. Sim, J. S. Kim, J. Kim, H. Lee, S.-G. Ihn, S. Kim and J. Hong, High-efficiency blue organic light-emitting Diodes using emissive carbazole-triazine-based donor-acceptor molecules with high reverse intersystem crossing rates, *Org. Electron.*, 2019, **75**, 105399.

101 X. Zheng, F. Cao, C. Wang, T. Tsuboi, Y. Zhu, Q. Ai, C. Deng, D. Wang, L. Su, Z. Liu and Q. Zhang, Expanding

the hole delocalization range in excited molecules for stable organic light-emitting diodes employing thermally activated delayed fluorescence, *J. Mater. Chem. C*, 2020, **8**, 10021–10030.

102 Z. Zhang, E. Crovini, P. L. dos Santos, B. A. Naqvi, D. B. Cordes, A. M. Z. Slawin, P. Sahay, W. Brütting, I. D. W. Samuel, S. Bräse and E. Zysman-Colman, Efficient Sky-Blue Organic Light-Emitting Diodes Using a Highly Horizontally Oriented Thermally Activated Delayed Fluorescence Emitter, *Adv. Opt. Mater.*, 2020, **8**, 2001354.

103 E. Crovini, Z. Zhang, Y. Kusakabe, Y. Ren, Y. Wada, B. A. Naqvi, P. Sahay, T. Matulaitis, S. Diesing, I. D. W. Samuel, W. Brütting, K. Suzuki, H. Kaji, S. Bräse and E. Zysman-Colman, Effect of a twin-emitter design strategy on a previously reported thermally activated delayed fluorescence organic light-emitting diode, *Beilstein J. Org. Chem.*, 2021, **17**, 2894–2905.

104 D. H. Ahn, S. W. Kim, H. Lee, I. J. Ko, D. Karthik, J. Y. Lee and J. H. Kwon, Highly efficient blue thermally activated delayed fluorescence emitters based on symmetrical and rigid oxygen-bridged boron acceptors, *Nat. Photonics*, 2019, **13**, 540–546.

105 Y. H. Lee, S. Park, J. Oh, S.-J. Woo, A. Kumar, J.-J. Kim, J. Jung, S. Yoo and M. H. Lee, High-Efficiency Sky Blue to Ultradeep Blue Thermally Activated Delayed Fluorescent Diodes Based on Ortho-Carbazole-Appended Triarylboron Emitters: Above 32% External Quantum Efficiency in Blue Devices, *Adv. Opt. Mater.*, 2018, **6**, 1800385.

106 A. Shuto, T. Kushida, T. Fukushima, H. Kaji and S. Yamaguchi, π-Extended Planarized Triphenylboranes with Thiophene Spacers, *Org. Lett.*, 2013, **15**, 6234–6237.

107 Y. Kitamoto, T. Namikawa, D. Ikemizu, Y. Miyata, T. Suzuki, H. Kita, T. Sato and S. Oi, Light blue and green thermally activated delayed fluorescence from 10H-phenoxaborin-derivatives and their application to organic light-emitting diodes, *J. Mater. Chem. C*, 2015, **3**, 9122–9130.

108 Y. Kitamoto, T. Namikawa, T. Suzuki, Y. Miyata, H. Kita, T. Sato and S. Oi, Dimesitylarylborane-based luminescent emitters exhibiting highly-efficient thermally activated delayed fluorescence for organic light-emitting diodes, *Org. Electron.*, 2016, **34**, 208–217.

109 K. Suzuki, S. Kubo, K. Shizu, T. Fukushima, A. Wakamiya, Y. Murata, C. Adachi and H. Kaji, Triarylboron-Based Fluorescent Organic Light-Emitting Diodes with External Quantum Efficiencies Exceeding 20%, *Angew. Chem., Int. Ed.*, 2015, **54**, 15231–15235.

110 M. Numata, T. Yasuda and C. Adachi, High efficiency pure blue thermally activated delayed fluorescence molecules having 10*H*-phenoxaborin and acridan units, *Chem. Commun.*, 2015, **51**, 9443–9446.

111 J. Hwang, C. W. Koh, J. M. Ha, H. Y. Woo, S. Park, M. J. Cho and D. H. Choi, Aryl-Annulated[3,2-*a*]Carbazole-Based Deep-Blue Soluble Emitters for High-Efficiency Solution-Processed Thermally Activated Delayed Fluorescence Organic Light-Emitting Diodes with $CIE_y < 0.1$, *ACS Appl. Mater. Interfaces*, 2021, **13**, 61454–61462.

112 J. Hwang, H. Kang, J.-E. Jeong, H. Y. Woo, M. J. Cho, S. Park and D. H. Choi, Donor engineered Deep-Blue emitters for tuning luminescence mechanism in Solution-Processed OLEDs, *Chem. Eng. J.*, 2021, **416**, 129185.

113 G. Meng, H. Dai, Q. Wang, J. Zhou, T. Fan, X. Zeng, X. Wang, Y. Zhang, D. Yang, D. Ma, D. Zhang and L. Duan, High-efficiency and stable short-delayed fluorescence emitters with hybrid long- and short-range charge-transfer excitations, *Nat. Commun.*, 2023, **14**, 2394.

114 D. Zhang, C. Zhao, Y. Zhang, X. Song, P. Wei, M. Cai and L. Duan, Highly Efficient Full-Color Thermally Activated Delayed Fluorescent Organic Light-Emitting Diodes: Extremely Low Efficiency Roll-Off Utilizing a Host with Small Singlet–Triplet Splitting, *ACS Appl. Mater. Interfaces*, 2017, **9**, 4769–4777.

115 X. Lv, R. Huang, S. Sun, Q. Zhang, S. Xiang, S. Ye, P. Leng, F. B. Dias and L. Wang, Blue TADF Emitters Based on Indenocarbazole Derivatives with High Photoluminescence and Electroluminescence Efficiencies, *ACS Appl. Mater. Interfaces*, 2019, **11**, 10758–10767.

116 M. Inoue, T. SereviŁius, H. Nakanotani, K. Yoshida, T. Matsushima, S. JurškŁnas and C. Adachi, Effect of reverse intersystem crossing rate to suppress efficiency roll-off in organic light-emitting diodes with thermally activated delayed fluorescence emitters, *Chem. Phys. Lett.*, 2016, **644**, 62–67.

117 Y. Im, M. Kim, Y. J. Cho, J.-A. Seo, K. S. Yook and J. Y. Lee, Molecular Design Strategy of Organic Thermally Activated Delayed Fluorescence Emitters, *Chem. Mater.*, 2017, **29**, 1946–1963.

118 G. H. Kim, R. Lampande, J. B. Im, J. M. Lee, J. Y. Lee and J. H. Kwon, Controlling the exciton lifetime of blue thermally activated delayed fluorescence emitters using a heteroatom-containing pyridoindole donor moiety, *Mater. Horiz.*, 2017, **4**, 619–624.

119 J. S. Ward, R. S. Nobuyasu, M. A. Fox, A. S. Batsanov, J. Santos, F. B. Dias and M. R. Bryce, Bond Rotations and Heteroatom Effects in Donor–Acceptor–Donor Molecules: Implications for Thermally Activated Delayed Fluorescence and Room Temperature Phosphorescence, *J. Org. Chem.*, 2018, **83**, 14431–14442.

120 Z. Chen, F. Ni, Z. Wu, Y. Hou, C. Zhong, M. Huang, G. Xie, D. Ma and C. Yang, Enhancing Spin–Orbit Coupling by Introducing a Lone Pair Electron with p Orbital Character in a Thermally Activated Delayed Fluorescence Emitter: Photophysics and Devices, *J. Phys. Chem. Lett.*, 2019, **10**, 2669–2675.

121 K. Matsuo and T. Yasuda, Blue thermally activated delayed fluorescence emitters incorporating acridan analogues with heavy group 14 elements for high-efficiency doped and non-doped OLEDs, *Chem. Sci.*, 2019, **10**, 10687–10697.

122 X.-K. Chen, B. W. Bakr, M. Auffray, Y. Tsuchiya, C. D. Sherrill, C. Adachi and J.-L. Bredas, Intramolecular Noncovalent Interactions Facilitate Thermally Activated Delayed Fluorescence (TADF), *J. Phys. Chem. Lett.*, 2019, **10**, 3260–3268.

123 T. Agou, K. Matsuo, R. Kawano, I. S. Park, T. Hosoya, H. Fukumoto, T. Kubota, Y. Mizuhata, N. Tokitoh and T. Yasuda, Pentacyclic Ladder-Heteraborin Emitters Exhibiting High-Efficiency Blue Thermally Activated Delayed Fluorescence with an Ultrashort Emission Lifetime, *ACS Mater. Lett.*, 2020, **2**, 28–34.

124 D. R. Lee, S.-H. Hwang, S. K. Jeon, C. W. Lee and J. Y. Lee, Benzofurocarbazole and benzothienocarbazole as donors for improved quantum efficiency in blue thermally activated delayed fluorescent devices, *Chem. Commun.*, 2015, **51**, 8105–8107.

125 H. Uoyama, K. Goushi, K. Shizu, H. Nomura and C. Adachi, Highly efficient organic light-emitting diodes from delayed fluorescence, *Nature*, 2012, **492**, 234–238.

126 D. R. Lee, J. M. Choi, C. W. Lee and J. Y. Lee, Ideal Molecular Design of Blue Thermally Activated Delayed Fluorescent Emitter for High Efficiency, Small Singlet–Triplet Energy Splitting, Low Efficiency Roll-Off, and Long Lifetime, *ACS Appl. Mater. Interfaces*, 2016, **8**, 23190–23196.

127 X. Zhang, C. Fuentes-Hernandez, Y. Zhang, M. W. Cooper, S. Barlow, S. R. Marder and B. Kippelen, High performance blue-emitting organic light-emitting diodes from thermally activated delayed fluorescence: A guest/host ratio study, *J. Appl. Phys.*, 2018, **124**, 55501.

128 H. Abroshan, E. Cho, V. Coropceanu and J.-L. Brédas, Suppression of Concentration Quenching in Ortho-Substituted Thermally Activated Delayed Fluorescence Emitters, *Adv. Theory Simul.*, 2020, **3**, 1900185.

129 D. J. Shin, J. Lim and J. Y. Lee, Combinatorial donor engineering for highly efficient blue thermally activated delayed fluorescence emitters with low efficiency roll-off, *J. Mater. Chem. C*, 2021, **9**, 15276–15283.

130 D. S. Kim, S. J. Yoon, K. H. Lee, J. Y. Lee and W. P. Hong, Starburst Type Benzofuroindolocarbazole Donor for High Efficiency and Long Lifetime in Thermally Activated Delayed Fluorescence Emitters, *Adv. Opt. Mater.*, 2021, **9**, 2001432.

131 Q. Zhang, S. Xiang, Z. Huang, S. Sun, S. Ye, X. Lv, W. Liu, R. Guo and L. Wang, Molecular engineering of pyrimidine-containing thermally activated delayed fluorescence emitters for highly efficient deep-blue ($CIE_y < 0.06$) organic light-emitting diodes, *Dyes Pigm.*, 2018, **155**, 51–58.

132 M. Cai, M. Auffray, D. Zhang, Y. Zhang, R. Nagata, Z. Lin, X. Tang, C.-Y. Chan, Y.-T. Lee, T. Huang, X. Song, Y. Tsuchiya, C. Adachi and L. Duan, Enhancing spin–orbital coupling in deep-blue/blue TADF emitters by minimizing the distance from the heteroatoms in donors to acceptors, *Chem. Eng. J.*, 2021, **420**, 127591.

133 D. J. Shin, S. J. Hwang, J. Lim, C. Y. Jeon, J. Y. Lee and J. H. Kwon, Reverse intersystem crossing accelerating assistant dopant for high efficiency and long lifetime in red hyperfluorescence organic light-emitting diodes, *Chem. Eng. J.*, 2022, **446**, 137181.

134 J. Lee, U. Jo and J. Y. Lee, Suppression of Dexter Energy Transfer through Modulating Donor Segments of Thermally Activated Delayed Fluorescence Assistant Dopants, *ACS Appl. Mater. Interfaces*, 2023, **15**, 21261–21269.

135 J.-A. Seo, Y. Im, S. H. Han, C. W. Lee and J. Y. Lee, Unconventional Molecular Design Approach of High-Efficiency Deep Blue Thermally Activated Delayed Fluorescent Emitters Using Indolocarbazole as an Acceptor, *ACS Appl. Mater. Interfaces*, 2017, **9**, 37864–37872.

136 Y. Im, S. H. Han and J. Y. Lee, Deep blue thermally activated delayed fluorescent emitters using CN-modified indolocarbazole as an acceptor and carbazole-derived donors, *J. Mater. Chem. C*, 2018, **6**, 5012–5017.

137 P. L. dos Santos, J. S. Ward, D. G. Congrave, A. S. Batsanov, J. Eng, J. E. Stacey, T. J. Penfold, A. P. Monkman and M. R. Bryce, Triazatruxene: A Rigid Central Donor Unit for a D–A3 Thermally Activated Delayed Fluorescence Material Exhibiting Sub-Microsecond Reverse Intersystem Crossing and Unity Quantum Yield via Multiple Singlet–Triplet State Pairs, *Adv. Sci.*, 2018, **5**, 1700989.

138 T. J. Penfold and J. Eng, Mind the GAP: quantifying the breakdown of the linear vibronic coupling Hamiltonian, *Phys. Chem. Chem. Phys.*, 2023, **25**, 7195–7204.

139 P. L. dos Santos, D. de Sa Pereira, J. Eng, J. S. Ward, M. R. Bryce, T. J. Penfold and A. P. Monkman, Fine-Tuning the Photophysics of Donor–Acceptor (D–A3) Thermally Activated Delayed Fluorescence Emitters Using Isomerisation, *ChemPhotoChem*, 2023, **7**, e202200248.

140 K. J. Kim, G. H. Kim, R. Lampande, D. H. Ahn, J. B. Im, J. S. Moon, J. K. Lee, J. Y. Lee, J. Y. Lee and J. H. Kwon, A new rigid diindolocarbazole donor moiety for high quantum efficiency thermally activated delayed fluorescence emitter, *J. Mater. Chem. C*, 2018, **6**, 1343–1348.

141 L. Chen, C. Li, E. Fu, M. Li, Y. Kuboi, Z.-Y. Li, Z. Chen, J. Chen, X. Liu, X. Tang, L. Frédéric, F. Maurel, C. Adachi, F. Mathevet and S. Zhang, A Donor–Acceptor Cage for Thermally Activated Delayed Fluorescence: toward a New Kind of TADF Exciplex Emitters, *ACS Mater. Lett.*, 2023, **5**, 1450–1455.

142 Y. Chen, S. Wang, X. Wu, Y. Xu, H. Li, Y. Liu, H. Tong and L. Wang, Triazatruxene-based small molecules with thermally activated delayed fluorescence, aggregation-induced emission and mechanochromic luminescence properties for solution-processable nondoped OLEDs, *J. Mater. Chem. C*, 2018, **6**, 12503–12508.

143 Y. Liu, X. Wu, Y. Chen, L. Chen, H. Li, W. Wang, S. Wang, H. Tian, H. Tong and L. Wang, Triazatruxene-based thermally activated delayed fluorescence small molecules with aggregation-induced emission properties for solution-processable nondoped OLEDs with low efficiency roll-off, *J. Mater. Chem. C*, 2019, **7**, 9719–9725.

144 Y. Liu, Y. Chen, H. Li, S. Wang, X. Wu, H. Tong and L. Wang, High-Performance Solution-Processed Red Thermally Activated Delayed Fluorescence OLEDs Employing Aggregation-Induced Emission-Active Triazatruxene-Based Emitters, *ACS Appl. Mater. Interfaces*, 2020, **12**, 30652–30658.

145 S. K. Pathak, H. Liu, C. Zhou, G. Xie and C. Yang, Triazatruxene based star-shaped thermally activated delayed fluorescence emitters: modulating the performance of solution-processed non-doped OLEDs via side-group engineering, *J. Mater. Chem. C*, 2021, **9**, 7363–7373.

146 N. Aizawa, Y.-J. Pu, Y. Harabuchi, A. Nihonyanagi, R. Ibuka, H. Inuzuka, B. Dhara, Y. Koyama, K. Nakayama, S. Maeda, F. Araoka and D. Miyajima, Delayed fluorescence from inverted singlet and triplet excited states, *Nature*, 2022, **609**, 502–506.

147 H. L. Lee, C. S. Oh, K. H. Lee, J. Y. Lee and W. P. Hong, Lifetime-Extending 3-(4-Phenylbenzo[4,5]thieno[3,2-*d*]pyrimidin-2-yl)benzonitrile Acceptor for Thermally Activated Delayed Fluorescence Emitters, *ACS Appl. Mater. Interfaces*, 2021, **13**, 2908–2918.

148 J. H. Maeng, R. Braveenth, Y. H. Jung, S. J. Hwang, H. Lee, H. L. Min, J. Y. Kim, C. W. Han and J. H. Kwon, Efficiency enhancement in orange red thermally activated delayed fluorescence OLEDs by using a rigid di-indolocarbazole donor moiety, *Dyes Pigm.*, 2021, **194**, 109580.

149 Q. Zhang, S. Sun, W. J. Chung, S. J. Yoon, Y. Wang, R. Guo, S. Ye, J. Y. Lee and L. Wang, Highly efficient TADF OLEDs with low efficiency roll-off based on novel acridine–carbazole hybrid donor-substituted pyrimidine derivatives, *J. Mater. Chem. C*, 2019, **7**, 12248–12255.

150 Q. Zhang, S. Sun, W. Liu, P. Leng, X. Lv, Y. Wang, H. Chen, S. Ye, S. Zhuang and L. Wang, Integrating TADF luminogens with AIE characteristics using a novel acridine–carbazole hybrid as donor for high-performance and low efficiency roll-off OLEDs, *J. Mater. Chem. C*, 2019, **7**, 9487–9495.

151 D. Yang, J.-S. Huh and J.-I. Hong, Spiro−type TADF emitters based on acridine donors and anthracenone acceptor, *Dyes Pigm.*, 2022, **197**, 109873.

152 Y. Fu, H. Liu, B. Z. Tang and Z. Zhao, Realizing efficient blue and deep-blue delayed fluorescence materials with record-beating electroluminescence efficiencies of 43.4%, *Nat. Commun.*, 2023, **14**, 2019.

153 H. Hirai, K. Nakajima, S. Nakatsuka, K. Shiren, J. Ni, S. Nomura, T. Ikuta and T. Hatakeyama, One-Step Borylation of 1,3-Diaryloxybenzenes Towards Efficient Materials for Organic Light-Emitting Diodes, *Angew. Chem., Int. Ed.*, 2015, **54**, 13581–13585.

154 K. Stavrou, A. Danos, T. Hama, T. Hatakeyama and A. Monkman, Hot Vibrational States in a High-Performance Multiple Resonance Emitter and the Effect of Excimer Quenching on Organic Light-Emitting Diodes, *ACS Appl. Mater. Interfaces*, 2021, **13**, 8643–8655.

155 S. Oda, W. Kumano, T. Hama, R. Kawasumi, K. Yoshiura and T. Hatakeyama, Carbazole-Based DABNA Analogues as Highly Efficient Thermally Activated Delayed Fluorescence Materials for Narrowband Organic Light-Emitting Diodes, *Angew. Chem., Int. Ed.*, 2021, **60**, 2882–2886.

156 Y. Zhang, D. Zhang, J. Wei, Z. Liu, Y. Lu and L. Duan, Multi-Resonance Induced Thermally Activated Delayed Fluorophores for Narrowband Green OLEDs, *Angew. Chem., Int. Ed.*, 2019, **58**, 16912–16917.

157 X.-F. Luo, H.-X. Ni, H.-L. Ma, Z.-Z. Qu, J. Wang, Y.-X. Zheng and J.-L. Zuo, Fused π-Extended Multiple-Resonance Induced Thermally Activated Delayed Fluorescence Materials for High-Efficiency and Narrowband OLEDs with Low Efficiency Roll-Off, *Adv. Opt. Mater.*, 2022, **10**, 2102513.

158 Y. Zhang, D. Zhang, T. Huang, A. J. Gillett, Y. Liu, D. Hu, L. Cui, Z. Bin, G. Li, J. Wei and L. Duan, Multi-Resonance Deep-Red Emitters with Shallow Potential-Energy Surfaces to Surpass Energy-Gap Law, *Angew. Chem., Int. Ed.*, 2021, **60**, 20498–20503.

159 X.-F. Luo, S.-Q. Song, H.-X. Ni, H. Ma, D. Yang, D. Ma, Y.-X. Zheng and J.-L. Zuo, Multiple-Resonance-Induced Thermally Activated Delayed Fluorescence Materials Based on Indolo[3,2,1-*jk*]carbazole with an Efficient Narrowband Pure-Green Electroluminescence, *Angew. Chem., Int. Ed.*, 2022, **61**, e202209984.

160 M. Yang, I. S. Park and T. Yasuda, Full-Color, Narrowband, and High-Efficiency Electroluminescence from Boron and Carbazole Embedded Polycyclic Heteroaromatics, *J. Am. Chem. Soc.*, 2020, **142**, 19468–19472.

161 Y. Zhang, G. Li, L. Wang, T. Huang, J. Wei, G. Meng, X. Wang, X. Zeng, D. Zhang and L. Duan, Fusion of Multi-Resonance Fragment with Conventional Polycyclic Aromatic Hydrocarbon for Nearly BT.2020 Green Emission, *Angew. Chem., Int. Ed.*, 2022, **61**, e202202380.

162 Y.-C. Cheng, X.-C. Fan, F. Huang, X. Xiong, J. Yu, K. Wang, C.-S. Lee and X.-H. Zhang, A Highly Twisted Carbazole-Fused DABNA Derivative as an Orange-Red TADF Emitter for OLEDs with Nearly 40% EQE, *Angew. Chem., Int. Ed.*, 2022, **61**, e202212575.

163 Y. Sano, T. Shintani, M. Hayakawa, S. Oda, M. Kondo, T. Matsushita and T. Hatakeyama, One-Shot Construction of BN-Embedded Heptadecacene Framework Exhibiting Ultra-narrowband Green Thermally Activated Delayed Fluorescence, *J. Am. Chem. Soc.*, 2023, **145**, 11504–11511.

164 H. Lee, R. Braveenth, J. Do Park, C. Y. Jeon, H. S. Lee and J. H. Kwon, Manipulating Spectral Width and Emission Wavelength towards Highly Efficient Blue Asymmetric Carbazole Fused Multi-Resonance Emitters, *ACS Appl. Mater. Interfaces*, 2022, **14**, 36927–36935.

165 E. Ravindran, H. E. Baek, H. W. Son, J. H. Park, Y.-H. Kim and M. C. Suh, Steric Rooted Multi-Resonant Thermally Activated Delayed Fluorescent Emitters for Pure Blue Organic Light Emitting Diodes with Ultralow Efficiency Roll-Off, *Adv. Funct. Mater.*, 2023, 2213461.

166 Y.-T. Lee, C.-Y. Chan, M. Tanaka, M. Mamada, K. Goushi, X. Tang, Y. Tsuchiya, H. Nakanotani and C. Adachi, Tailor-Made Multi-Resonance Terminal Emitters toward Narrowband, High-Efficiency, and Stable Hyperfluorescence Organic Light-Emitting Diodes, *Adv. Opt. Mater.*, 2022, **10**, 2200682.

167 I. S. Park, H. Min and T. Yasuda, Ultrafast Triplet–Singlet Exciton Interconversion in Narrowband Blue Organoboron Emitters Doped with Heavy Chalcogens, *Angew. Chem., Int. Ed.*, 2022, **61**, e202205684.

168 X. Cao, K. Pan, J. Miao, X. Lv, Z. Huang, F. Ni, X. Yin, Y. Wei and C. Yang, Manipulating Exciton Dynamics toward Simultaneous High-Efficiency Narrowband Electroluminescence and Photon Upconversion by a Selenium-Incorporated Multiresonance Delayed Fluorescence Emitter, *J. Am. Chem. Soc.*, 2022, **144**, 22976–22984.

169 F. Liu, Z. Cheng, Y. Jiang, L. Gao, H. Liu, H. Liu, Z. Feng, P. Lu and W. Yang, Highly Efficient Asymmetric Multiple

Resonance Thermally Activated Delayed Fluorescence Emitter with EQE of 32.8% and Extremely Low Efficiency Roll-Off, *Angew. Chem., Int. Ed.*, 2022, **61**, e202116927.

170 X. Xiong, Y.-C. Cheng, K. Wang, J. Yu and X.-H. Zhang, A comparative study of two multi-resonance TADF analogous materials integrating chalcogen atoms of different periods, *Mater. Chem. Front.*, 2023, **7**, 929–936.

171 Y. X. Hu, J. Miao, T. Hua, Z. Huang, Y. Qi, Y. Zou, Y. Qiu, H. Xia, H. Liu, X. Cao and C. Yang, Efficient selenium-integrated TADF OLEDs with reduced roll-off, *Nat. Photonics*, 2022, **16**, 803–810.

172 D. Hall, K. Stavrou, E. Duda, A. Danos, S. Bagnich, S. Warriner, A. M. Z. Slawin, D. Beljonne, A. Köhler, A. Monkman, Y. Olivier and E. Zysman-Colman, Diindolocarbazole – achieving multi-resonant thermally activated delayed fluorescence without the need for acceptor units, *Mater. Horiz.*, 2022, **9**, 1068–1080.

173 H. L. Lee, S. O. Jeon, I. Kim, S. C. Kim, J. Lim, J. Kim, S. Park, J. Chwae, W.-J. Son, H. Choi and J. Y. Lee, Multiple-Resonance Extension and Spin-Vibronic-Coupling-Based Narrowband Blue Organic Fluorescence Emitters with Over 30% Quantum Efficiency, *Adv. Mater.*, 2022, **34**, 2202464.

174 Q. Peng, W. Yang, N. Li, S. Gong, X. Gao, C. Ye, Y. Zou and C. Yang, Indolocarbazole-based deep-blue multiple-resonance narrowband emitters and efficient organic light-emitting diodes, *Chem. Eng. J.*, 2023, **466**, 143423.

175 G. Meng, D. Zhang, J. Wei, Y. Zhang, T. Huang, Z. Liu, C. Yin, X. Hong, X. Wang, X. Zeng, D. Yang, D. Ma, G. Li and L. Duan, Highly efficient and stable deep-blue OLEDs based on narrowband emitters featuring an orthogonal spiro-configured indolo[3,2,1-*de*]acridine structure, *Chem. Sci.*, 2022, **13**, 5622–5630.

176 A. Pershin, D. Hall, V. Lemaur, J.-C. Sancho-Garcia, L. Muccioli, E. Zysman-Colman, D. Beljonne and Y. Olivier, Highly emissive excitons with reduced exchange energy in thermally activated delayed fluorescent molecules, *Nat. Commun.*, 2019, **10**, 597.

177 S. K. Jeon, H. L. Lee, K. S. Yook and J. Y. Lee, Recent Progress of the Lifetime of Organic Light-Emitting Diodes Based on Thermally Activated Delayed Fluorescent Material, *Adv. Mater.*, 2019, **31**, 1803524.

178 S. Sudheendran Swayamprabha, D. K. Dubey, Shahnawaz, R. A. K. Yadav, M. R. Nagar, A. Sharma, F.-C. Tung and J.-H. Jou, Approaches for Long Lifetime Organic Light Emitting Diodes, *Adv. Sci.*, 2021, **8**, 2002254.

179 C. Li, A. K. Harrison, Y. Liu, Z. Zhao, F. B. Dias, C. Zeng, S. Yan, M. R. Bryce and Z. Ren, TADF dendronized polymer with vibrationally enhanced direct spin-flip between charge-transfer states for efficient non-doped solution-processed OLEDs, *Chem. Eng. J.*, 2022, **435**, 134924.

180 S. Liu, Y. Tian, L. Yan, S. Wang, L. Zhao, H. Tian, J. Ding and L. Wang, Color Tuning in Thermally Activated Delayed Fluorescence Polymers with Carbazole and Tetramethylphenylene Backbone, *Macromolecules*, 2023, **56**, 876–882.

181 Y. Liu, Y. Xie, L. Hua, X. Tong, S. Ying, Z. Ren and S. Yan, Realizing External Quantum Efficiency over 25% with Low Efficiency Roll-Off in Polymer-Based Light-Emitting Diodes Synergistically Utilizing Intramolecular Sensitization and Bipolar Thermally Activated Delayed Fluorescence Monomer, *CCS Chem.*, 2022, **5**, 1005–1017.

182 P. Khammultri, P. Chasing, C. Chitpakdee, S. Namuangruk, T. Sudyoadsuk and V. Promarak, Red to orange thermally activated delayed fluorescence polymers based on 2-(4-(diphenylamino)-phenyl)-9H-thioxanthen-9-one-10,10-dioxide for efficient solution-processed OLEDs, *RSC Adv.*, 2021, **11**, 24794–24806.

183 X.-Y. Zeng, Y.-Q. Tang, X.-Y. Cai, J.-X. Tang and Y.-Q. Li, Solution-processed OLEDs for printing displays, *Mater. Chem. Front.*, 2023, **7**, 1166–1196.

184 N. R. Paisley, C. M. Tonge and Z. M. Hudson, Stimuli-Responsive Thermally Activated Delayed Fluorescence in Polymer Nanoparticles and Thin Films: Applications in Chemical Sensing and Imaging, *Front. Chem.*, 2020, **8**, 229.

185 7th International TADF Workshop, 2022, **https://www.tadf.jp**.

186 13th International Conference on Electroluminescence, 2022, **https://icel2022.org**.

187 O. Graydon, OLEDs are more than just displays, *Nat. Photonics*, 2023, **17**, 216–217.

188 W. Ma, Y. Su, Q. Zhang, C. Deng, L. Pasquali, W. Zhu, Y. Tian, P. Ran, Z. Chen, G. Yang, G. Liang, T. Liu, H. Zhu, P. Huang, H. Zhong, K. Wang, S. Peng, J. Xia, H. Liu, X. Liu and Y. M. Yang, Thermally activated delayed fluorescence (TADF) organic molecules for efficient X-ray scintillation and imaging, *Nat. Mater.*, 2022, **21**, 210–216.

189 M. Jian, Z. Song, X. Chen, J. Zhao, B. Xu and Z. Chi, Afterglows from the indolocarbazole families, *Chem. Eng. J.*, 2022, **429**, 132346.